

University of Nebraska - Lincoln

DigitalCommons@University of Nebraska - Lincoln

Biological Systems Engineering--Dissertations,
Theses, and Student Research

Biological Systems Engineering

5-2021

CONTROL SYSTEM FOR VARIABLE-ORIFICE MECHATRONIC SPRAY NOZZLE FOR REGULATION OF APPLICATION RATE AND DROPLET SIZE SPECTRA

Rodney Rohrer

University of Nebraska-Lincoln, rodneyrohrer01@gmail.com

Follow this and additional works at: <https://digitalcommons.unl.edu/biosysengdiss>



Part of the [Bioresource and Agricultural Engineering Commons](#)

Rohrer, Rodney, "CONTROL SYSTEM FOR VARIABLE-ORIFICE MECHATRONIC SPRAY NOZZLE FOR REGULATION OF APPLICATION RATE AND DROPLET SIZE SPECTRA" (2021). *Biological Systems Engineering--Dissertations, Theses, and Student Research*. 125.
<https://digitalcommons.unl.edu/biosysengdiss/125>

This Article is brought to you for free and open access by the Biological Systems Engineering at DigitalCommons@University of Nebraska - Lincoln. It has been accepted for inclusion in Biological Systems Engineering--Dissertations, Theses, and Student Research by an authorized administrator of DigitalCommons@University of Nebraska - Lincoln.

CONTROL SYSTEM FOR VARIABLE-ORIFICE MECHATRONIC SPRAY NOZZLE FOR
REGULATION OF APPLICATION RATE AND DROPLET SIZE SPECTRA

by

Rodney A. Rohrer

A DISSERTATION

Presented to the Faculty of
The Graduate College at the University of Nebraska
In Partial Fulfillment of Requirements
For the Degree of Doctor of Philosophy

Major: Biological Engineering
(Agricultural & Biological Systems Engineering)

Under the Supervision of Professor Joe Luck

Lincoln, Nebraska

May, 2021

CONTROL SYSTEM FOR VARIABLE-ORIFICE MECHATRONIC SPRAY NOZZLE FOR
REGULATION OF APPLICATION RATE AND DROPLET SIZE SPECTRA

Rodney A. Rohrer, Ph.D.

University of Nebraska, 2021

Advisor: Joe Luck

Traditional fixed-orifice spray nozzles are selected for flow rate and droplet spectra required for a given pesticide application. Although limited variation in flow can be achieved by adjusting system pressure, this can adversely affect spray quality. Other nozzle configurations, such as Pulse Width Modulated (PWM) nozzles or passive variable-orifice designs, are intended to maintain consistent droplet size and spray pattern as flow rate is changed but those too have limitations.

A variable-orifice nozzle modified by Luck (2012) can span multiple droplet spectra and offers independent control of flow and droplet size; however, an advanced control system must be developed to make it practical for field use. The primary goal of this research was to develop such control logic by managing four system variables: flow rate, pressure, droplet size, and effective orifice size. A five-nozzle spray system was built as a testbed to develop and evaluate the control method which automatically targeted desired droplet spectra and flow rate. Performance characteristics of five sizes of variable-orifice nozzles were evaluated which showed that two nozzles, spanning fine to very coarse droplet spectra, could replace four of the five nozzles.

Validation tests confirmed the control method could independently vary flow rate and droplet size. Droplet volume mean diameter was within $\pm 10\%$ of desired size for all

operating points. Actual flow rate was within $\pm 10\%$ of desired flow at nearly all operating points above 207 kPa. Optimization of the control method showed promise to reduce flow error to less than $\pm 10\%$ across the entire operating envelope but future work remains to fully implement and validate this in the control system.

Although the control method was developed with a modified variable-orifice nozzle, literature implies there is potential for it to be applied to PWM nozzles. This adaptable control method provides a foundation for development of site-specific droplet size control, weather-based droplet size control, and it is well suited for robotic and autonomous spray systems.

ACKNOWLEDGEMENTS

I would like to acknowledge the following people and organizations and thank them for their support during my graduate program:

- My family: Mary, Anna, Elizabeth, Ben
- Graduate committee: Joe Luck (graduate advisor), Santosh Pitla, Yeyin Shi, Greg Kruger
- Nebraska Tractor Test Laboratory: Doug Triplett, Justin Geyer, Roger Hoy
- Sam Marx
- Pesticide Application Technology Lab: Jeff Golus, Barbara Vukaja
- Biological Systems Engineering Research Shop: Scott Minchow
- Lincoln Machine, Inc.

GRANT INFORMATION

This research was complete under a USDA National Institute of Food and Agriculture Foundational Program grant for “Next-Generation Spray Drift Mitigation via Field-Deployable, Real-Time Weather Monitoring and Novel Spray Nozzle Control Technologies.”

Copyright 2021, Rodney Rohrer

TABLE OF CONTENTS

LIST OF FIGURES	viii
LIST OF TABLES.....	xiii
CHAPTER 1 INTRODUCTION.....	1
1.1 PESTICIDE DRIFT	1
1.2 METHODS AND TECHNOLOGIES FOR DRIFT REDUCTION	2
1.3 PROJECT GOALS AND OBJECTIVES	9
CHAPTER 2 NOZZLE DROPLET SPECTRA CHARACTERIZATION	10
2.1 INTRODUCTION.....	10
2.2 DROPLET SPECTRA MEASUREMENT	10
2.3 RESULTS AND DISCUSSION	12
2.4 CONCLUSION	16
CHAPTER 3 MULTI-NOZZLE SPRAY SYSTEM INTEGRATION AND ACTUATOR CONTROL DEVELOPMENT	17
3.1 INTRODUCTION.....	17
3.2 SPRAY SYSTEM HARDWARE	17
3.3 SOFTWARE FOR ACTUATOR CONTROL.....	23
3.3.1 LabVIEW FPGA SOFTWARE	24
3.3.2 LabVIEW REAL-TIME SOFTWARE.....	26
3.3.3 LabVIEW USER INTERFACE ON HOST PC.....	29

3.4	SPRAY SYSTEM FUNCTIONAL VALIDATION.....	32
3.4.1	ACTUATOR DISPLACEMENT	32
3.4.2	ACTUATOR RESPONSE TIME.....	33
3.4.3	PRESSURE SENSOR CALIBRATION	36
3.4.4	NOZZLE DISCHARGE RATE AND FLOW SENSOR CALIBRATION	38
3.4.5	SPRAY VOLUME DISTRIBUTION.....	41
3.5	CONCLUSION	44
CHAPTER 4	METHOD FOR ACTIVE NOZZLE CONTROL.....	46
4.1	INTRODUCTION.....	46
4.2	VARIABLE-ORIFICE NOZZLE CONTROL ALGORITHM	46
4.3	SYSTEM MODELING.....	48
4.4	VARIABLE-ORIFICE NOZZLE CONTROL IMPLEMENTATION.....	53
4.4.1	FIELD PROGRAM REAL-TIME SOFTWARE LAYER.....	53
4.4.2	FIELD PROGRAM UI SOFTWARE LAYER	57
4.5	CONCLUSION	61
CHAPTER 5	SPRAY SYSTEM CONTROL VALIDATION	63
5.1	FLOW VALIDATION.....	63
5.2	SPRAY SYSTEM DROPLET SIZE VALIDATION.....	73
5.3	FIELD PROGRAM VALIDATION.....	78
5.4	CONCLUSION	90

CHAPTER 6	RECOMMENDATIONS FOR FUTURE WORK AND SUMMARY ..	93
6.1	REDUCING FLOW ERROR WITH HIGHER ORDER CURVE FITS.....	93
6.2	POTENTIAL APPLICATION OF CONTROL METHOD TO PWM NOZZLES	
	97	
6.3	POTENTIAL CONTROL FEATURES ENABLED BY GPS	101
6.4	OTHER POTENTIAL CONTROL FEATURES, DESIGN OPORTUNITIES, AND APPLICATIONS.....	102
6.5	SUMMARY	103
REFERENCES	105
APPENDIX A	DRAWINGS OF SYSTEM COMPONENTS.....	108
APPENDIX B	DROPLET SPECTRA CHARACTERIZATION DATA	116
APPENDIX C	FLOW VALIDATION DATA.....	119

LIST OF FIGURES

Figure 1 – Nozzle body turret (left) and stackable nozzle bodies (right)	4
Figure 2 - Micromax rotary, or controlled droplet, atomizer.....	5
Figure 3 – Prototype electromechanical variable-orifice spray nozzle.....	8
Figure 4 - Low speed wind tunnel and laser diffraction instrument at the PAT Lab.	11
Figure 5 - Nozzle Tips available for VariTarget nozzle system	12
Figure 6 – Example of cumulative volume fraction vs. droplet size for green nozzle at 276 kPa and 500 motor steps.	13
Figure 7 - Reference nozzle droplet size vs. cumulative volume fraction for data collected at PAT Lab March 2019.	14
Figure 8 - Section view showing internal parts of nozzle assembly.....	19
Figure 9 - Nozzle assembly components.	20
Figure 10 - Thermocouple installed through front of enclosure (left) to measure temperature inside the enclosure (right).	22
Figure 11 - Failures of the sealing diaphragm at outer sealing joint (top) and inner sealing joint (bottom).	23
Figure 12 – FPGA software front panel for NI cRIO embedded controller.	24
Figure 13 - Real-Time software layer front panel.	27
Figure 14 - Front panel for graphic user interface that runs on the host PC.....	29
Figure 15 - Service and calibration program interactions and logic.	31
Figure 16 - Dial indicator set up to measure nozzle metering stem displacement.	32
Figure 17 - Actuator response during full retract and full extend.....	36
Figure 18 –Dead-weight tester applying known pressure for sensor calibration.....	37

Figure 19 - Graduated cylinder capturing spray to evaluate nozzle flow rate.	38
Figure 20 - Flow meter response for each nozzle at various flow rates	40
Figure 21 - Nozzles installed on patternator at W. F. Splinter Labs.....	42
Figure 22 - Example of patternator output for blue nozzle operating at 276 kPa and 400 steps.....	43
Figure 23 – Example of time history data at 25 operating points for five blue nozzles. ..	49
Figure 24 - Scatter plot of mean steady-state values from time history data.....	50
Figure 25 - Relationship between metering stem position and orifice size.	50
Figure 26 – Plot of linear regression of pressure and actuator position on flow for blue nozzle01.	51
Figure 27 – Plot of linear regression of pressure and actuator position on droplet size for blue nozzle01.	52
Figure 28 - Real Time layer front panel displaying (a) constants read from calibration file and (b) nozzle characteristics loaded from parameter file.	55
Figure 29 - User interface front panel setup tab.	57
Figure 30 - User interface front panel control tab. a.) nozzle type selector, b.) droplet spectra selector, c.) selection complete button, d.) system controls, e.) system feedback, f.) graph of system model.	58
Figure 31 - Field program software interactions and logic.....	60
Figure 32 – Detailed view from fig. 33 showing data for blue nozzle01 for varying actuator settings at lowest pressure setting.	64
Figure 33 – Plot of flow validation data for blue nozzle01 for various pressures and actuator positions.	65

Figure 34 - Scatter plot of flow error at 135 operating points for blue nozzle01.	67
Figure 35 - Scatter plot of pressure and position vs flow error at 135 operating points for blue nozzle01.	67
Figure 36 - Scatter plot of flow error at 135 operating points for green nozzle01.	68
Figure 37 - Scatter plot of pressure and position vs. flow error at 135 operating points for green nozzle01.	68
Figure 38 – Measured flow vs. actuator position for blue nozzle01 at nine pressure settings.	70
Figure 39 – Measured flow vs. actuator position for green nozzle01 at nine pressure settings.	70
Figure 40 - Percent error between measured flow and expected flow using blue nozzle01 polynomial coefficients for each of five blue nozzles.	71
Figure 41 – Percent error between measured flow and expected flow using green nozzle01 polynomial coefficients for each of five green nozzles.	72
Figure 42 - Reference nozzle droplet size vs. cumulative volume fraction for curve fit and validation data collected at PAT Lab 7Dec2020.	74
Figure 43 - Operating points for droplet size curve fit and validation data sets.	74
Figure 44 - Error between measured and expected $D_{v0.5}$ for blue nozzle validation data.	77
Figure 45 - Error between measured and expected $D_{v0.5}$ for green nozzle validation data.	78
Figure 46 - Reference nozzle droplet size vs. cumulative volume fraction for field program data collected at PAT Lab 8Dec2020.	79
Figure 47 - Operating envelope for blue nozzle spanning three droplet spectra.	81

Figure 48 - Operating envelope for green nozzle spanning three droplet spectra.	82
Figure 49 - Nine operating points with blue nozzle01 at constant flow rate (i.e., speed) but varying droplet size ($D_{v0.5}$) spanning three droplet spectra categories.	83
Figure 50 - Nine operating points with green nozzle01 at constant flow rate (i.e., speed) but varying droplet size ($D_{v0.5}$) spanning three droplet spectra categories.	84
Figure 51 - Three operating points on a line of constant droplet size but varying flow rate for blue nozzle01.....	86
Figure 52 - Three operating points on a line of constant droplet size but varying flow rate for green nozzle01.....	87
Figure 53 -Variation in droplet size measured from reference nozzles on three different days but at the same laboratory and with the same operator.	90
Figure 54 – Plot of blue nozzle01 measured flow along with four variations of expected flow calculated from alternative polynomial curve fits.	94
Figure 55 - Plot of blue nozzle01 measured flow along with four variations of expected flow calculated from alternative polynomial curve fits.	95
Figure 56 - Flow error vs. pressure and position for five nozzles using nozzle01 coefficients with a polynomial first-order on pressure and second-order on position.....	96
Figure 57 - Flow error vs. pressure for five blue nozzles using nozzle01 coefficients with a polynomial first-order on pressure and second-order on position.	97
Figure 58 - Spray volume median diameter for various pressures and flow rates achieved by 10% – 100% modulation of control valve with an 8004 nozzle (Giles, 1996).	99

Figure 59 - Surface plot created from data published by Butts, et al. (2019) showing the relationship between pressure, duty cycle and volume median diameter for SR11004c nozzle.	100
Figure 60 - Engineering drawing for nozzle assembly adapter block sheet 1.	108
Figure 61 - Engineering drawing for nozzle assembly adapter block sheet 2.	109
Figure 62 - Engineering drawing for nozzle assembly adapter cylinder.	110
Figure 63 - Engineering drawing for nozzle assembly metering stem extension.	111
Figure 64 - Engineering drawing for nozzle assembly metering stem.	112
Figure 65 - Engineering drawing for nozzle assembly metering tip.....	113
Figure 66 - Engineering drawing for nozzle assembly enclosure.....	114
Figure 67 - Engineering drawing for nozzle assembly enclosure lid.....	115
Figure 68 - Detailed view from fig. 69 showing data for varying actuator settings at lowest pressure setting (green nozzle01 flow coefficients).	119
Figure 69 - Plot of time history data for nozzle flow evaluation (green nozzle01 flow coefficients).....	120

LIST OF TABLES

Table 1 - Performance specifications for Micromax CDA.....	6
Table 2 - Reference nozzle mean droplet diameter for nozzle evaluation at the PAT Lab March 2019.....	13
Table 3 - Range of droplet size observed for each nozzle.....	15
Table 4 - Summary of droplet spectra performance of the five nozzles tested with modified seal.....	15
Table 5 - Summary of actuator position evaluation.....	33
Table 6 - Summary of pressure sensor error after calibration.....	38
Table 7 - Summary of flow meter measurement error as percent of reading.....	40
Table 8 – Range of flow observed for each nozzle.....	41
Table 9 - Spray pattern coefficient of variation across nozzle operating range.....	44
Table 10 - Polynomial coefficients, coefficient of determination, and root mean square error for regression of pressure and actuator position on flow.....	51
Table 11 - Polynomial coefficients, coefficient of determination, and root mean square error for regression of pressure and actuator position on droplet size.....	52
Table 12 - Example of parameter file for green nozzle tip.....	55
Table 13 - Range of measured flow for five blue nozzles and five green nozzles.....	69
Table 14 - Flow error for five blue nozzles and five green nozzles where expected flow was based on polynomial coefficients from nozzle01.....	72
Table 15 - Reference nozzle droplet diameters for curve fit and validation data collected at PAT Lab 7Dec2020.....	73
Table 16 - Dv0.1, Dv0.5, and Dv0.9 droplet diameters for droplet validation data set....	75

Table 17 - Droplet classifications for validation data set.	76
Table 18 - Error between measured and expected $D_{v0.5}$ for validation data set.	76
Table 19 - Reference nozzle droplet diameters for field program data collected at PAT Lab 8Dec2020.....	79
Table 20 - Operating points for field program data collection.	81
Table 21 - UI settings for field program validation.	82
Table 22 - Summary of blue nozzle01 validation data with field program.	84
Table 23 - Summary of green nozzle01 validation data with field program.	85
Table 24 - Variation in droplet size measured from reference nozzles on three different days but at the same laboratory and with the same operator.	89
Table 25 - Higher order polynomial curve fits done on blue nozzle flow validation data.	93
Table 26 - Average measured pressure, measured flow, and volume median diameter ($D_{v0.1}$, $D_{v0.5}$, and $D_{v0.9}$) for five nozzles.....	116

CHAPTER 1 INTRODUCTION

1.1 PESTICIDE DRIFT

Modern agriculture has achieved unprecedented levels of production and quality of agricultural products that provide society with food, fiber, and feedstock for biofuels and other products derived from crops. Many factors contribute to this success including the ability to control agricultural pests. Spray-applied liquid pesticides are an effective part of integrated pest management in modern agriculture. In 2012 pesticide expenditures in the U.S. were approximately \$14 billion at the user level with pesticide usage of over 1.1 billion pounds on 390 million acres (EPA, 2017). Spray application methods are well developed and have widespread use, but some problems remain to be addressed and new pesticides can present new challenges. A significant challenge is spray drift during application where a pesticide is carried by wind to off-target areas. According to EPA estimates, approximately ten percent of agricultural pesticide sprays miss or move from intended application sites and an estimated seventy million pounds of pesticide active ingredient are wasted to drift annually (Leonard, 2016). Drift can cause many problems including harm to off-target crops and vegetation, reduced effectiveness on the target crop, and environmental and economic damage and pollution to sensitive areas (Kruger et al., 2013). The Nebraska Department of Agriculture investigates approximately 10 complaints involving alleged drift each year with the belief that this represents only a fraction of drift events as not all incidents of drift are reported (Leonard, 2016). Hanna et al. (2009) report that in an average year approximately 200 to 300 pesticide drift complaints are investigated in Iowa.

Dicamba, a broadleaf herbicide that has been in use in the U.S. since the late 1960s, provides a recent example of problems with spray drift. Starting in 2017 dicamba tolerant cotton and soybeans have been grown in the U.S. A 2017 report on dicamba-injured soybean acres indicates there were 2,708 dicamba-related crop injury cases under investigation by state departments of agriculture in the U.S. and approximately 3.6 million acres of soybeans were injured by off-site movement of dicamba (Bradley, 2017).

1.2 METHODS AND TECHNOLOGIES FOR DRIFT REDUCTION

Several best practices for pesticide application can be employed to reduce and mitigate drift. In many cases, drift can be minimized by simply avoiding spray applications during windy conditions, however pesticide application must be timely to be successful and may not be effective if weeds or other pests are not controlled before reaching specific growth or population thresholds. Chemical adjuvants can be mixed with pesticides to change their properties, making them less susceptible to drift. While this offers some success in minimizing drift, it requires additional cost and labor and may not be compatible with all pesticides. Changing pesticide mix concentration by increasing the carrier (water) volume in the mixture allows higher flow rates, at lower pressure, through larger fixed-orifice spray nozzles with the effect of producing larger droplets which are less susceptible to movement by wind. However, this introduces additional costs and other logistics problems where more carrier must be transported to the field and requires refilling the sprayer more often. Additionally, the pesticide carrier volume can affect the efficacy of the pesticide application (Butts et al., 2018).

Although larger droplets are beneficial to minimizing drift, droplet size can affect pesticide efficacy and coverage and so larger droplets may not be appropriate for all

pesticide applications (Creech et al., 2016). For example, finer droplets may be more effective for contact herbicides, insecticides, and fungicides where consistent coverage is important, whereas large droplets may be better for systemic herbicides that translocate within a plant (Fischel et al., 2016; Hanna et al., 2009; Butts et al., 2018).

Proper nozzle selection is important for achieving the application rate and droplet size specified on the pesticide product label. A wide variety of spray nozzles are commercially available, but their performance is generally limited to a fixed spray pattern and droplet size and so different nozzles are required to achieve distinct application parameters. Traditional fixed orifice nozzles can in some cases operate at more than one droplet size category by adjusting system pressure. However, this will also change the nozzle flow rate (l/min) and, in turn, change the application rate (l/ha). Application rate must then be managed by adjusting travel speed. If the required application rate or droplet size is outside the nozzle's operating envelope, or if the required travel speed becomes impractical, then the physical nozzle tip must be changed, and the system readjusted. For modern sprayers with booms up to 40 meters wide, this could mean changing dozens of nozzle tips which is not only expensive and time consuming but leads to increased pesticide exposure for the operator. Conventional sprayers can be configured with nozzle body turrets (fig. 1 left) or stackable nozzle bodies (fig. 1 right) to make it easier to change nozzle tips. While this does add convenience, the operator is still required to manually rotate the turret for each nozzle or activate the correct stacked nozzle to make a discrete change in sprayer performance. Butts et al. (2018) cites a survey reporting that more than 62% of applicators changed nozzles less than 50% of the time when changing herbicide products, potentially leading to inaccurate applications.



Figure 1 – Nozzle body turret (left) and stackable nozzle bodies (right) (Spray Systems Co., 2014).

Funseth et al. (2014) conceived of a rotary manifold connected to multiple standard fixed-orifice nozzles. In this configuration, a drive motor would be actuated to automatically switch between nozzles to change application rate on-the-go to compensate for changes in ground speed. This is further evidence of the need for solutions to maintaining proper droplet size and spray pattern as flow rate is changed.

Rotary atomizers, or controlled droplet atomizers (CDA), can also be used for liquid pesticide application. With these devices droplets are formed as the liquid is cast from a spinning disk where smaller droplets are generated at faster rotational speeds and are of a more uniform size than pressurized nozzle atomizers (Srivastava et al., 2006). However, rotary atomizers are also more mechanically complex than fixed orifice nozzles and require external hydraulic or electric motor to spin the disk. As atomizer speed is varied, pesticide distribution can also change.

An example of a rotary atomizer marketed for agricultural use is the Micromax CDA (Micron Group, 2021) (fig. 2). This atomizer has three operating speeds, producing three different droplet sizes (table 1). Speed is adjusted by manually moving a drive belt to a different set of pulleys between the drive motor and the disk. Flow rate is adjusted by installing restrictors and regulating supply system pressure (Micron Group, 2002). CDA applicators are not in widespread use in production agriculture but are primarily used for low-volume applications where smaller droplet sizes are needed.

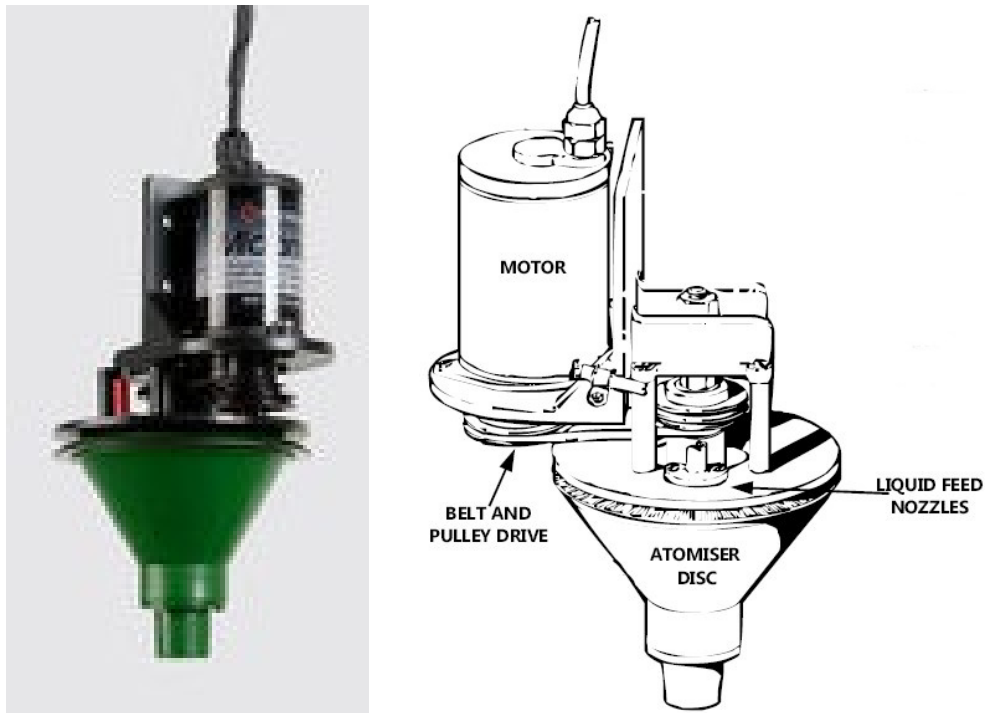


Figure 2 - Micromax rotary, or controlled droplet, atomizer. Left: (Micron Group, 2021)
Right: (Micron Group, 2002)

Table 1 - Performance specifications for Micromax CDA (Micron Group, 2002).

disc speed (rpm)	liquid feed rate (l/min)	spray droplet size (μm)	application volume (l/ha)
2000	0.5-3	200-500	30-200
3500	0.25-1	100-300	20-80
5000	0.125-0.5	75-150	10-40

Pulse-width-modulated (PWM) solenoid-controlled nozzles developed several decades ago (Giles and Comino, 1992) are now in widespread use in production agriculture.

These nozzles use a fixed orifice spray tip where flow is turned on and off several times per second, typically at 10 Hz, by the solenoid to vary the flow rate while maintaining consistent droplet size and spray pattern (Sharda et al., 2016). However, some studies indicate that because this system does not have a continuous spray pattern it may not produce a uniform application resulting in areas with under- or over-application (Magnus et al., 2017). Although a primary feature of these nozzles is to maintain the same droplet size at varying flow rates, Giles et al. (1996) has confirmed that flow and droplet size can be controlled independently with a PWM, however, this functionality has not been commercially developed.

Kruckeberg (2011) developed an automated control system to mitigate spray drift based on local weather conditions where the system would activate one of three installed spray nozzles to provide the desired droplet size. The physical system required multiple nozzle assemblies, each providing a distinct droplet spectra and at a discrete flow rate. Flow to each nozzle was controlled by a separate solenoid-activated valve. As local weather conditions changed, the control system activated a different nozzle to provide the droplets of the desired size category. As different nozzles were activated, a rate controller was used to adjust system flow and pressure to maintain the required application rate. This

control system was successful in modeling spray drift potential and determining a droplet size required to minimize drift, however, the system required multiple spray tips installed on redundant nozzle bodies to enable changing droplet spectra on-the-go. Although the objective of their research was not to create a system with continuously variable droplets size and flow capability, this work does highlight the significance of this gap in variable-orifice nozzle technology.

Bui (2006) patented a novel nozzle design, now commercially marketed as VariTarget nozzles, that, like a PWM nozzle, is intended to maintain constant droplet size and spray pattern as flow rate is varied. Unlike the PWM system that uses fixed-orifice nozzles operated at constant pressure, with the VariTarget nozzle, system pressure is adjusted to change flow rate and the nozzle geometry is changed accordingly to maintain consistent droplet size and spray pattern. In the commercial implementation of this design, the nozzle orifice geometry is changed by an internal metering element that is passively controlled by a spring reacting to changes in system pressure. Bui (2006) described alternate implementations where the “biasing element could be a controlled fluid, gas, or motor-controlled linkage” which could receive commands from a controller to position the metering element in the valve. Additionally, Bui described implementations where the same controller could control a throttle valve or variable speed pump to regulate system pressure as well as including position information from a GPS or additional inputs that “account for wind, boom height, sunlight and water received by the crops, variations in insect infestation, etc.” (Bui, 2006). However, no evidence has been found in the literature showing any of these alternate hardware implementations or control schemes.

A variable-orifice electromechanical spray nozzle was prototyped by Luck (2012) based on a modified version of the VariTarget nozzle (SprayTarget, Laguna Niguel, CA). Luck replaced the internal bias spring with a stepper motor linear actuator and had the insight to modify the internal nozzle seal to increase the operating envelope of the nozzle performance (fig 3). The result was an electronically controlled nozzle capable of varying droplet size and flow rate independently, and continuously, across several droplet size spectra using a single nozzle tip. Preliminary research demonstrated this nozzle could span four standard droplet size classifications (ANSI/ASABE, 2018) across flow and pressure ranges seen on typical commercial sprayers. No commercially available products exist that can generate a range of droplet sizes with continuous flow; the design intent of commercial nozzles has generally been to maintain constant droplet size. Although the active electromechanical nozzle is novel, it can still be attached to industry standard nozzle bodies allowing it to be retrofitted onto existing commercial sprayers. This innovative nozzle, however, requires an advanced control system.



Figure 3 – Prototype electromechanical variable-orifice spray nozzle.

No control algorithms exist that manage the four variables which characterize the variable-orifice nozzle system: flow rate, pressure, effective orifice size, and droplet size. The variable-orifice spray nozzle prototyped by Luck (2012) was used as a development platform for a control system that allows a user to specify application rate, travel speed,

and droplet size for a specific pesticide type, or mode-of-action. Although the novel nozzle control algorithm was developed with a particular nozzle platform, it is applicable to other variable-orifice nozzle variations that may be developed in the future and is not limited to use with the existing electromechanical nozzle prototype discussed above.

1.3 PROJECT GOALS AND OBJECTIVES

The primary goal of this research was to develop a control system for a variable-orifice spray nozzle. Specific objectives for this research were:

1. Develop operating envelopes (i.e., flow and droplet spectra) for five variable-orifice nozzle tips with modified seals.
2. Develop control logic for an electromechanical variable-orifice nozzle.
3. Implement a control system to automatically target (via carrier pressure and metering stem position settings) a desired droplet spectra and desired flow rate based on product application rate.

CHAPTER 2 NOZZLE DROPLET SPECTRA CHARACTERIZATION

2.1 INTRODUCTION

When developing the prototype variable-orifice nozzle described above, Luck (2012) found that modifying the seal between the nozzle tip and the VariTarget nozzle body, by removing the inner ‘collar’ of the seal, increased the range of flow through the nozzle. Luck mapped flow rate, system pressure, effective orifice size, and droplet size for a green (coarse) VariTarget nozzle tip. Although the system was not integrated with automated control, by manually adjusting system pressure and nozzle actuator position the prototype demonstrated the capability to produce droplets sizes across several droplet spectra with a single spray tip.

In fulfillment of the first project objective, five VariTarget nozzles were evaluated to characterize the operating envelope of each and identify overlap in their performance. Results of this evaluation revealed opportunities to disregard spray tips whose performance overlapped with another’s or was not practically useful when developing the variable-orifice spray control system for typical agricultural field applications.

2.2 DROPLET SPECTRA MEASUREMENT

The Pesticide Application Technology (PAT) Laboratory at the University of Nebraska-Lincoln’s (UNL) West Central Research and Extension Center (WCREC) in North Platte, Nebraska includes a low-speed wind tunnel with a laser diffraction instrument (Helos/Kr-Vario, Sympatec, Clausthal-Zellerfeld, Germany) for measuring droplet size (fig. 4).

When equipped with a R7 lens, the laser diffraction instrument can detect particles from

18 to 3500 micrometers (μm). Air flow in the wind tunnel prevented droplets from recirculating as the flat fan spray pattern traversed the laser. The flat fan distribution of the spray stream was perpendicular to, and 305 mm from, the path of the laser beam as the nozzle was moved on a linear actuator to traverse the path of the laser.

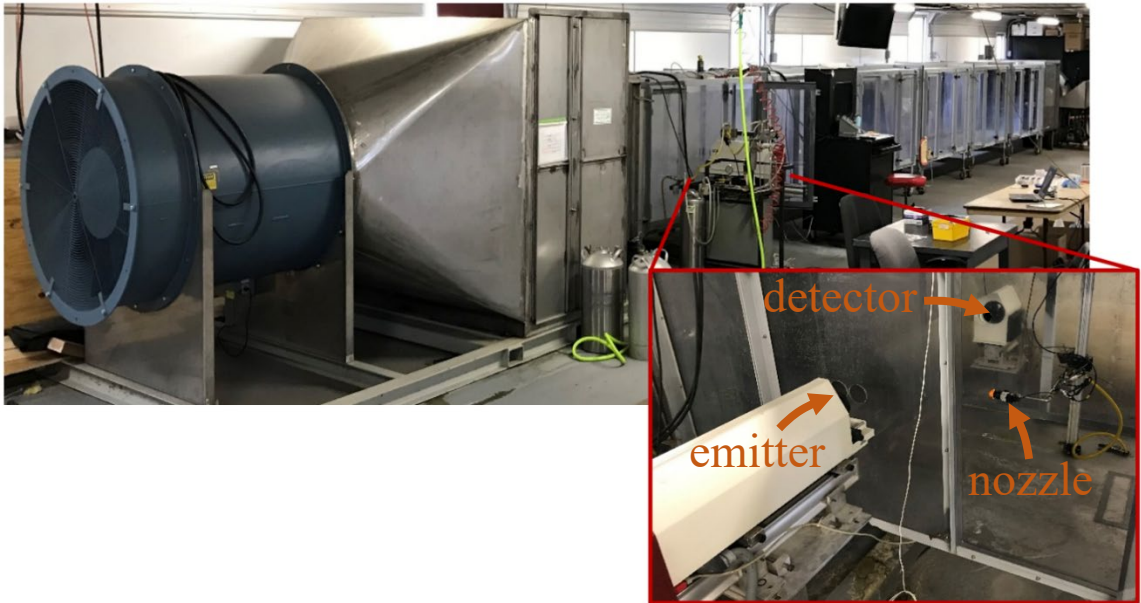


Figure 4 - Low speed wind tunnel and laser diffraction instrument at the PAT Lab.

Each of the five nozzle tips available for the VariTarget nozzle system (fig. 5) were evaluated to measure their droplet spectra at various system pressures from 138 to 552 kilopascal (kPa) and various effective orifice sizes (i.e., 400 to 800 motor steps). Because effective orifice size is a function of actuator position, motor steps of the actuator's stepper motor is a proxy for effective orifice size for this variable-orifice nozzle configuration. Droplet spectra for standard reference nozzles described in ANSI/ASABE Standard S572.2 were measured during the same test to be used as a reference in determining the droplet classification for each operating point (ANSI/ASABE, 2018). All

tests were done with water. System pressure was managed by regulating air pressure in pneumatic supply tanks. Three iterations were done at each operating point.



Figure 5 - Nozzle Tips available for VariTarget nozzle system (SprayTarget, 2009).

Although spray pattern was not evaluated during this nozzle testing it was observed at each operating point. When the red nozzle was operated at low pressures it was obvious that the spray pattern was not uniform and was poorly distributed, so this nozzle was not evaluated at pressures below 207 kPa. Similarly, the green nozzle was not evaluated at pressures above 414 kPa.

2.3 RESULTS AND DISCUSSION

Output from the nozzle testing included droplet size for each observation, in micrometers, at 10%, 50%, and 90% of cumulative volume fraction, designated as $D_{v0.1}$, $D_{v0.5}$, and $D_{v0.9}$ respectively, as shown in the example in figure 6. The reference nozzles provided a method to ‘calibrate’ droplet size measurements to standard droplet spectra categories as defined in ANSI/ASABE S527.2 (2018). Boundaries between droplet spectra categories are delineated by lines connecting points that are one standard deviation above the average $D_{v0.1}$, $D_{v0.5}$, and $D_{v0.9}$ for each respective reference nozzle. Results for the reference nozzles used for this evaluation are shown in table 2 and figure 7.

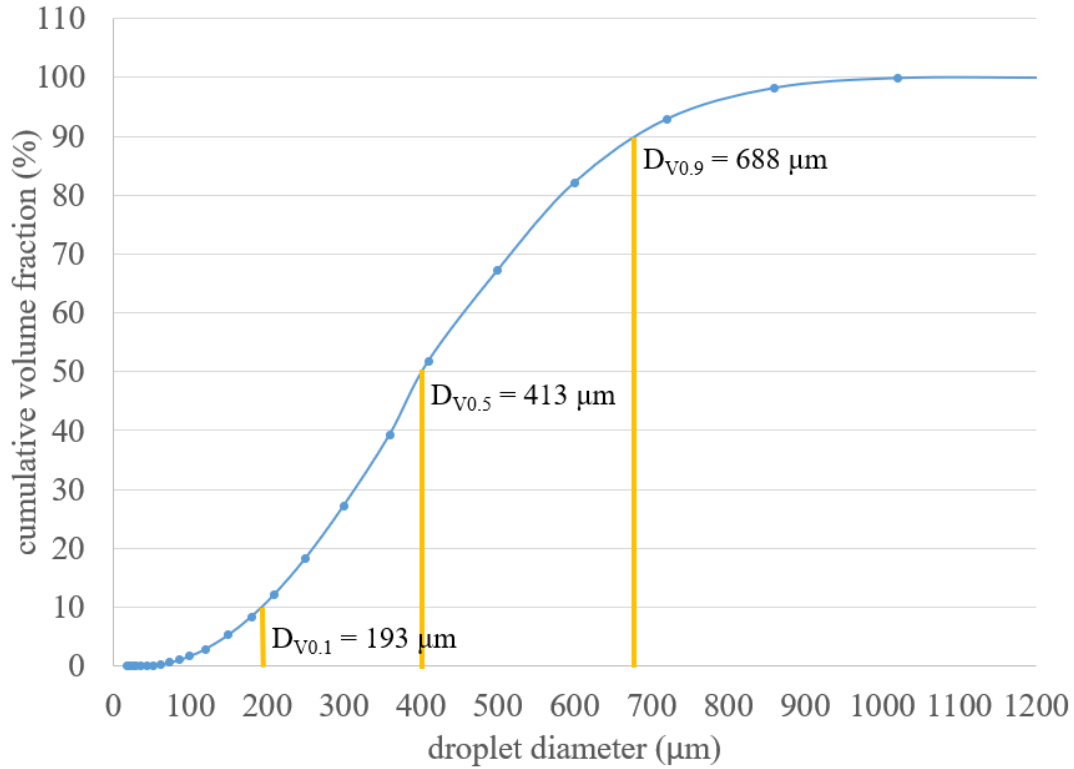


Figure 6 – Example of cumulative volume fraction vs. droplet size for green nozzle at 276 kPa and 500 motor steps.

Table 2 - Reference nozzle mean droplet diameter for nozzle evaluation at the PAT Lab March 2019.

Droplet Spectra Classification Boundaries									
categories [†]	mean diameter (μm)								
	D _{v0.1}			D _{v0.5}			D _{v0.9}		
	avg	std. dev.	sum	avg	std. dev.	sum	avg	std. dev.	sum
VF/F	65	0.3	65	141	0.4	141	239	1.5	241
F/M	120	1.1	121	261	1.0	262	424	1.5	425
M/C	177	2.3	180	377	3.1	380	587	3.2	590
C/VC	207	0.4	207	446	0.7	446	747	0.9	748
VC/XC	255	0.5	256	542	0.8	542	856	0.3	856
XC/UC	339	0.5	340	690	1.5	692	1082	3.7	1086

[†]VF = very fine

F = fine

M = medium

C = coarse

VC = very coarse

XC = extremely coarse

UC = ultra coarse

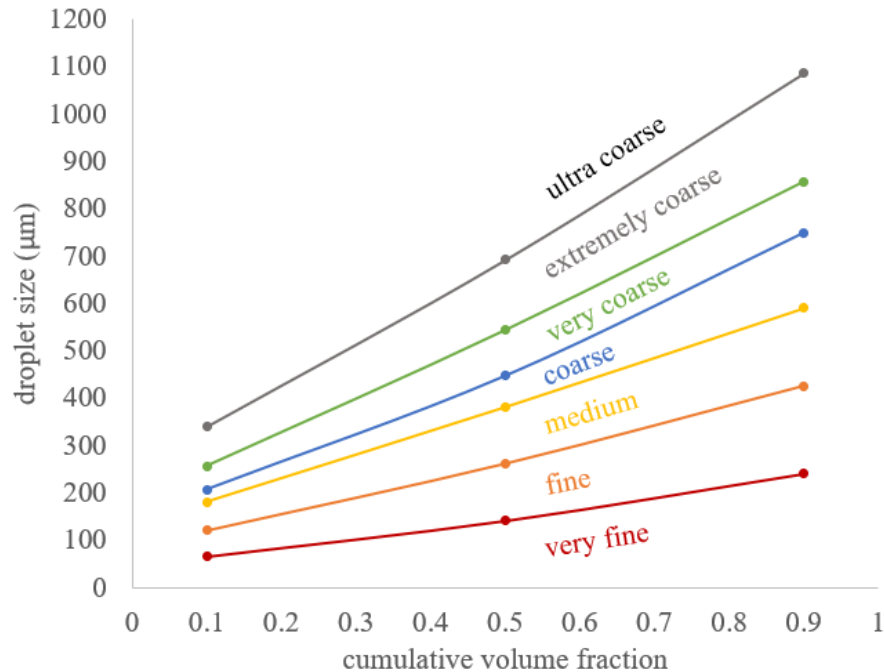


Figure 7 - Reference nozzle droplet size vs. cumulative volume fraction for data collected at PAT Lab March 2019.

Average measured pressure, measured flow rate, and $D_{v0.1}$, $D_{v0.5}$, and $D_{v0.9}$ droplet sizes for the three iterations at each test nozzle operating point are summarized in table 26 in Appendix B: Nozzle Droplet Spectra Characterization Data. The range of droplet diameters achieved by each nozzle are summarized in table 3 where minimum operating point is at highest pressure and smallest orifice and maximum operating point is at lowest pressure and largest orifice. This table also reports relative span, the difference between $D_{v0.9}$ and $D_{v0.1}$ divided by $D_{v0.5}$, which is an indication of the width of the droplet size distribution. The $D_{v0.1}$, $D_{v0.5}$, and $D_{v0.9}$ volume diameters were compared to the droplet spectra boundaries generated from reference nozzle data to determine droplet size classifications which are summarized in table 4. Note that droplet size increases as effective orifice size increases (i.e., lower motor steps) and as pressure decreases.

Table 3 - Range of droplet size observed for each nozzle.

	operating point	pressure (kPa)	position (steps)	droplet size range			relative span
				Dv0.1 (μm)	Dv0.5 (μm)	Dv0.9 (μm)	
red	min	552	800	42	98	181	1.42
	max	207	400	67	175	381	1.79
orange	min	552	800	80	190	335	1.34
	max	138	400	128	286	474	1.21
yellow	min	552	800	83	193	341	1.34
	max	138	400	142	324	543	1.24
blue	min	552	800	102	233	398	1.27
	max	138	400	207	439	714	1.15
green	min	414	800	127	284	477	1.23
	max	138	400	253	525	837	1.11

Table 4 - Summary of droplet spectra performance of the five nozzles tested with modified seal.

nozzle	position (steps)	pressure (kPa)						
		138	207	276	345	414	483	552
red	400	--	F	VF	VF	VF	VF	VF
	500	--	F	VF	VF	VF	VF	VF
	600	--	VF	VF	VF	VF	VF	VF
	700	--	F	VF	VF	VF	VF	VF
	800	--	F	VF	VF	VF	VF	VF
orange	400	M	F	F	F	F	F	F
	500	F	F	F	F	F	F	F
	600	F	F	F	F	F	F	F
	700	F	F	F	F	F	F	F
	800	F	F	F	F	F	F	F
yellow	400	M	M	M	M	M	M	M
	500	M	M	M	M	F	F	F
	600	F	F	F	F	F	F	F
	700	F	F	F	F	F	F	F
	800	F	F	F	F	F	F	F
blue	400	C	C	M	M	M	M	M
	500	M	M	M	M	M	M	M
	600	M	M	M	M	M	F	F
	700	M	M	F	F	F	F	F
	800	M	M	M	F	F	F	F
green	400	VC	VC	C	C	M	--	--
	500	VC	C	C	M	M	--	--
	600	C	M	M	M	M	--	--
	700	C	M	M	M	M	--	--
	800	C	M	M	M	M	--	--

VF = very fine M = medium VC = very coarse
F = fine C = coarse XC = extremely coarse

2.4 CONCLUSION

The first project objective to develop operating envelopes (i.e., flow and droplet spectra) for five variable-orifice nozzle tips was accomplished with the work described in this chapter. The red nozzle produced very fine droplets across most of its operating range with fine droplets produced at only 207 kPa. While appropriate for some applications, very fine droplets are not typically used for commercial agricultural pesticide application, therefore the red nozzle was not considered further in this project. The fine and medium droplet spectra produced by the orange and yellow nozzles were also available at several operating points with the blue nozzle and so were not considered further.

Performance of the blue nozzle spanned three droplet size categories, fine, medium, and coarse, while the green nozzle was able to span medium, coarse, and very coarse. The blue and green nozzles were able to span the droplet size performance of four of the five nozzles tested with the modified seal, with the fifth nozzle (red) of lesser commercial interest and so only the blue and green nozzles were considered during the subsequent variable-orifice spray system development.

CHAPTER 3 MULTI-NOZZLE SPRAY SYSTEM INTEGRATION AND ACTUATOR CONTROL DEVELOPMENT

3.1 INTRODUCTION

The variable-orifice nozzle prototyped by Luck (2012) was used as a concept design to be scaled up to a multi-nozzle sprayer for further spray system development. Upon successful completion of the variable-orifice nozzle control system, future plans included development of additional spray system features along with assembly of a demonstration sprayer for a utility vehicle. This seven-nozzle demonstration unit would be used to showcase the variable-orifice spray technology in agronomic research and other field trials. Deploying the variable-orifice nozzle assembly in the field requires addition of an enclosure to protect the stepper motor linear actuator and motor driver circuit board from dirt and moisture. Mounting provisions were also needed to allow the nozzle to be attached to a spray boom along with integration of sensors and fittings to create a compact nozzle assembly.

This chapter describes spray system hardware and low-level software design and integration needed for future field deployment. Discussion includes development of control logic, positioning validation, and dynamic response for the linear actuator. This is followed by discussion on pressure and flow sensor calibration and evaluation of spray volume distribution.

3.2 SPRAY SYSTEM HARDWARE

The basic features of the prototype nozzle developed by Luck were retained in the updated design, but additional features were added to create a practical nozzle assembly

for the field demonstration sprayer. The same stepper motor linear actuator (Zaber NA1416A, Zaber Technologies, Vancouver, BC) was used in place of the factory installed spring in the VariTarget nozzle body to allow active control of the internal metering stem. The linear actuator had a range of 16 mm with 200 steps per revolution and 1.2192 mm per revolution. Although the motor driver and actuator enabled micro-stepping, micro-stepping was not used for this application. The linear actuator included an integral Hall-effect sensor that was used to detect when the actuator was fully retracted to its home position. The physical design of the nozzle body and adapter block required that the metering stem be limited to no more than approximately 750 steps to prevent damaging the spray tip by pushing the metering tip too far into the nozzle.

The metering stem extension adapter, metering stem, adapter cylinder, and internal features of the adapter block (fig. 8, component drawings in Appendix A: Drawings of System Components figures 60-67) were nominally the same as those of Luck's (2012) design but with special consideration given to the length tolerance of these parts to ensure consistent metering tip displacement among different nozzle assemblies. Even with this attention to length tolerance, the assembly included two soft joints that caused some variation in the tolerance stack-up. The soft joints occurred where a rubber diaphragm was installed to allow the metering stem to move while sealing fluid from leaking to the top of the nozzle body and flooding the linear actuator. A weep hole was added to the adapter cylinder to allow fluid to drain externally in the event of leakage past the diaphragm. Features were added to the nozzle adapter block to provide mounting provisions so the nozzles could be attached to a spray boom and to attach an enclosure to protect the stepper motor and motor driver.

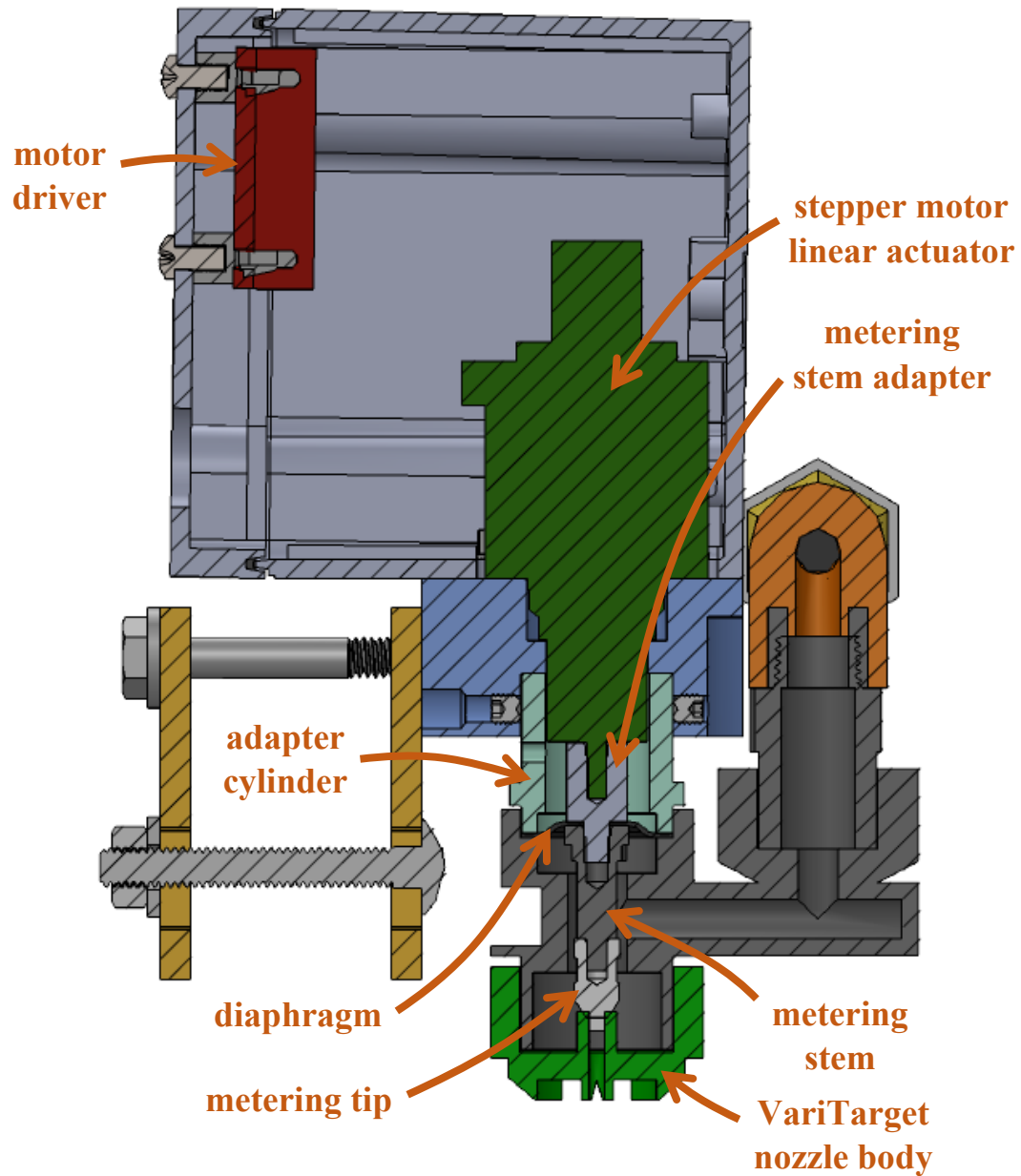


Figure 8 - Section view showing internal parts of nozzle assembly.

Pressure sensors (PX09-100G5V, Omega Engineering Inc., Norwalk, CT) and turbine flow meters (FTB-430, Omega Engineering Inc., Norwalk, CT) were installed on each nozzle assembly (fig. 9). The pressure sensors had a range of 0 to 689 kPa with 0 to 5 volt output. The flow meters had a range of 0.76 to 7.57 liters per minute with an output of 34 to 343 Hz. While only one pressure sensor would be required for a fully developed

multi-nozzle spray system, pressure sensors were included in each nozzle assembly for development. Data from these sensors were logged during control system development to understand variation in performance of the nozzle assemblies. Flow meters were installed on each nozzle assembly to provide a data for characterizing nozzle performance and are not required for a fully developed spray system. A 21 kPa check valve (SM650-6F6FB check valve, Dultmeier Sales, Omaha, NE) was included to prevent fluid from draining when the system was turned off.

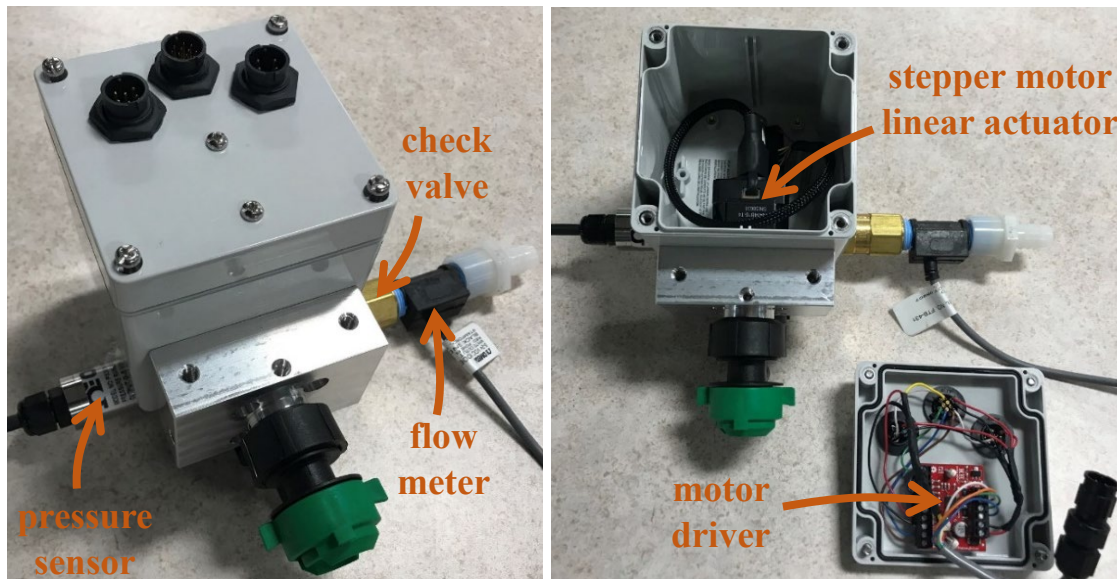


Figure 9 - Nozzle assembly components.

The seal between the VariTarget nozzle body and spray tip was modified by removing the inner ‘collar’ of the seal in the same manner as done by Luck (2012) to increase the operating range of the variable-orifice nozzle.

The system was controlled with a National Instruments (NI) compact reconfigurable input output (cRIO) embedded controller (cRIO-9068, National Instruments, Austin, TX) with Field Programmable Gate Array (FPGA) and Real-Time (RT) processor. The cRIO controller was configured with one NI 9403 32-channel TTL digital IO module and one

NI 9205 32-channel 16-bit analog input module (National Instruments, Austin, TX). The stepper motor linear actuators were interfaced with the controller using Big Easy Driver stepper motor drivers (SparkFun Electronics, Niwot, CO). Although the motor drivers allowed micro-stepping, they were configured to use only a full step for each digital pulse generated by the controller. Motor driver current limits were adjusted to rated motor current of 0.57 amps. Each motor driver used three channels from the NI 9403 module, one each for stepping, direction, and home signal, with one additional digital channel for each flowmeter. Each pressure sensor used one analog channel on the NI 9205 module.

During development it was observed that the temperature of the linear actuators would get hot when the stepper motors were powered continuously even when no motion is commanded. The motor drivers include a feature where they can be disabled with a digital signal to minimize power consumption and reduce heat buildup in the linear actuators when not in motion. However, it was discovered that if the actuators were not continuously powered, they could be back-driven by the fluid pressure acting on the diaphragm in the nozzle assembly and would not be able to hold their position when under load. A thermocouple was installed in one of the nozzle assemblies to evaluate temperature rise of a continuously powered actuator (fig. 10). When the nozzle assembly was not installed on the metal spray boom, and with no fluid flowing through the nozzle, the temperature rose to 63 degrees Celsius and was still rising slightly when the evaluation was stopped. When mounted to the metal spray boom, the temperature stabilized at approximately 49 degrees Celsius when no fluid was flowing through the nozzle and at approximately 35 degrees Celsius when fluid was flowing. The linear

actuator manufacturer confirmed the need to leave the actuators powered to better hold their position and recommended to install a heat sink to manage temperature.

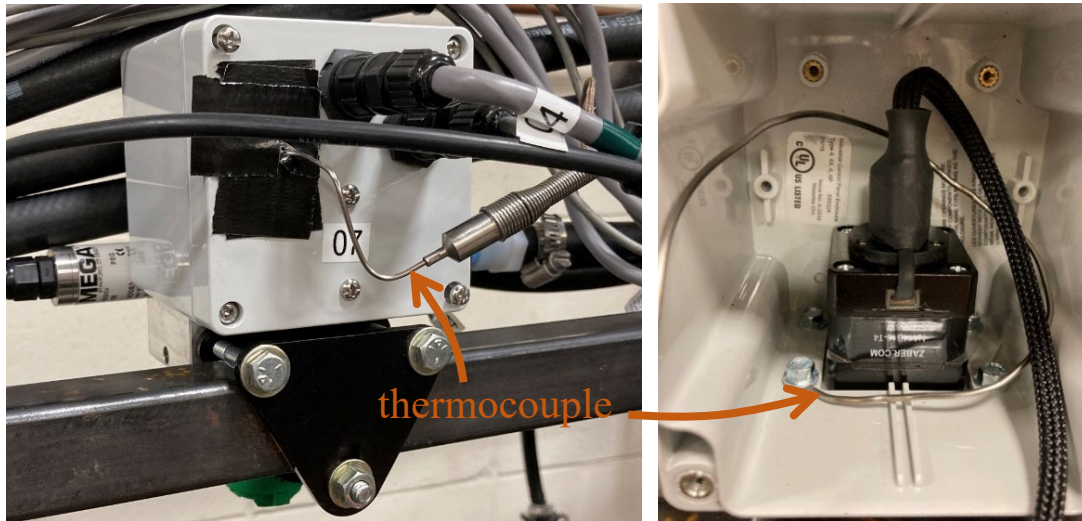


Figure 10 - Thermocouple installed through front of enclosure (left) to measure temperature inside the enclosure (right).

Another issue discovered during system development was that the diaphragm clamped in the joint between the nozzle body and adapter cylinder and between the metering stem extension and metering stem could slip out of the clamped joint and allow fluid to leak into the actuator and enclosure. Although no actuators failed because of this leakage, several motor drivers shorted and failed when water entered the enclosure. The failure at the external edge of the diaphragm (fig. 11, top), clamped between the nozzle body and adapter cylinder, was resolved by additional tightening of the nut on nozzle assembly to increase clamping force on outer diameter. The failure at the inner edge of the diaphragm (fig. 11 bottom), clamped between the metering stem extension and metering stem, was resolved by roughing the machined surfaces on both parts and applying additional tightening. The final step in avoiding further failures was to limit operating pressures to 414 kPa.

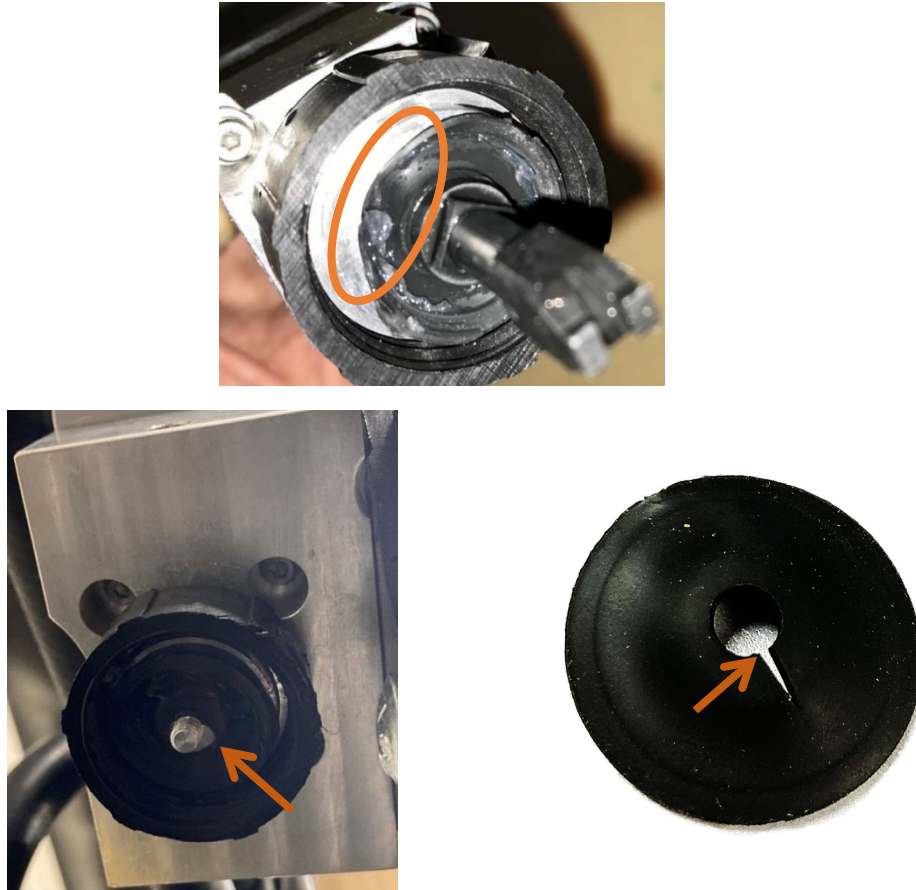


Figure 11 - Failures of the sealing diaphragm at outer sealing joint (top) and inner sealing joint (bottom).

3.3 SOFTWARE FOR ACTUATOR CONTROL

LabVIEW software (National Instruments, Austin, TX) along with LabVIEW Real-Time Module and LabVIEW FPGA Module were required to operate the NI cRIO-9068 embedded controller. Although it was possible for the embedded controller to run as a headless system, i.e., as an embedded system with no external computer or user interface, this project required a user interface on a connected PC to allow the user to perform sensor calibrations and manually command actuator positions. A service and calibration program was created which consisted of three main software layers: FPGA, RT, and user interface (UI) on the host PC.

3.3.1 LabVIEW FPGA SOFTWARE

The lowest level software was for the FPGA layer where the most basic interaction with actuators and sensors occurred. The FPGA front panel is shown in figure 12. It was in this software layer that analog voltage from the pressure sensors was sampled and passed directly to the RT software layer. In a separate FPGA processing loop, the period between flow meter pulses was measured by monitoring changes in the rising edge of each flow meter's digital input. With each new rising edge detected, elapsed time from the previous rising edge was calculated and passed to the RT software layer before the elapsed timer reset.

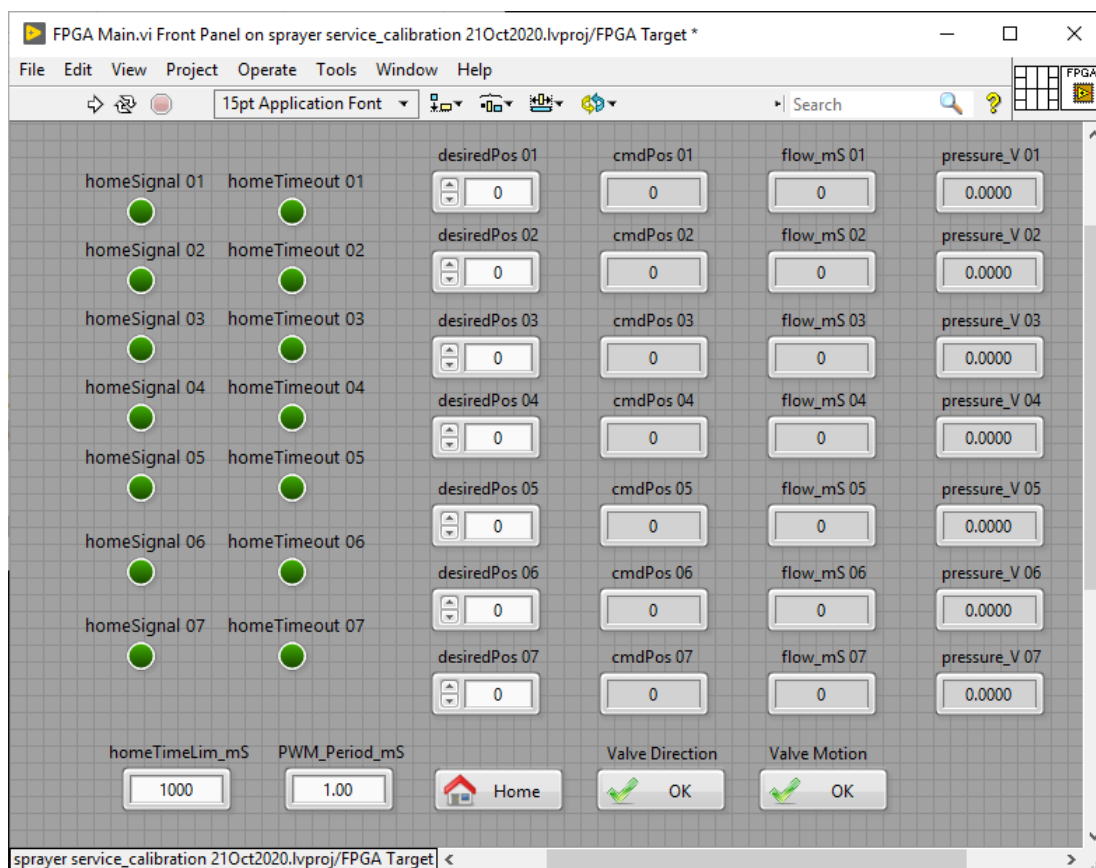


Figure 12 – FPGA software front panel for NI cRIO embedded controller.

A third processing loop in the FPGA software contained the basic logic for controlling the linear actuators. This involved two digital outputs, for direction and step, and one digital input for home position. If home position was detected then no step command was given, actual position was set to zero, and direction was set to extend; the actuator would stop and remain in standby mode in its fully retracted position. If actuator motion was commanded, the program would determine the position error, in units of motor steps, between current position and desired position. Direction was determined by the sign of the error, if desired position minus actual position was positive then direction was set to extend, if negative, retract. Actuator motion was accomplished by sending a digital pulse to the motor driver for each step until position error was zero. This digital signal was set up in similar fashion as a pulse width modulated (PWM) signal but with duty cycle fixed at fifty percent and with a variable frequency. The period of the pulse train could be adjusted with a value sent from the RT software layer. Various values were evaluated down to one millisecond (ms) per step where the actuators were able to reach the desired position quickly, accurately, and consistently.

Although the actuators included a Hall-effect sensor that provided an indication of fully retracted, or home, position, no other feedback was available to indicate actual position when extended away from home position. Due to the deterministic nature of a stepper motor, it was possible to accurately position the actuators with open-loop control, i.e., with no position feedback, by counting motor steps. With every loop executed in the FPGA software, the program checked the status of the home signal and, if not fully retracted, calculated position, set direction, generated a pulse for each step, and counted ascending or descending steps to maintain a record of actual position.

The Hall-effect sensor integrated into the stepper motor linear actuator would be damaged if the stepper motor was not stopped immediately when the actuator reached the fully retracted position. The logic described above accomplished this during normal operation but during development a situation was encountered where the home signal was not received by the controller due to a broken wire. This caused the stepper motor to continue to attempt to retract even though it was already in the home position. Logic was added to the actuator control scheme to cause the program to timeout and stop if the actuator was attempting to retract for a duration longer than the time expected to retract from the fully extended position. If this timeout occurred, the program would stop commanding motion for that actuator, send a timeout signal to the RT layer, and then to the UI at the host PC to alert the operator. This would mitigate potential damage to the Hall-effect sensors and signal the operator that an error had occurred.

3.3.2 LabVIEW REAL-TIME SOFTWARE

The RT operating system running on the embedded controller was where most of the data acquisition and control logic resided. The RT front panel is shown in figure 13. This layer contained the logic to send actuator commands to the FPGA, retrieve sensor values from the FPGA, filter sensor signals, scale sensor values to engineering units, record sensor values and actuator status to a log file, read and write sensor calibration files, and send information to and from the UI on the host PC.

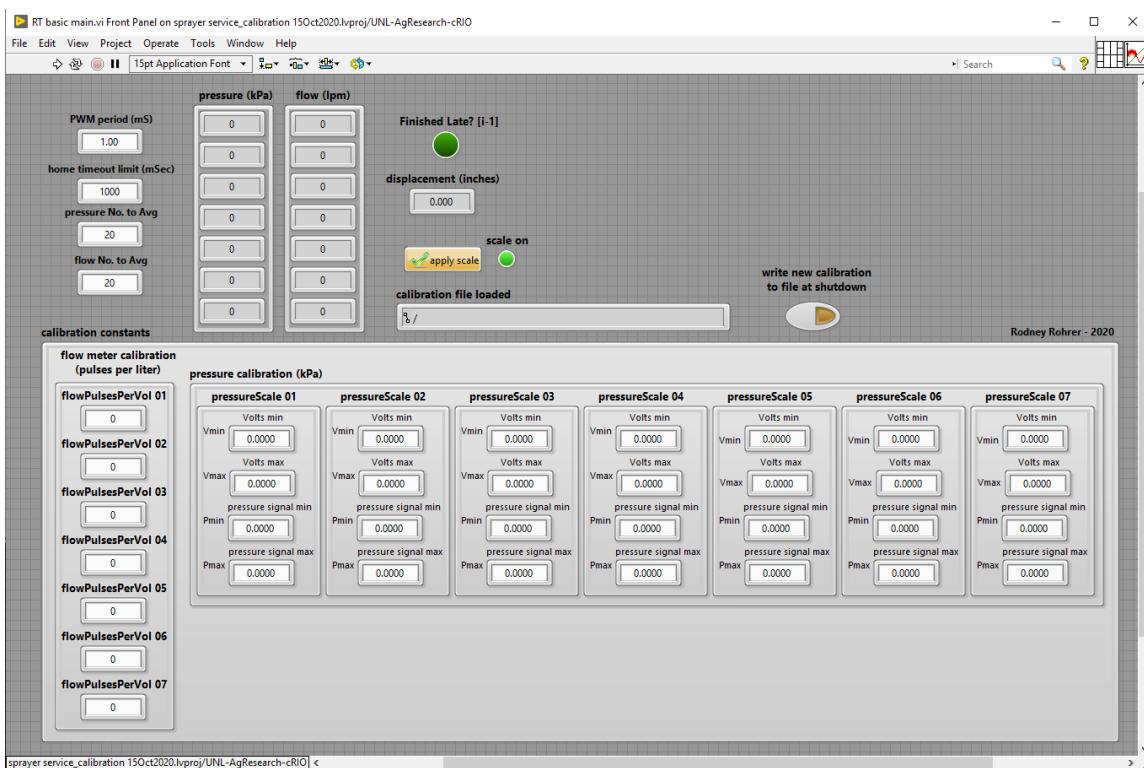


Figure 13 - Real-Time software layer front panel.

A producer-consumer architecture was used in the RT software to allow multiple processing loops to share data while running at different rates. In this way, high priority and time critical tasks could run in the high-speed producer loop which produces data and sends it to the slower consumer loop via a queue. The consumer loop processed data that it consumed from the queue and handled lower priority tasks that were not time critical.

The producer loop was a timed loop that sent and receive information from the FPGA at a frequency of 20 Hz. Signals sent to the FPGA include desired actuator position (steps), period of motor step pulses (ms), home sensor timeout limit (ms), and home button command. These values were used in the FPGA software processes described above. Pressure sensor voltage and flow meter period (ms/pulse) received from the FPGA were smoothed with a moving average filter before being scaled to engineering units. The number of samples to filter was programmed as a configurable input from the RT front

panel. A variety of values were evaluated and a twenty-point moving average was found to offer adequate smoothing of the pressure and flow signals without creating excessive delay in their response, effectively resulting in a one-second moving average filter.

Sensor calibration constants were read from an extensible markup language (xml) file and were used to scale raw sensor values to engineering units. The RT software included provisions to toggle the scale on/off as needed depending on the current activity. In calibration mode, the scales would be turned off so raw sensor values were recorded in the log file. These data could be post processed along with the corresponding known applied pressure or flow to create the calibration scale values. The calibration constants were input into the RT front panel and could be written to a new, unique xml calibration file. Each time the program started it automatically loaded the newest calibration file. In this way the program was set up to maintain the best practice of avoiding hard-coding calibration values in the software.

The consumer loop in the RT software received information from the producer loop via a queue and recorded it to a log file in National Instruments Technical Data Management Streaming (tdms) format. The log file included four channels for each nozzle (measured pressure, measured flow, desired position, and commanded position) along with operator name, test description, units for data channels, sample rate, and other metadata.

The final function of the RT software was to communicate with the UI software layer on the host PC. Information sent from the RT layer to the UI included filtered and scaled pressure and flow signals, commanded actuator position, home position status, and home timeout status for each nozzle. Information received from the UI included desired

actuator position(s), command from the home button, and metadata to be included in the log file (e.g., log file name, operator name, description, etc.).

3.3.3 LabVIEW USER INTERFACE ON HOST PC

The highest-level software layer was the UI running on the host PC. The UI front panel is shown in figure 14. The UI allowed the operator to input desired actuator position(s) individually or as a single command to move all actuators simultaneously. The operator could also actuate a home button that would return all actuators from their current position to their fully retracted home position. These operator commands were sent to the RT layer along with the log file metadata described above.

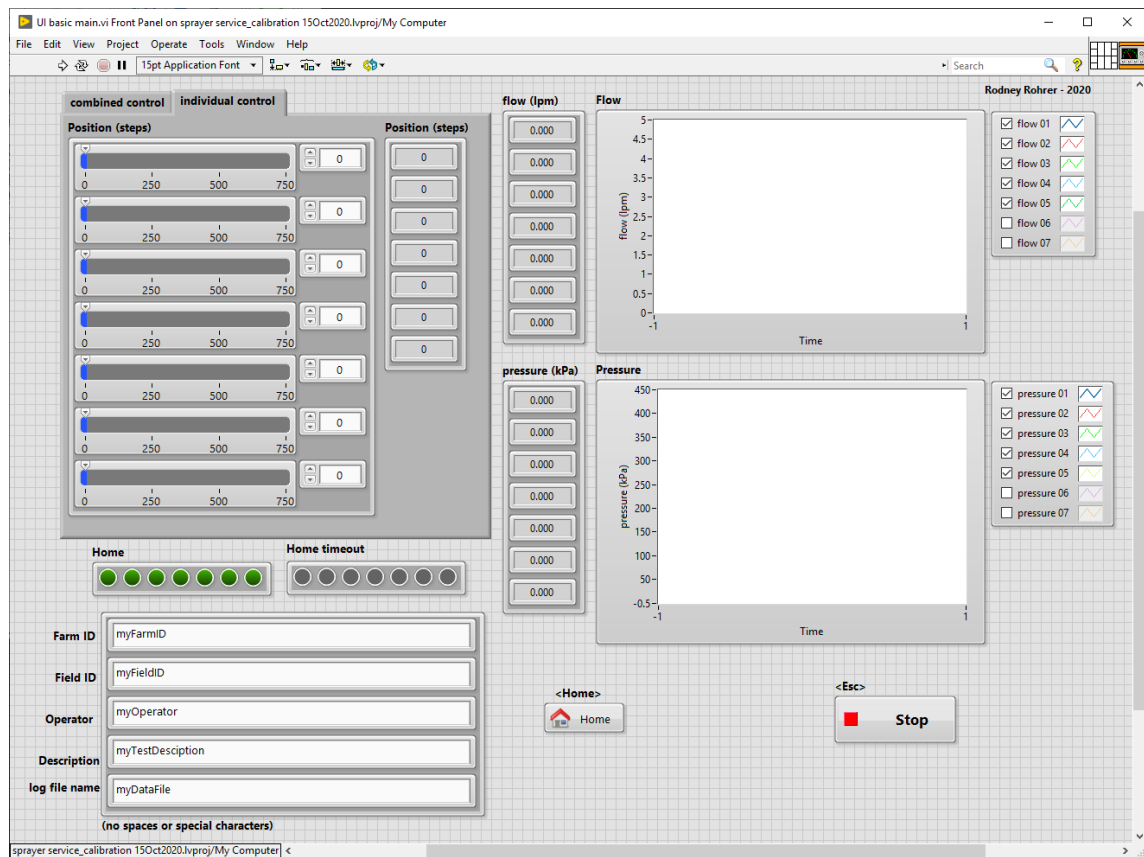


Figure 14 - Front panel for graphic user interface that runs on the host PC.

The UI received information from the RT layer which allowed the operator to monitor filtered and scaled pressure and flow signals. Actuator position, home status, and home timeout signals were also displayed for each nozzle. Service and calibration software logic described in sections 3.3.1 through 3.3.3 and is summarized in figure 15.

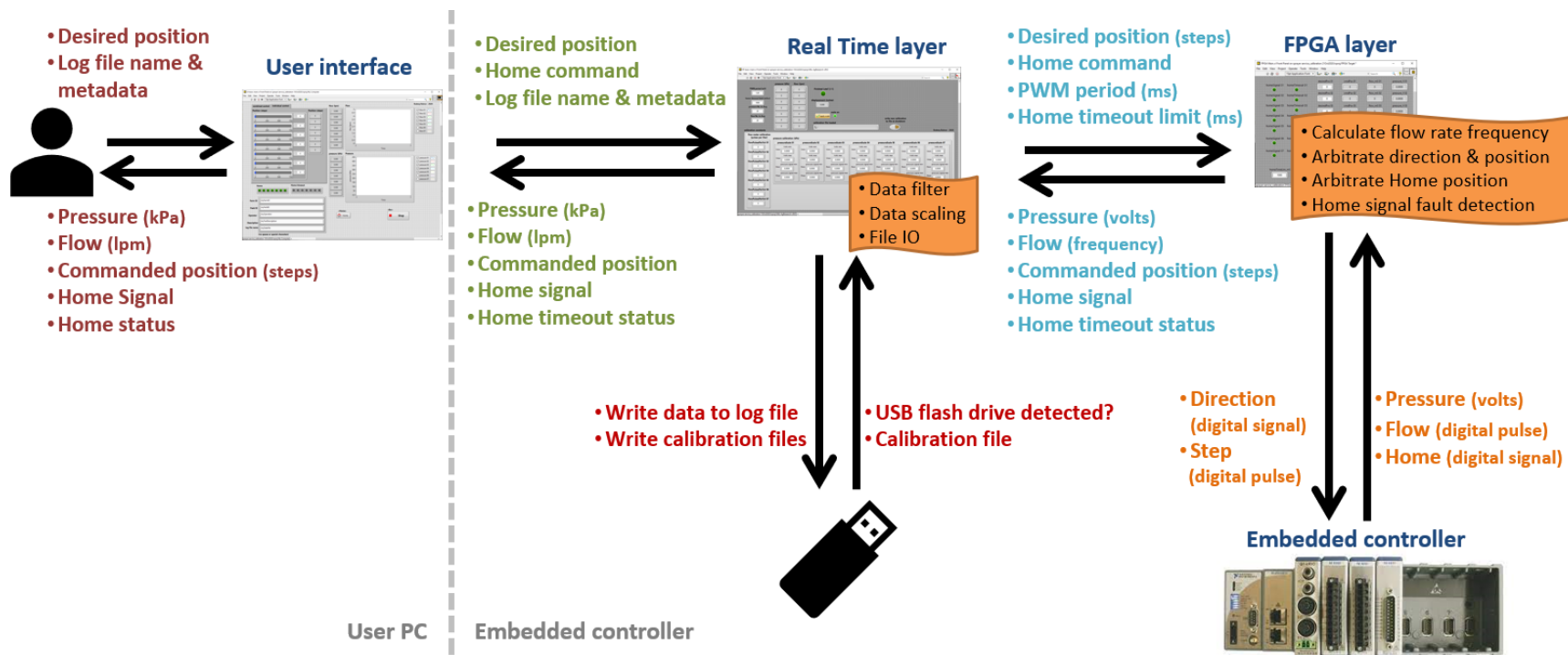


Figure 15 - Service and calibration program interactions and logic.

3.4 SPRAY SYSTEM FUNCTIONAL VALIDATION

With system hardware assembled, and software developed for basic actuator control and data logging, it was important to complete basic system validation before moving forward with development of automated variable-orifice nozzle control. This included checking functionality and positioning accuracy of the linear actuators, calibrating and checking accuracy of pressure and flow sensors, and checking spray volume distribution.

3.4.1 ACTUATOR DISPLACEMENT

The open-loop control strategy for actuator positioning required verification of accurate and repeatable displacement of the nozzle metering tip. To measure actuator displacement, a dial indicator (Starrett No. 650, L.S. Starrett Co., Athol, MA) was attached to the nozzle assembly with the plunger opposed to the end of the metering stem extension (fig. 16). The dial indicator had a resolution of 25.4 micrometers (μm); which, with actuator resolution of 6.1 μm per step, is equivalent to 4.2 motor steps.



Figure 16 - Dial indicator set up to measure nozzle metering stem displacement.

Each actuator was returned to its home position, and the dial indicator zeroed, before commanding the actuator to move a given number of steps. Displacement was read from the dial indicator as the actuator position was increased and then decreased.

Measurements were compared to the expected displacement to determine positioning error (table 5) and hysteresis. Maximum error observed was 2.1% and largest hysteresis was 25.4 μm , or less, as this is the resolution of the dial indicator.

Although displacements were consistent and repeatable, it was through this evaluation where it was discovered that the metering stem in some of the nozzle assemblies could bottom-out inside the nozzle bodies just before reaching 800 steps. Because of this, the operating range was reduced to 750 steps for the remainder of the project.

Table 5 - Summary of actuator position evaluation.

	actuator position steps	nominal displacement mm (in)	nozzle no.					nozzle no.				
			1	2	3	4	5	1	2	3	4	5
			measured displacement mm (in)					displacement error %				
increasing displacement	400	2.438 (0.096)	2.413 (0.095)	2.413 (0.095)	2.413 (0.095)	2.388 (0.094)	2.413 (0.095)	1.0	1.0	1.0	2.1	1.0
	600	3.658 (0.144)	3.581 (0.141)	3.607 (0.142)	3.607 (0.142)	3.607 (0.142)	3.607 (0.142)	2.1	1.4	1.4	1.4	1.4
	750	4.572 (0.180)	4.496 (0.177)	4.496 (0.177)	4.521 (0.178)	4.521 (0.178)	4.547 (0.179)	1.7	1.7	1.1	1.1	0.6
decreasing displacement	600	3.658 (0.144)	3.607 (0.142)	3.607 (0.142)	3.607 (0.142)	3.607 (0.142)	3.607 (0.142)	1.4	1.4	1.4	1.4	1.4
	400	2.438 (0.096)	2.438 (0.096)	2.413 (0.095)	2.413 (0.095)	2.413 (0.095)	2.413 (0.095)	0.0	1.0	1.0	1.0	1.0

3.4.2 ACTUATOR RESPONSE TIME

Development of the spray system hardware and actuator control logic was done to support the higher-level project objective to implement a control system to automatically

target a desired droplet spectra and desired flow rate, as such, the objective did not include characterization or optimization of system dynamic response. However, the example below is included to provide an indication of system response.

Actuator response time is important to ensure the nozzle system achieves desired flow rate and droplet size in a timely manner. For example, if the operator adjusts the target ground speed during in-field application, or if the system is set up to react to a real-time ground speed signal, application rate may be incorrect while the system is adjusting to new parameters. A quick response time is necessary to ensure proper application rate and desired droplet size during transient operation.

An example of actuator response time can be seen in figure 17 where the system was operating at steady state with the actuator fully extended when the desired position on the UI was set to zero to fully retract to the home position. Although there is no feedback signal for actuator position, it was verified earlier that tracking position by counting motor steps is reliable. Accordingly, the time to retract the actuator was determined from the commanded position which is a signal from the FPGA generated at the last point in the software control sequence where a digital pulse is sent to the motor driver for each commanded step. In this way the commanded position signal excludes as much software delay as possible. Based on this commanded position signal, time to fully retract from 750 steps to home position was 0.9 seconds. During this event, the flow and pressure responded immediately reaching a new steady state at approximately the same time the actuator reached its final position. It is important to note that the one-second moving average on the pressure and flow signals skews the response time which was faster than the filtered data implies.

Continuing with the sequence shown in figure 17, the actuator was then commanded to move from home position to fully extended position of 750 steps which took 1.0 seconds. The 0.1 second difference in response time between extend vs. retract is believed to be due to the 50 ms resolution in the software loop timing in the RT layer where the command from the user for desired position may have occurred early or late in the loop cycle and, likewise, the commanded position signal returned from the FPGA layer could have been received early or late in the loop cycle. Another contributing factor is that when the actuator is extending it must work against additional force, created by the fluid pressure working on the area of the diaphragm, making extending relatively more difficult than retracting.

Although there was an immediate flow response when the actuator retracted, it is clear in figure 17 that the flow response was delayed when the actuator was extended. This is a characteristic of the nozzle assembly where the metering stem does not engage in the nozzle tip until approximately 400 steps and therefore the working range is 400 to 750 steps. During normal operation, the response time would not include deadband from 0 to 400 steps. Relating to the example in figure 17, the system response would be expected to be proportional to the 0.9 second response for full travel from 0 to 750 steps. The proportional response time for just the working range of 400 to 750 steps would be approximately 0.42 seconds.

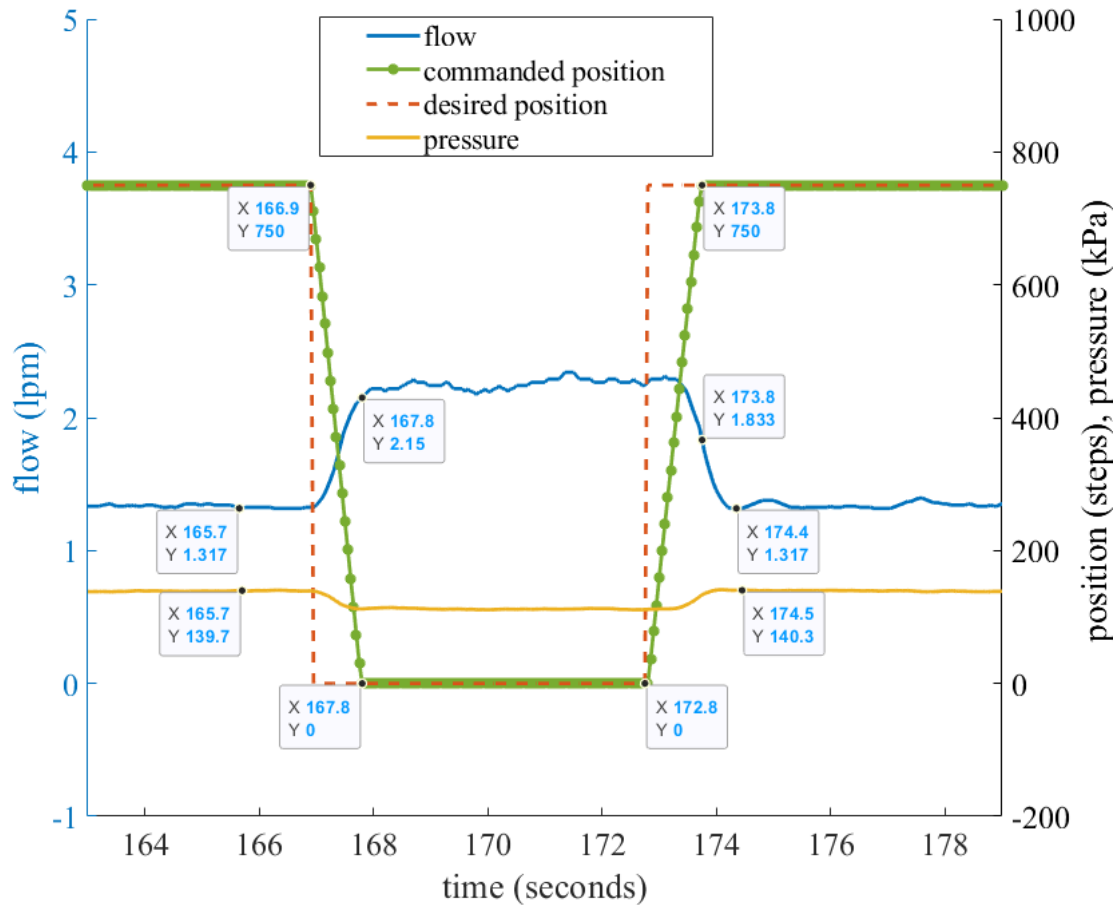


Figure 17 - Actuator response during full retract and full extend.

Further evaluation of system response could be done in a manner like that done by Luck, Shearer, et al. (2015) who did a thorough analysis of dynamic response of the nozzle prototyped by Luck (2012). Although the software and control implementation was not the same, their work does provide some indication of the response capability of the actuator with closed loop flow control.

3.4.3 PRESSURE SENSOR CALIBRATION

Each nozzle assembly included a pressure sensor (PX309-100G5V, Omega Engineering Inc., Norwalk, CT) with an operating range of 0 to 689 kPa which was proportional to the 0 to 5 volt output. Each sensor was calibrated by applying known pressures with a

portable dead weight tester (1305-D, Ashcroft, Newtown, CT) (fig. 18) as described in section 4.2.3 of ASTM Standard E641-01 for testing hydraulic spray nozzles used in agriculture (ASTM, 2006). The calibration was defined by the sensor's linear response between min and max system operating pressures: 138 kPa and 414 kPa. The sensor outputs at these pressures were applied in the software program to convert sensor voltage to engineering units of kPa. After the calibration scales were applied, each pressure sensor was evaluated again by applying known pressures at 138, 276, and 414 kPa. Pressure sensor accuracy ranged from -0.30% – 0.29% of the respective reading which is within the $\pm 2\%$ accuracy at actual working pressure as recommended in ASTM Standard E641-01. A summary of this evaluation is shown in table 6.

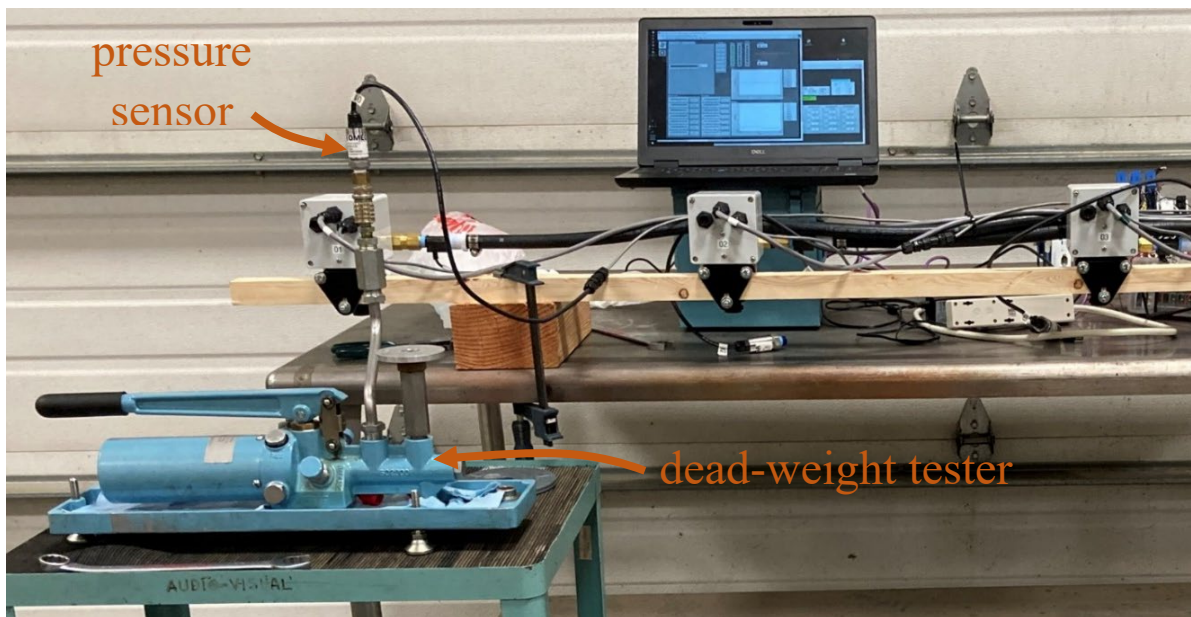


Figure 18 –Dead-weight tester applying known pressure for sensor calibration.

Table 6 - Summary of pressure sensor error after calibration.

applied pressure kPa	sensor no.					sensor no.				
	1	2	3	4	5	1	2	3	4	5
	measured pressure kPa					error %				
137.9	137.5	138.0	137.8	138.3	138.1	-0.30	0.08	-0.10	0.29	0.12
275.8	275.7	276.0	275.5	276.1	276.1	-0.04	0.09	-0.09	0.12	0.12
413.7	413.4	413.9	413.3	414.2	413.8	-0.06	0.04	-0.10	0.13	0.03
	mean					-0.13	0.07	-0.10	0.18	0.09

3.4.4 NOZZLE DISCHARGE RATE AND FLOW SENSOR CALIBRATION

Each nozzle assembly included a turbine flow meter (FTB-430, Omega Engineering Inc., Norwalk, CT).

Although these flow meters are not required for system operation, they were included to provide a reference for characterizing nozzle performance and determining flow error when the nozzles were operating with the control algorithm. These flow meters have a nominal operating range of 0.76 to 7.57 lpm with an output frequency of 34 to 343 Hz. Although a nominal calibration was provided with sensor data sheets, each flow meter was calibrated in-situ to get a more accurate measurement. The manual calibration included capturing a volume of fluid in a graduated cylinder (fig. 19) during a measured period as described in ASTM Standard E641-01 (ASTM, 2006).

Time was measured with the stopwatch function on an

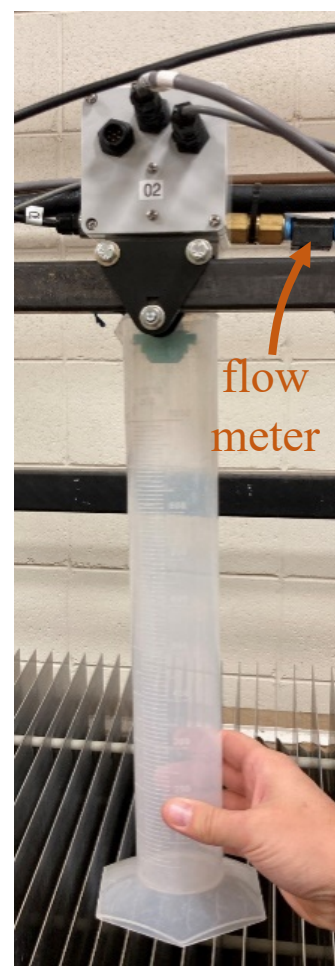


Figure 19 - Graduated cylinder capturing spray to evaluate nozzle flow rate.

iPhone SE with software version 14.0. Three to four iterations were completed for each nozzle at four flow rates spanning the system's operating range: minimum pressure and orifice setting for the blue and green nozzle tips and medium and maximum pressure and orifice settings for the green nozzle tip.

During calibration, the period between flow meter pulses (ms/pulse) was logged with the DAQ controller. Average period during each steady-state operating point was calculated with Matlab. Actual flow rate was calculated from the volume captured in the graduated cylinder (ml) and the measured time (sec) to determine flow rate in lpm for each steady-state operating point. The steady-state flow rate (lpm) and period (ms/pulse) were used to calculate a calibration constant for each flow meter in pulses per liter.

With calibration constants applied to the flow signals in the controller software, a check was done to validate the calibration. Again, three to four iterations of flow measurement were done at four different flow rates spanning the system operating range (fig. 20).

Error, as percent of reading, for all nozzles and all operating points ranged from -1.62% – 1.55% (table 7).

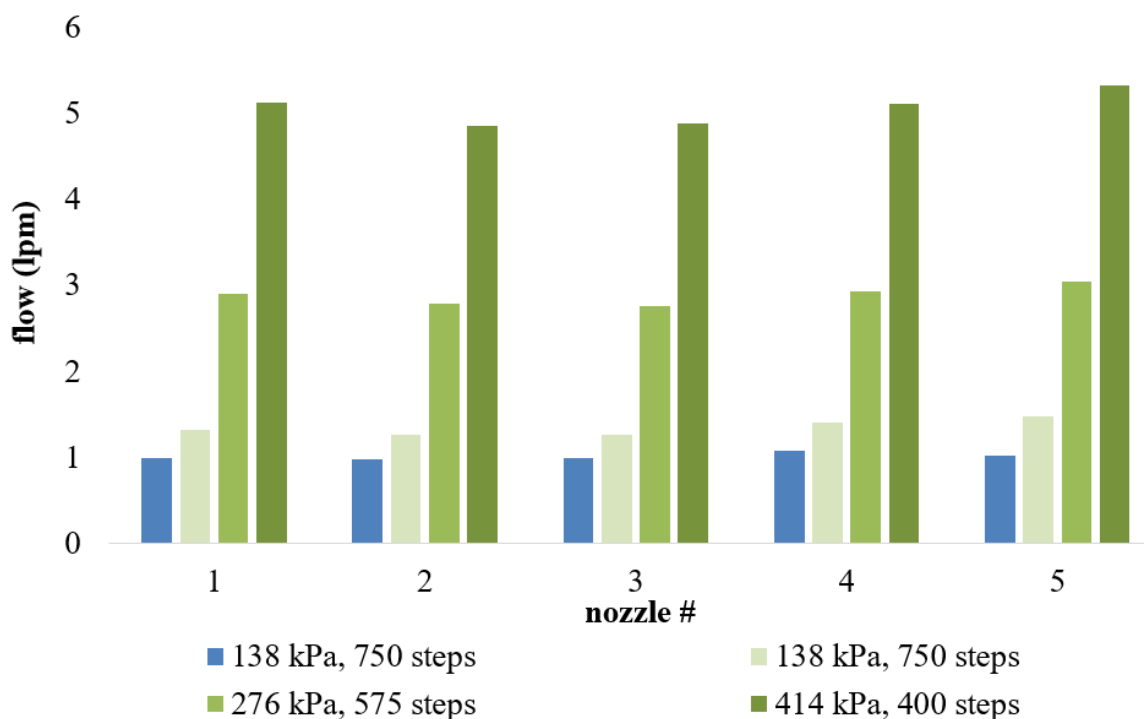


Figure 20 - Flow meter response for each nozzle at various flow rates (blue bar for blue nozzle tip, green bars for green nozzle tip).

Table 7 - Summary of flow meter measurement error as percent of reading.

nozzle type	operating point	nozzle no.					nozzle no.					nozzle no.					
		1	2	3	4	5	1	2	3	4	5	1	2	3	4	5	
		manual measurement					sensor measurement					error					
kPa	steps	lpm					lpm					%					
blue	138	750	0.99	0.97	0.98	1.07	1.01	1.00	0.98	0.98	1.08	1.02	1.36	1.10	-0.17	1.35	0.84
	138	750	1.32	1.26	1.26	1.40	1.47	1.33	1.27	1.28	1.41	1.49	1.18	1.07	1.55	0.79	1.04
green	276	575	2.91	2.78	2.76	2.92	3.04	2.91	2.78	2.79	2.92	3.02	0.02	-0.05	1.13	-0.29	-0.41
	414	400	5.12	4.85	4.88	5.11	5.32	5.10	4.80	4.89	5.07	5.24	-0.47	-1.12	0.32	-0.72	-1.62

The range of flow rate and turn down ratio (i.e., ratio of maximum to minimum flow) observed for each of the five modified VariTarget nozzle are shown in table 8.

Table 8 – Range of flow observed for each nozzle.

nozzle	minimum flow			maximum flow			turndown ratio
	flow (lpm)	pressure (kPa)	position (steps)	flow (lpm)	pressure (kPa)	position (steps)	
red	--*	207	800	0.82	552	400	--
orange	0.82*	138	800	2.38	552	400	>2.9 [†]
yellow	0.80*	138	800	3.48	552	400	>2.8 [†]
blue	0.83	138	800	4.83	552	400	5.8
green	1.16	138	800	5.27	414	400	4.6

* some flow rates were below the sensor operating range and so minimum measurable flow is reported

† tumdown ratio was calculated from minimum measurable flow rate and so actual tumdown ratio would be greater than what is reported here

3.4.5 SPRAY VOLUME DISTRIBUTION

Uniform spray pattern is important for even pesticide application and effective coverage.

Five nozzles were installed on a patternator at W. F. Splinter Labs at UNL (fig. 21) to evaluate spray volume distribution in accordance with procedures outlined in ASTM Standard E641-01 (ASTM, 2006). The nozzles were spaced 508 millimeters (mm) apart at a height of 508 mm above the top of the patternator baffles. The patternator was configured with baffles spaced 25 mm apart which captured flow from the spray plume and directed it to tubes with 166 ml volume where it accumulated. A 762-mm-wide section of spray plume, centered under the middle of the five nozzles, was evaluated by capturing fluid in 30 tubes under each respective baffle.



Figure 21 - Nozzles installed on patternator at W. F. Splinter Labs.

A signal generated by an optical liquid level sensor near the top of each tube indicated when the tube was full, allowing software to determine the amount of time for each tube to fill. Three repetitions were completed at each of three pressures and three actuator positions for both the blue and green nozzles. The time to fill each tube was proportional to the spray volume applied between each respective set of baffles. An example of patternator output is shown in figure 22 where the graph shows duration, in seconds, for each tube to fill. Tube 15 was centered directly under the middle of the five nozzles.

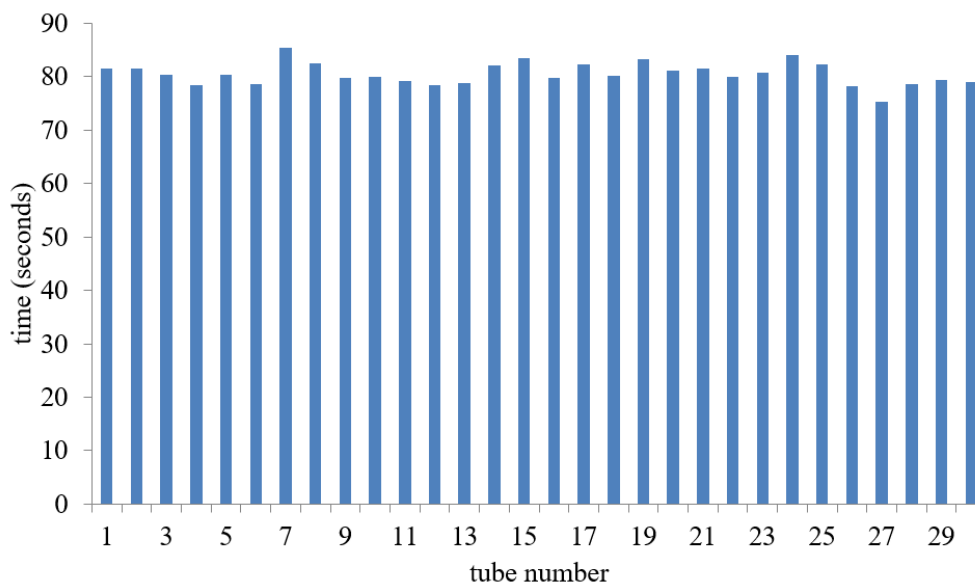


Figure 22 - Example of patternator output for blue nozzle operating at 276 kPa and 400 steps.

The mean (μ) and standard deviation (σ) of the fill times were used to calculate a coefficient of variation, or CV (equation 3.1), for each operating point.

$$CV = \frac{\sigma}{\mu} \quad \text{Equation 3.1}$$

A summary of the average CV for the three repetitions at each operating point is shown in table 9. CV for the blue tip ranged from 2.7 to 6.1% across its operating range where it was generally larger at lower pressures and smaller orifice sizes (i.e., higher motor steps). CV for the green tip ranged from 3.6% – 8.1% where it was generally larger for higher pressures and larger orifice sizes (i.e., lower motor steps). CV values below 10% are desirable but up to 15% is acceptable (Luck, Pitla, et al., 2015).

Table 9 - Spray pattern coefficient of variation across nozzle operating range.

Coefficient of variation (%)						
pressure (kPa)	blue nozzle tip			green nozzle tip		
	position (steps)					
	400	600	800	400	600	800
138	2.7	3.3	5.6	3.8	4.0	5.1
276	3.0	5.1	6.1	6.4	3.6	4.0
414	4.1	5.0	4.1	8.1	3.6	3.9

3.5 CONCLUSION

A five-nozzle spray system was created based on the variable-orifice nozzle prototyped by Luck (2012). Additional features were added to the prototype design to provide protection for the stepper motor linear actuator and motor driver circuit board. Pressure and flow sensors and mounting features were added to complete the assembly and to allow this to be scaled up to a demonstration spray system for a utility vehicle in future work. Special attention was paid to length tolerances of machined parts to minimize variability in performance between nozzle assemblies.

Software for an embedded controller was developed in LabVIEW for basic actuator control and data logging. This consisted of three layers of software: FGPA, RT, and UI for host PC. Other software features included provisions for sensor calibration and error detection when actuators failed to return to home position.

System validation included checking actuator functionality and positioning accuracy; the open loop control scheme was able to position the metering stem within 2.1% of desired position. Pressure sensors were calibrated and checked with a dead weight tester; error ranged from -0.30% – 0.29% of the respective reading which is within the $\pm 2\%$ accuracy

at actual working pressure that is recommended in ASTM Standard E641-01. Accuracy of flow meter calibration was found to be within -1.62% – 1.55% of reading. Flow rates across the five modified VariTarget nozzles ranged from 0.82 to 5.27 lpm with some flow rates not reported because they were below the flow sensor operating range. The nozzles had turndown ratios of up to 5.8. Coefficient of variation for spray volume distribution was 6.1% or less for all operating points for blue nozzles and 8.1% or less for all operating points for green nozzles; all within the 10% desired maximum.

CHAPTER 4 METHOD FOR ACTIVE NOZZLE CONTROL

4.1 INTRODUCTION

In contrast to fixed-orifice nozzles, a variable-orifice nozzle can decouple pressure and flow in the sense that the same flow rate can be achieved at various system pressures by changing the orifice size. This can enable a wider range of flow rates and droplet spectra for a single nozzle tip. Changes in flow and droplet size are also continuous, with no discrete step changes in performance as would be experienced when changing fixed-orifice nozzle tips. Performance of the variable-orifice nozzle was characterized by four variables: system pressure, actuator position (i.e., effective orifice size), droplet size, and flow rate. These variables can be controlled to achieve a desired application rate (l/ha) and a desired droplet size for a given pesticide.

4.2 VARIABLE-ORIFICE NOZZLE CONTROL ALGORITHM

Chapter two described a method for measuring nozzle performance and collecting data to characterize the operating envelope of a variable-orifice nozzle. From those data, a mathematical model was derived by performing a curve fit, or regression, to get a best fit polynomial equation. The regression equation describing the relationship of the nozzle parameters was then used to devise a method to actively control a variable-orifice nozzle. In this case, two regressions were completed to create two equations which modeled the variable-orifice nozzle performance. The first was a linear regression of pressure and actuator position on flow, the second was of pressure and actuator position on volume mean diameter (i.e., droplet size).

The result was a set of two equations with four unknowns, equations 4.1 and 4.2.

$$Q = a + b * P + c * M \quad \text{Equation 4.1}$$

$$VMD = d + e * P + f * M \quad \text{Equation 4.2}$$

Q = flow rate (lpm)

VMD = droplet volume mean diameter (μm)

P = pressure (kPa)

M = metering stem position (steps)

a, b, c, d, e, f = polynomial coefficients

One of the four unknowns, droplet size (VMD), could be specified directly by the operator or input from an additional control algorithm based on wind speed or other relevant parameters. A second unknown, nozzle flow rate (Q), was determined from information provided by the operator: application rate (l/ha), nozzle spacing, and desired steady-state ground speed. Ground speed could also be an input from GPS, radar, or other ground speed sensor. With application rate, nozzle spacing, and ground speed known, required nozzle flow rate can be determined from equation 4.3.

$$Q = \text{rate} * \frac{\text{speed}}{600} * \text{nozzle spacing} \quad \text{Equation 4.3}$$

rate = application rate (l/ha)

speed = ground speed (kph)

nozzle spacing (m)

With droplet size specified and nozzle flow rate determined from operator inputs, two of the four variables were known and the remaining two, pressure (P) and actuator position (M) (i.e., effective orifice size), were found by solving equations 4.1 and 4.2 simultaneously to yield equations 4.4 and 4.5.

$$P = \frac{(Q-a)*f+(d-VMD)*c}{b*f-c*e} \quad \text{Equation 4.4}$$

$$M = \frac{(VMD-d)*b+(a-Q)*e}{b*f-c*e} \quad \text{Equation 4.5}$$

With these two equations, the control system could solve for the pressure and actuator position required to achieve the rate and droplet size desired by the operator.

4.3 SYSTEM MODELING

Nozzle assemblies were installed on a test bench where each of five blue and five green nozzles were operated at 25 steady-state operating points. These observations spanned the nozzle operating envelope with five pressures, every 69 kPa from 138 to 414 kPa, at each of five actuator positions, every 100 motor steps from 400 to 700 steps and at 750 steps. Pressure, flow, and commanded actuator position were recorded for each nozzle (fig.23). From this data, mean values were calculated for each steady-state operating point (fig. 24).

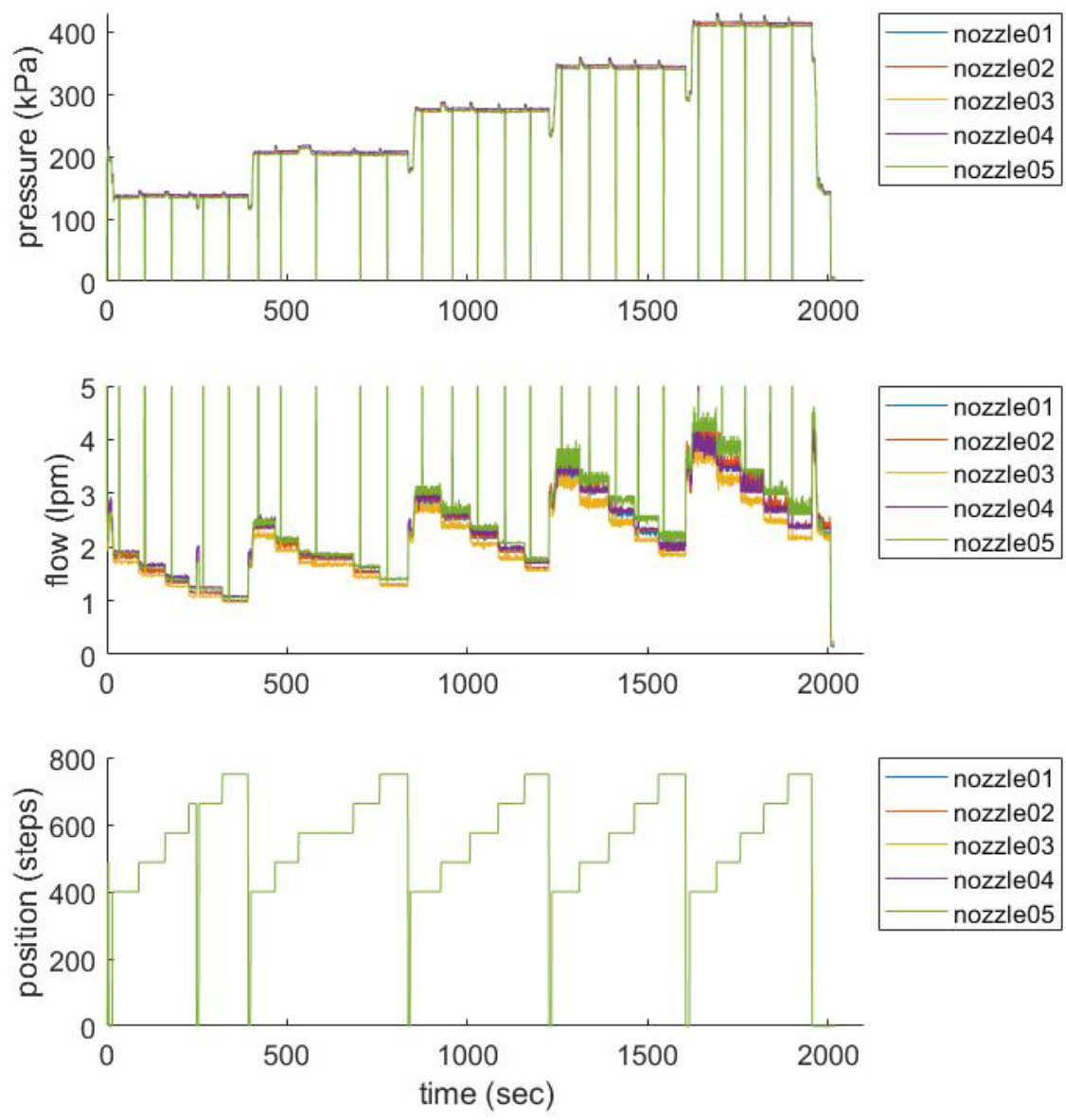


Figure 23 – Example of time history data at 25 operating points for five blue nozzles.
Note: vertical lines in pressure and flow plots mark the start of each observation.

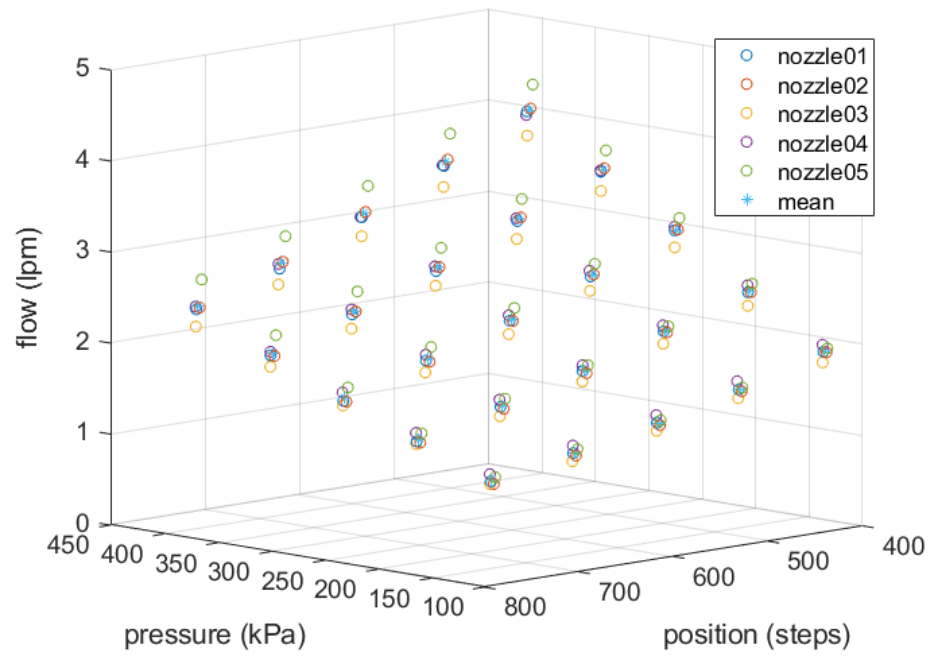


Figure 24 - Scatter plot of mean steady-state values from time history data.

An observation from the time-series data was that more flow variation existed at operating points with high pressure and low metering stem positions (fig. 23). This flow instability was thought to be the result of the spray tip being less supported when the metering stem was less engaged in the spray tip (fig. 25) and was accentuated with high flow rates induced by high pressure.

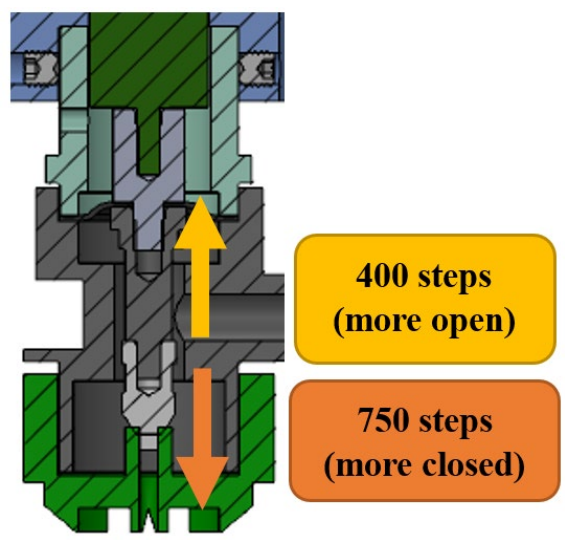


Figure 25 - Relationship between metering stem position and orifice size.

A linear regression was done on the 25 mean pressure, actuator position, and flow values for each nozzle with Matlab R2020a

(The Mathworks Inc., Natick, MA) (fig. 26). Polynomial coefficients, coefficient of determination, and root mean square error for the regression are summarized in table 10.

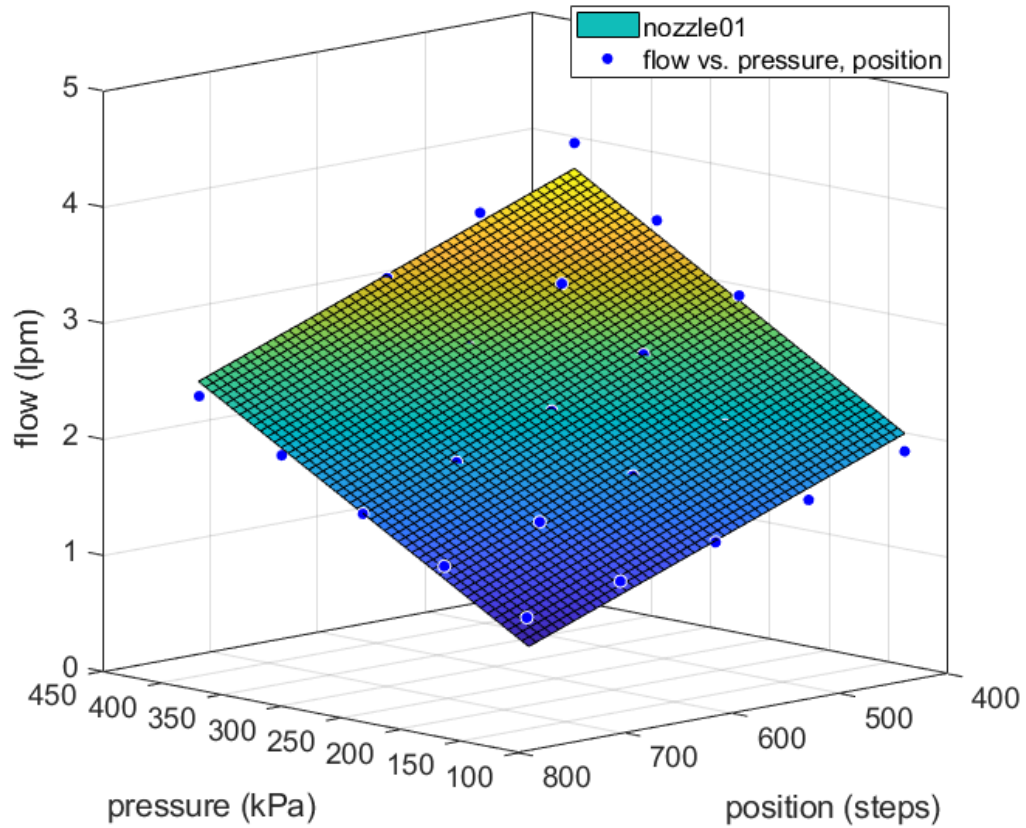


Figure 26 – Plot of linear regression of pressure and actuator position on flow for blue nozzle01.

Table 10 - Polynomial coefficients, coefficient of determination, and root mean square error for regression of pressure and actuator position on flow.

		polynomial coefficients			R^2	RMSE
		a	b	c		
blue	nozzle01	2.5647	0.0062	-0.0035	0.983	0.105
	nozzle02	2.5526	0.0065	-0.0036	0.984	0.105
	nozzle03	2.3944	0.0057	-0.0033	0.979	0.108
	nozzle04	2.6312	0.0059	-0.0034	0.984	0.097
	nozzle05	2.4283	0.0074	-0.0035	0.985	0.108
	mean	2.5136	0.0064	-0.0035	0.984	0.104
green	nozzle01	3.5099	0.0078	-0.0046	0.987	0.119
	nozzle02	3.4464	0.0074	-0.0045	0.987	0.112
	nozzle03	3.3714	0.0077	-0.0045	0.987	0.114
	nozzle04	3.4781	0.0079	-0.0045	0.984	0.130
	nozzle05	3.5650	0.0081	-0.0045	0.987	0.120
	mean	3.4741	0.0078	-0.0045	0.987	0.118

Linear regression was also performed on 25 mean pressure, actuator position, and $D_{v0.5}$ values measured at the PAT Lab for one blue and one green nozzle (fig. 27). Polynomial coefficients, coefficient of determination, and root mean square error for the regression are in table 11.

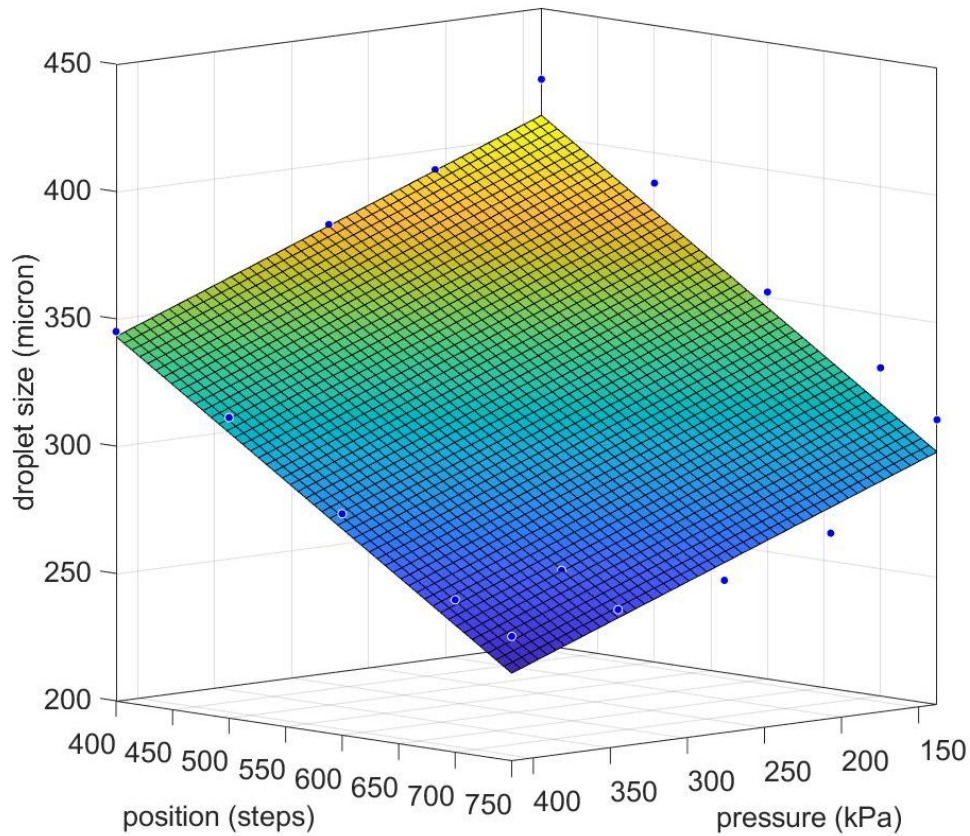


Figure 27 – Plot of linear regression of pressure and actuator position on droplet size for blue nozzle01.

Table 11 - Polynomial coefficients, coefficient of determination, and root mean square error for regression of pressure and actuator position on droplet size.

		polynomial coefficients			R^2	RMSE
		d	e	f		
blue	nozzle01	564	-0.2348	-0.3099	0.96	10.03
green	nozzle01	653	-0.4014	-0.3069	0.95	13.16

4.4 VARIABLE-ORIFICE NOZZLE CONTROL IMPLEMENTATION

While the service and calibration software offered an interface for the operator to monitor sensor signals and manually control actuator position, it provided only the most basic functionality. This software required the operator to return the actuators to home position and did not provide feedback for the pressure setting required to achieve a desired application rate or droplet spectra. A field program was created with LabVIEW software that incorporated the nozzle control algorithm described above to automate actuator positioning and determine system pressure required to achieve the application rate and droplet spectra specified by the operator.

The field program had a similar architecture to that of the service and calibration program but provided additional features in the RT and UI layers. The FPGA layer was identical to that described in section 3.3.1 and performed the same low level actuator control and sampling of sensor signals. The RT layer had the same interaction with the FPGA layer as that of the service and calibration software but included other features to facilitate the automated nozzle control with the algorithm described above.

4.4.1 FIELD PROGRAM REAL-TIME SOFTWARE LAYER

The RT software for the field program was deployed on the embedded controller and configured to run on startup. In this way, when the controller was powered, or reset, the RT software would start automatically and execute an initialization sequence before waiting in a standby mode for operator inputs.

If the controller were to lose power during operation, positions of the actuators would be unknown at the next startup. For the open-loop control to properly position the actuators their position had to be accurately known. Additionally, if the actuators were commanded

to extend from an already extended, but unknown, position, it may have been possible to for them to overextend and potentially damage the nozzle tips. To reset the actuators to a known position all actuators were returned to home position at startup. This was accomplished by an initialization sequence where, if any home signals were false, all actuators were commanded to retracted. Next, all actuators were commanded to extend to 400 steps so that they were past the hysteresis band of the hall-effect sensors. Finally, the actuators were once again fully retracted to their home positions before the program would standby to wait for information from the UI software layer.

During initialization, the RT program read sensor calibration information from an xml file. The calibration values displayed on the RT front panel (fig. 28a) and were used to scale raw sensor values to engineering units. This data was sent to the UI to be displayed for the operator and was also saved to a log file.

Polynomial coefficients and other nozzle-specific parameters were needed by the control algorithm to calculate the pressure and actuator position required to achieve the desired application rate and droplet size. At startup, the type of nozzle tip that was installed would be communicated to the RT layer once it was selected by the operator from the UI on the connected PC. When the waiting RT layer received that information, it loaded the appropriate comma separated variable (csv) parameter file for the installed nozzle (table 12). This nozzle specific information was also displayed on the RT front panel (fig. 28b). In addition to polynomial coefficients, the parameter file contained droplet classification boundaries, droplet spectra categories achievable by the installed nozzle, the nozzle operating envelope (i.e., minimum and maximum system pressure and linear actuator operating range), and a unique parameter file ID.

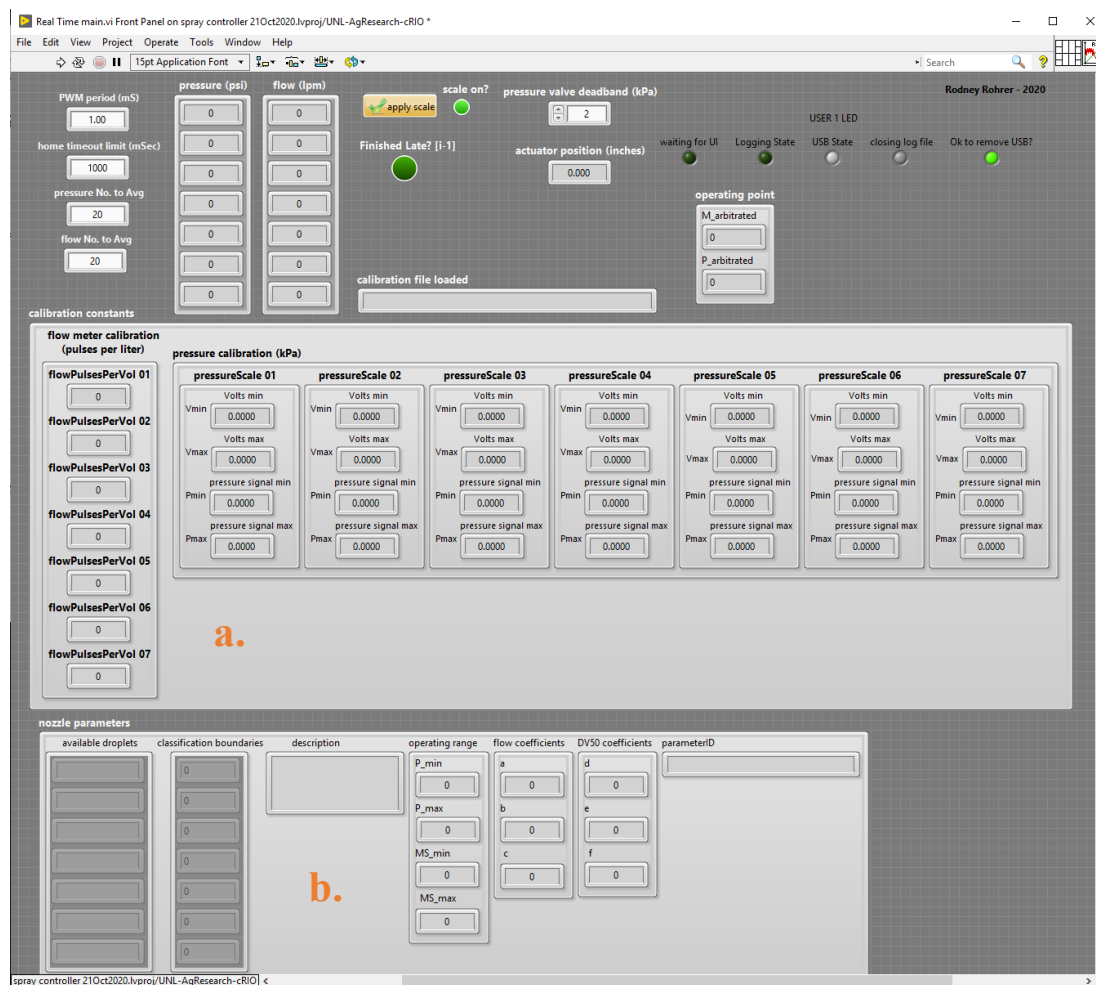


Figure 28 - Real Time layer front panel displaying (a) constants read from calibration file and (b) nozzle characteristics loaded from parameter file.

Table 12 - Example of parameter file for green nozzle tip.

flow polynomial coefficients	droplet DV50 polynomial coefficients	droplet classification boundaries (Dv50 micron)	operating range droplet categories	operating range	parameter file ID	description
3.5099	653.3	0	Medium (M)	138	G120720202301v3	nozzle01 flow polynomial coefficients from SPL
0.0078	-0.4014	142	Coarse (C)	414		
-0.0046	-0.3069	260	Very Coarse (VC)	400		
		376		750		
		438				
		522				
		662				
						Dec2020 WCREC DV50 polynomial coefficients & droplet classification boundaries

When the parameter file was read from the USB drive connected to the embedded controller, nozzle parameter information was stored in an array variable available to the UI and the algorithm embedded in the RT layer. The algorithm also required application rate, ground speed, nozzle spacing, and desired droplet size from operator inputs on the UI front panel. In addition to desired pressure and actuator position, the RT layer calculated the achievable minimum and maximum flow rate, ground speed, and droplet size which were sent to the UI for the operator's reference (fig. 30e).

A log file was created by the RT layer that was like that of the service and calibration software but with additional data channels and metadata. The field program log file included the following channels for each nozzle:

- Required flow (lpm)
- Measured flow (lpm)
- Desired pressure (kPa)
- Measured pressure (kPa)
- Desired position (steps)
- Commanded position (steps)
- Speed (kph)
- VMD desired (percent)
- VMD arbitrated (percent)

Metadata written to the log file included:

- Installed nozzle type
- Selected droplet spectra
- Specified application rate (l/ha)
- Nozzle spacing (m)
- Sensor calibration file ID
- Nozzle parameter file ID
- Droplet spectra boundaries (μm)
- polynomial coefficients for installed nozzle
- Optional: operator name, description, farm ID, field ID

The RT layer continued to run until it received a signal from the UI layer when the operator clicked the stop button. The shutdown sequence of the RT layer retracted the linear actuators to their home positions before stopping the data acquisition and control loop. The data logging loop continued to run until the data queue was empty and then the log file was closed. The operator could retrieve the log file from the USB drive attached to the embedded controller.

4.4.2 FIELD PROGRAM UI SOFTWARE LAYER

Before starting the UI, the operator could enter a farm ID, field ID, operator name, description, and log file name on the front panel setup tab (fig. 29). The setup tab included home timeout indicators and graphs to monitor flow and pressure signals.

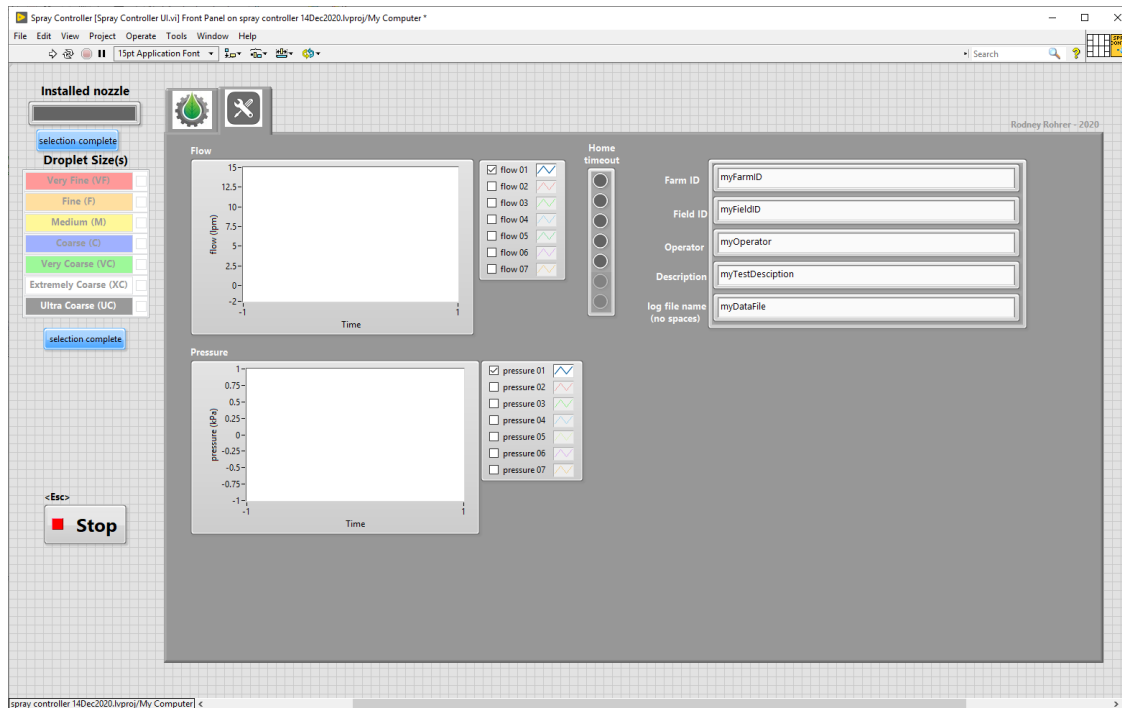


Figure 29 - User interface front panel setup tab.

Upon startup, the UI software on the host PC would enter a standby mode where it awaited interaction from the operator to select the installed nozzle type (fig. 30a) before loading the available droplet spectra for that nozzle (fig. 30b). One or more of the available droplet spectra could be chosen before completing the selection (fig. 30c) and starting the active control of the nozzles. To complete the setup, the operator also entered nozzle spacing (m) and desired application rate (l/ha) (fig. 30d).

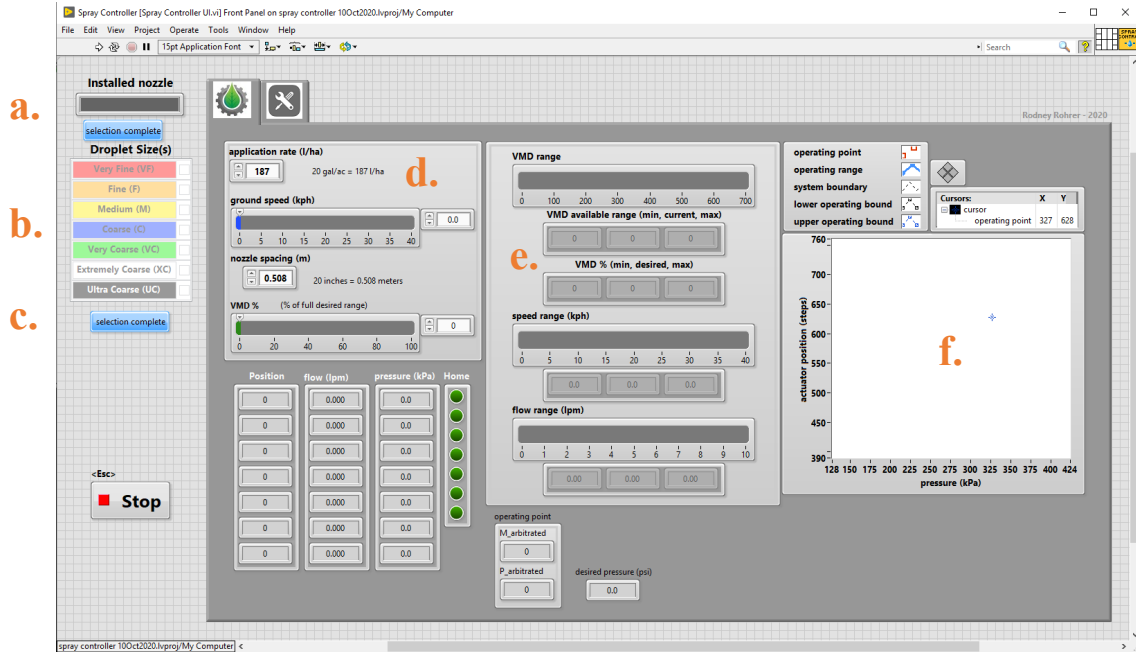


Figure 30 - User interface front panel control tab. a.) nozzle type selector, b.) droplet spectra selector, c.) selection complete button, d.) system controls, e.) system feedback, f.) graph of system model.

With the control system configured, the operator could adjust desired ground speed and droplet size (VMD%). This implementation of the system required the operator to indicate the intended steady-state ground speed. Future implementations could replace this operator control with an input from an active ground speed sensor such as from GPS or radar, and the system would automatically adjust the rate accordingly.

Droplet size control (VMD%) was configured as a percent of the range spanning the, one or more, droplet spectra selected by the operator at startup. For example, if the operator selected only medium droplet spectra, VMD% would be mapped across the range of medium droplet spectra (e.g., 260-376 μm) as 0% – 100%. If medium and coarse droplet spectra were selected, VMD% would be mapped across the range of 260-438 μm .

The range of available ground speed, flow, and droplet size (VMD% and μm) for the installed nozzle and selected droplet sizes were also displayed (fig. 30e). The final feature

on the front panel was a graph of the system model (fig. 30f) showing the boundary of the system operating envelope, boundaries of the selected droplet spectra, and the current operating point (i.e., pressure and actuator position). Field program software logic described in sections 4.4.1 through 4.4.2 and is summarized in figure 31.

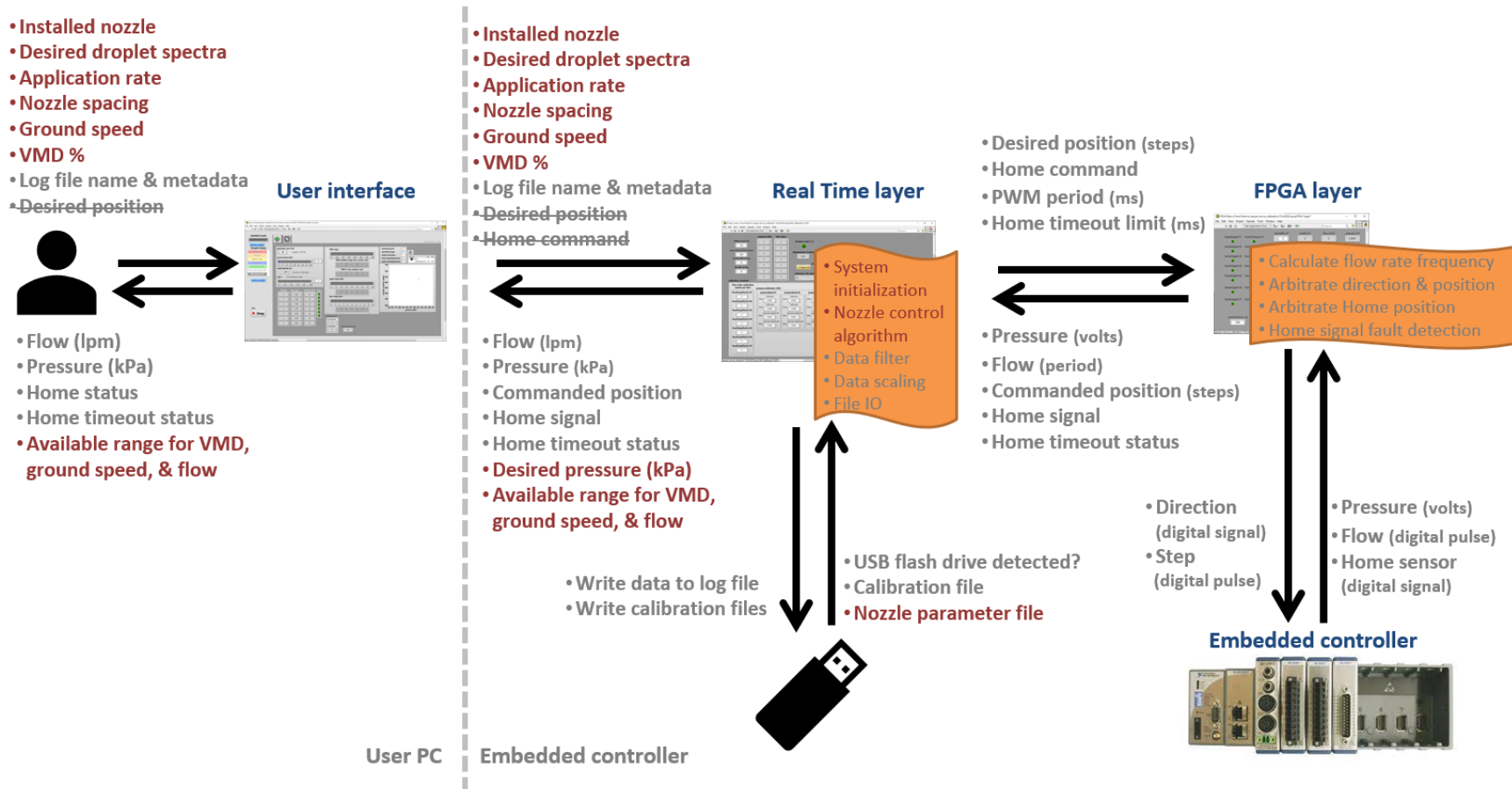


Figure 31 - Field program software interactions and logic. Items which are same as the service and calibration software are gray, new items for the field program software are red.

4.5 CONCLUSION

The project objective to develop control logic for electromechanical variable-orifice nozzles was accomplished with the work described in this chapter. Nozzle performance was characterized by four variables: flow rate, droplet size, system pressure, and effective orifice size. Data related to these variables were measured experimentally for two types of VariTarget nozzle tips. Linear regression performed on the nozzle data was used to create two polynomial equations that model nozzle performance: one equation for flow as a function of system pressure and actuator position and a second equation for droplet size as a function of system pressure and actuator position. This resulted in two equations and four unknowns. Two of the unknowns, nozzle flow rate and droplet size, were derived from operator inputs (i.e., application rate, nozzle spacing, ground speed, selected droplet spectra, and desired percent VMD) while the remaining two variables, system pressure and actuator position, were found by solving the polynomial equations simultaneously.

A control algorithm created from the system equations was implemented in LabVIEW software to create a field program to actively control the variable-orifice nozzles connected to the embedded controller. Operator inputs from the UI on a connected PC were passed to the RT software program running on the embedded controller. The RT software layer loaded sensor calibration data from an xml file and nozzle-specific parameters from a csv file, both stored on a USB drive connected to the embedded controller. With the nozzle parameters and operator inputs, the RT software calculated system pressure and actuator position required to achieve application criteria specified by the operator. The RT layer also filtered and scaled pressure and flow sensor signals sent from the FPGA layer. These data were saved to a log file on the USB drive. Low level

actuator control in the FGPA layer commanded movement of the actuators to achieve the desired effective orifice size while the RT layer communicated the required system pressure to the operator via the UI.

An initialization sequence programmed in the RT layer ensured that the actuators started operation from their home positions. This was needed to provide consistent positioning for open loop control and to protect the nozzle tips from over extension of the metering stem. At shutdown, the RT program commanded the actuators to fully retract and closed the log file once the data queue was empty.

Although the conceptual basis of the control algorithm is seemingly straight forward with the idea of solving the nozzle polynomial equations simultaneously, much of the effort and complexity was in the practical implementation of the algorithm. Logic was included to arbitrate desired pressure and position to ensure the desired operating point always remained within the boundaries of the selected droplet spectra and within the system operating envelope. The algorithm was also programmed in such a way that the nozzle parameters and operating range updated dynamically in the software when a selected nozzle parameter file was loaded.

CHAPTER 5 SPRAY SYSTEM CONTROL VALIDATION

Validation of the nozzle control algorithm and the field program software consisted of two parts: flow validation, and droplet size validation. Flow validation considered how well measured flow matched the flow required to achieve desired application rate (l/ha). Validation of nozzle droplet size performance considered how well measured droplet size matched desired droplet size specified by the nozzle control algorithm.

5.1 FLOW VALIDATION

There were three aspects to flow validation: 1) difference between required flow and expected flow, 2) difference between expected flow and measured flow, and 3) accuracy of measured flow. Evaluation of accuracy of measured flow, measured pressure, and actuator position was described in chapter 3 and so will not be discussed again here. Required nozzle flow rate was a function of application rate, ground speed, and nozzle spacing (equation 4.3), and expected nozzle flow rate was a function of actual system pressure and actuator position (equation 4.1). Because required and expected flow were well defined by these two math equations and several constants, differences between required and expected nozzle flow rates were then the result of error in actual system pressure and actuator position which were found to be quite small and so will not be explored further. This left investigation of error between expected flow and actual flow which was primarily the result of how well the regression curve fit was able to model flow at the nozzle level.

To evaluate flow error, data spanning the system operating envelope were collected with the service and calibration program. This data set included measured flow, measured pressure, and commanded actuator position for five nozzles and so could be used to

evaluate performance at the nozzle level and system level (i.e., variation between nozzles). Data were collected at fifteen actuator positions, every 25 steps from 400-750 steps, at each of nine system pressures, every 34.5 kPa from 138-414 kPa, for a total of 135 observations. At each operating point, actuator position was adjusted with the service and calibration program while system pressure was adjusted manually. A plot of the time history data for blue nozzle01 is shown in figure 32 for the operating points at the lowest pressure setting, while a plot of data for all operating points is shown in figure 33. Equivalent plots for green nozzle01 are shown in figures 68 and 69 in Appendix C: Flow Validation Data.

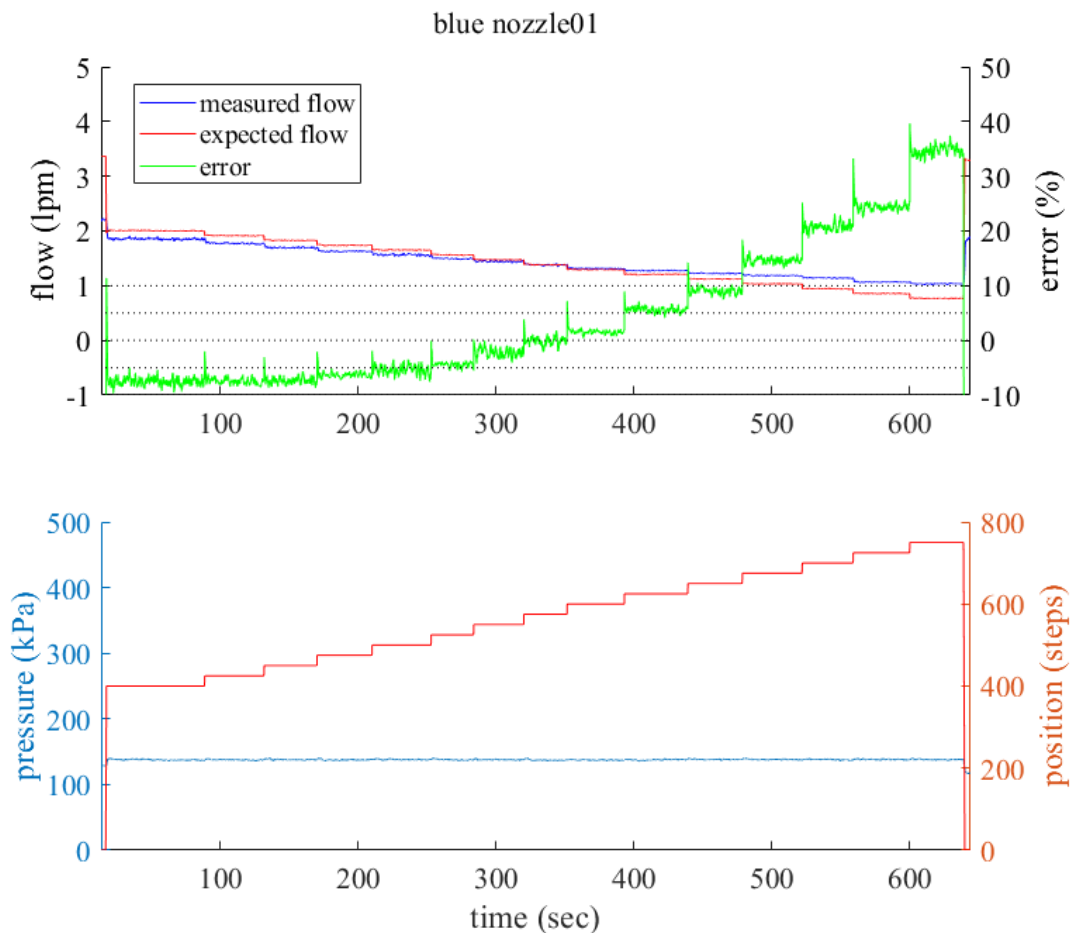


Figure 32 – Detailed view from fig. 33 showing data for blue nozzle01 for varying actuator settings at lowest pressure setting.

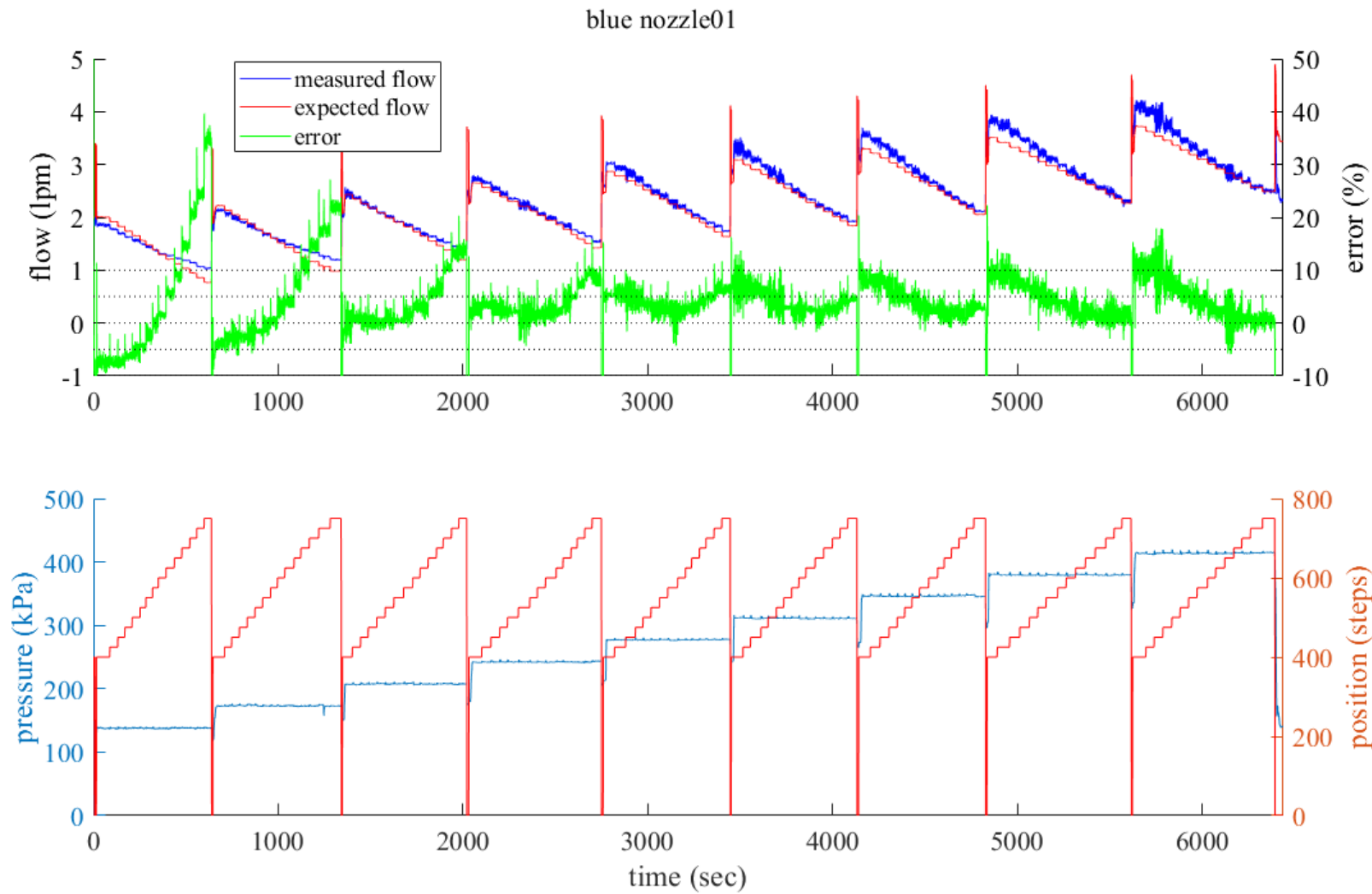


Figure 33 – Plot of flow validation data for blue nozzle01 for various pressures and actuator positions.

Polynomial coefficients for respective blue nozzle01 and green nozzle01 along with actuator position and pressure measured at each nozzle were used with equation 4.1 to calculate expected flow rate for each of the five nozzles. Error between expected and actual flow rate was then calculated.

The average percent error between expected flow and measured for blue nozzle01 was plotted vs. pressure and actuator position in figures 34 and 35. Flow error for this nozzle ranged from -7.5% – 34.8% with thirteen operating points having error greater than 10% (fig.35). A group of eleven points with the largest error was at low pressure and small effective orifice size (i.e., high number of actuator steps) while the remaining two points were at the highest pressure and large effective orifice size (i.e., low number of actuator steps).

For green nozzle01 the range of flow error was -10.4% – 22.9% with seven points outside of $\pm 10\%$ (fig. 36). A group of six points with the largest error was at low pressure and small effective orifice size (i.e., high number of actuator steps) with the remaining point at the lowest pressure and largest effective orifice size (i.e., low number of actuator steps) (fig. 37).

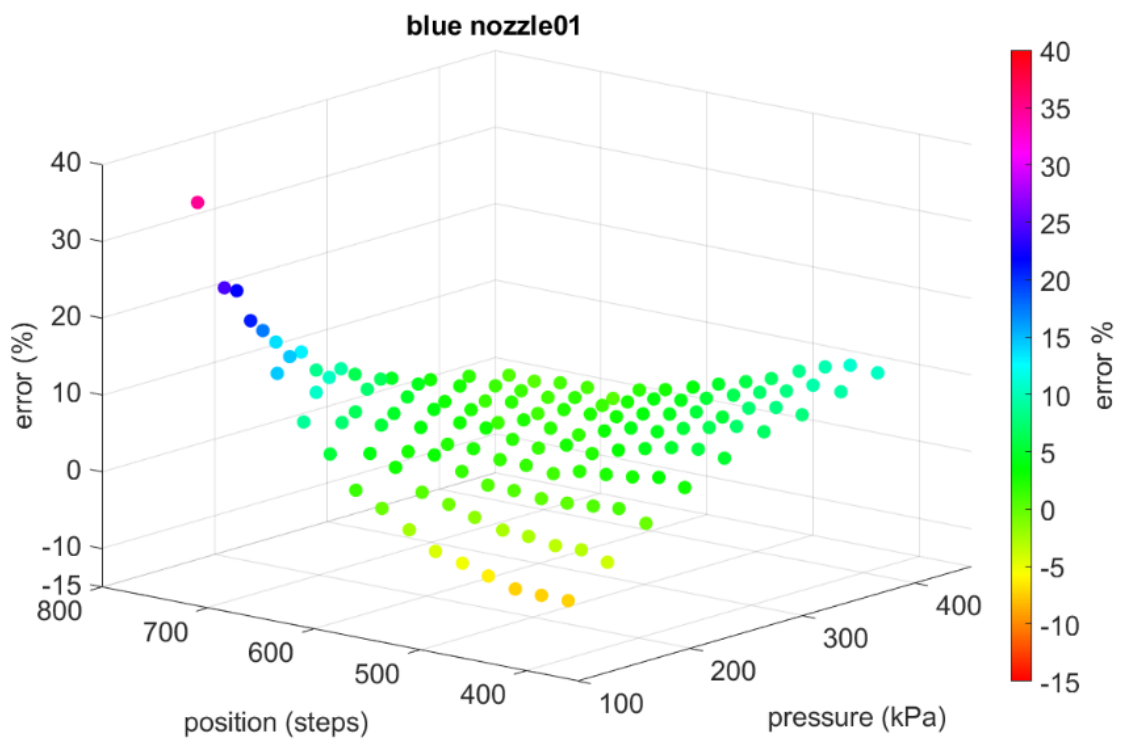


Figure 34 - Scatter plot of flow error at 135 operating points for blue nozzle01.

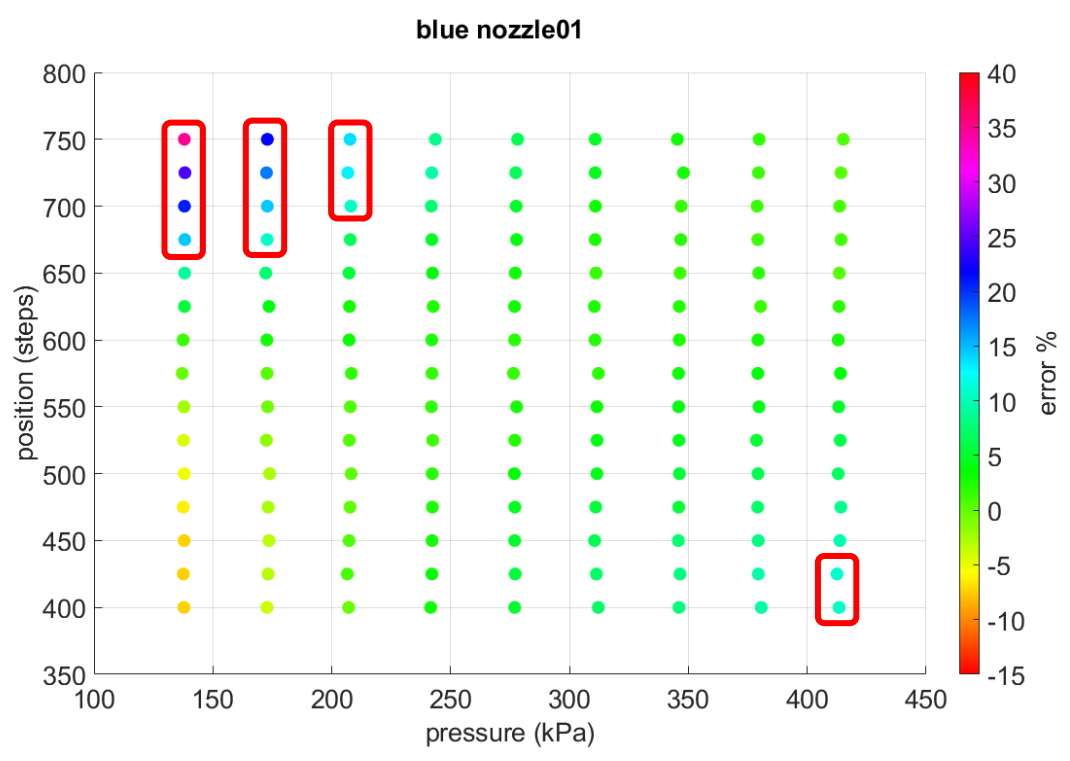


Figure 35 - Scatter plot of pressure and position vs flow error at 135 operating points for blue nozzle01. The outlined points have flow error greater than 10%.

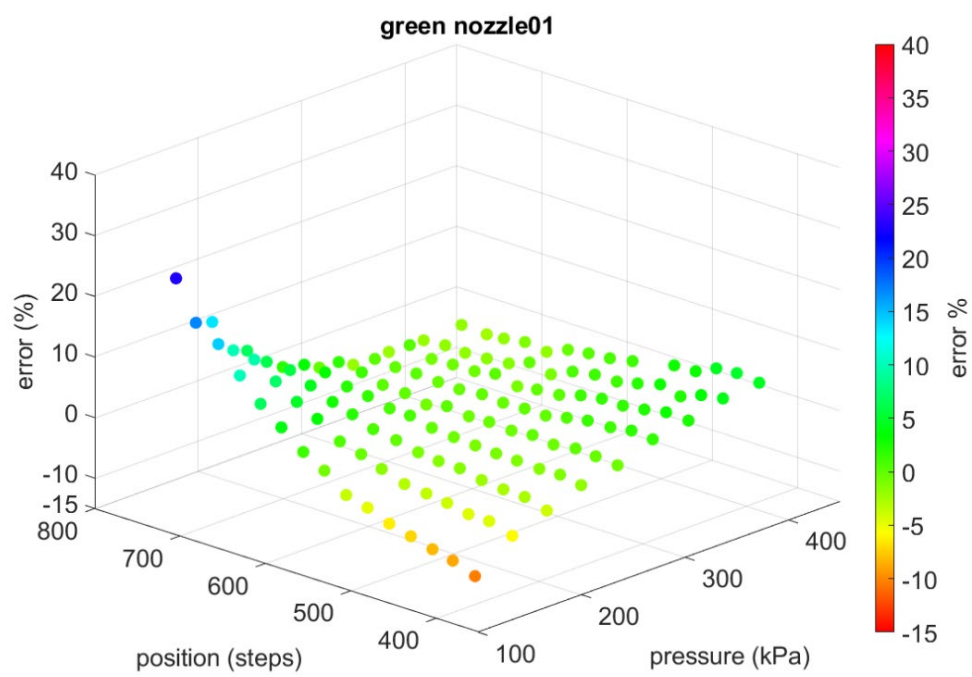


Figure 36 - Scatter plot of flow error at 135 operating points for green nozzle01.

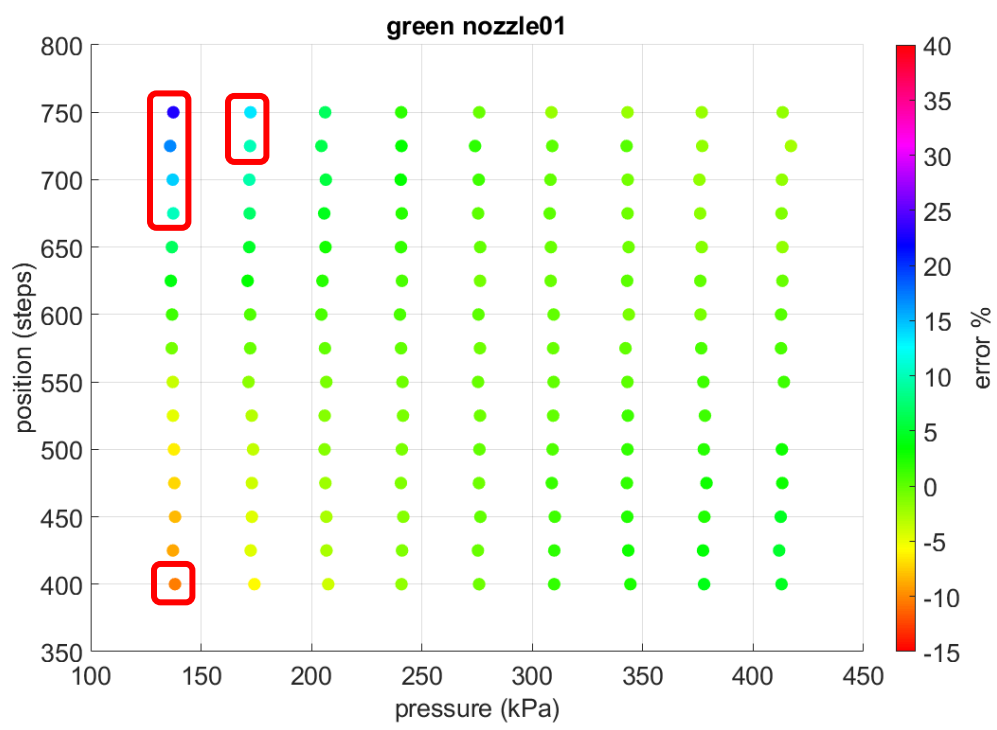


Figure 37 - Scatter plot of pressure and position vs. flow error at 135 operating points for green nozzle01. Seven outlined points have flow error greater than 10%.

The range of flow achieved by each nozzle is summarized in table 13 where minimum flow occurred at the lowest pressure and smallest orifice size (i.e., 138 kPa and 750 steps) and maximum flow occurred at the highest pressure and largest orifice size (i.e., 414 kPa and 400 steps). Across the five nozzles, the average flow for the blue nozzles ranged from 1.02 to 4.14 lpm with an average turndown ratio of 4.0, while the average flow rate for the green nozzles was from 1.40 to 5.14 lpm with an average turndown ratio of 3.7.

Table 13 - Range of measured flow for five blue nozzles and five green nozzles.

	flow (lpm)			
	blue nozzles		green nozzles	
	min	max	min	max
nozzle01	1.03	4.10	1.40	5.13
nozzle02	0.98	4.19	1.30	4.98
nozzle03	0.97	3.86	1.32	5.00
nozzle04	1.09	4.04	1.46	5.22
nozzle05	1.04	4.48	1.52	5.37
mean	1.02	4.14	1.40	5.14
turndown ratio	4.0		3.7	

Measured flow vs. actuator position at nine system pressures is shown in figure 38 for blue nozzle01 and figure 39 for green nozzle01. It is apparent from the graphs that the relationship between flow and actuator position is linear for both nozzle types and is consistent with evaluation done by Luck (2012).

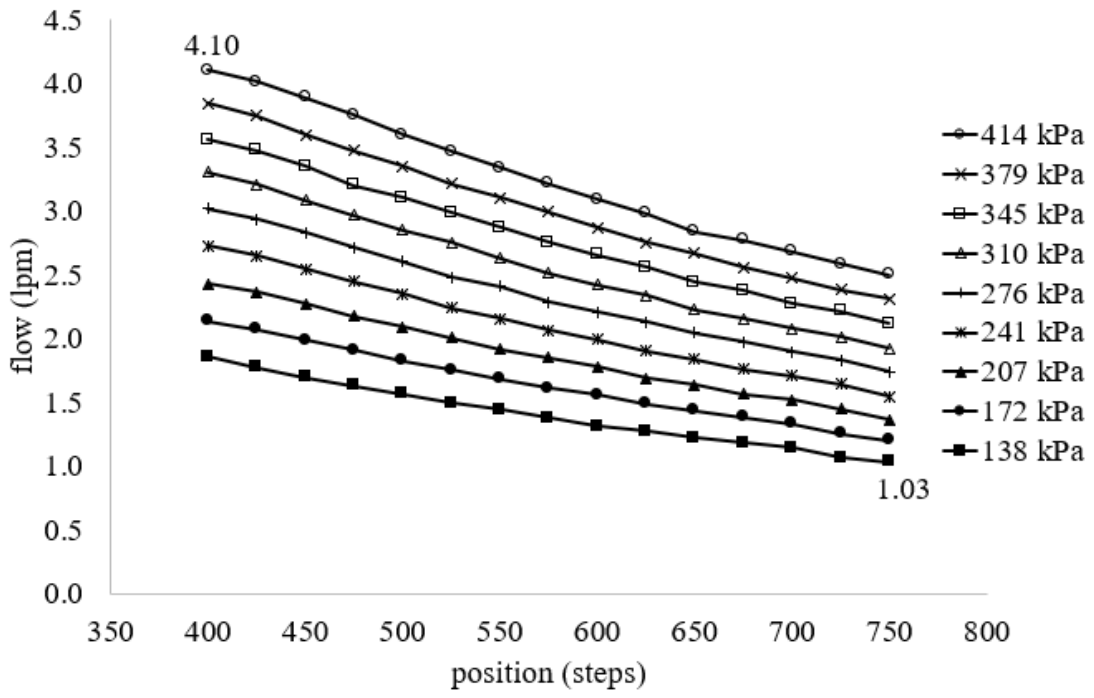


Figure 38 – Measured flow vs. actuator position for blue nozzle01 at nine pressure settings.

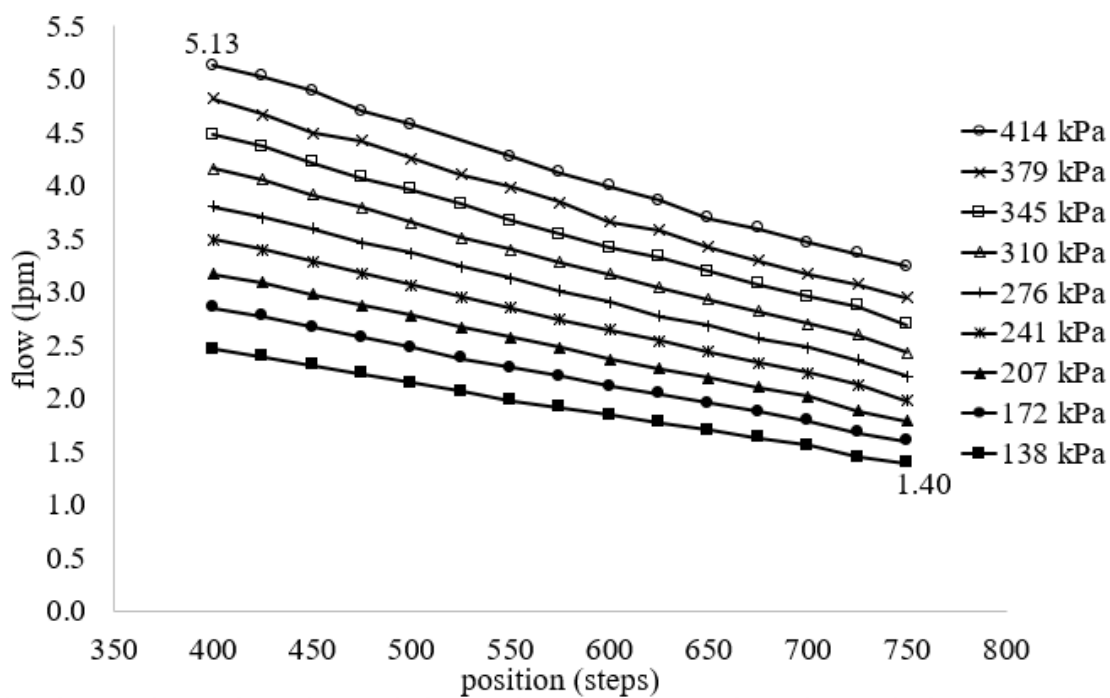


Figure 39 – Measured flow vs. actuator position for green nozzle01 at nine pressure settings.

Average flow error for each steady-state operating point is plotted vs. pressure and actuator position for five blue nozzles in figure 40 and five green nozzles in figure 41. From these figures it becomes apparent that, although the calculation for expected flow for each nozzle was done with the polynomial coefficients for nozzle01, the relative error across the operating envelope is quite similar in form for each nozzle. The largest errors were observed at extremes of the system operating envelope, especially at low system pressures and high metering stem positions. The range of error for each nozzle is summarized in table 14.

For the blue nozzles, the deviation of mean steady-state measured pressure from nominal pressure was -3.7 to 4.7 kPa across all operating points. For the green nozzles, the deviation of mean steady-state measured pressure from nominal pressure was -6.3 to 3.6 kPa across all operating points.

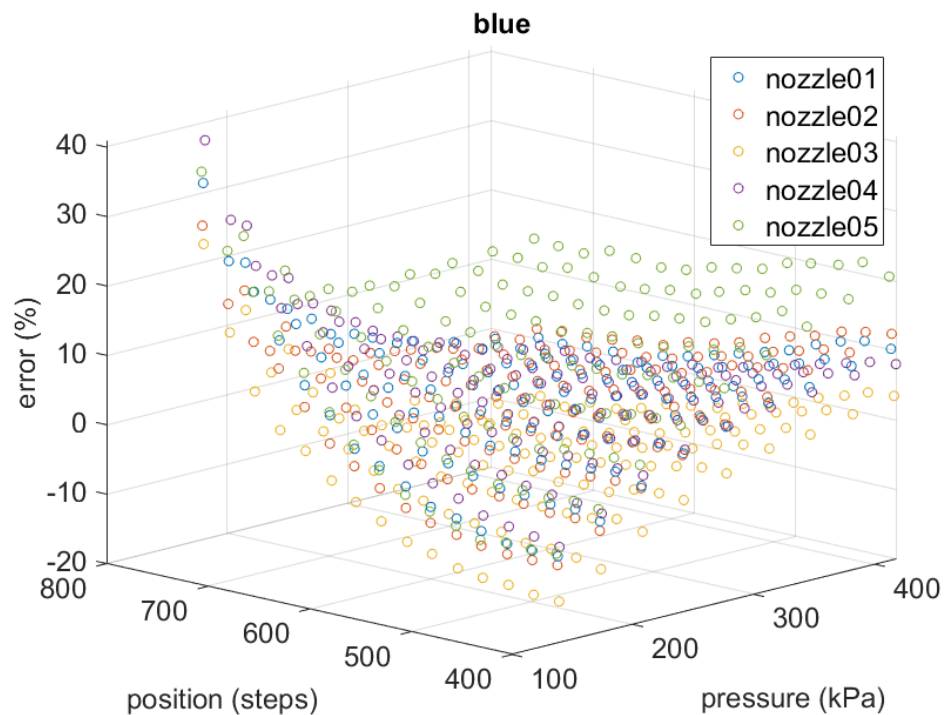


Figure 40 - Percent error between measured flow and expected flow using blue nozzle01 polynomial coefficients for each of five blue nozzles.

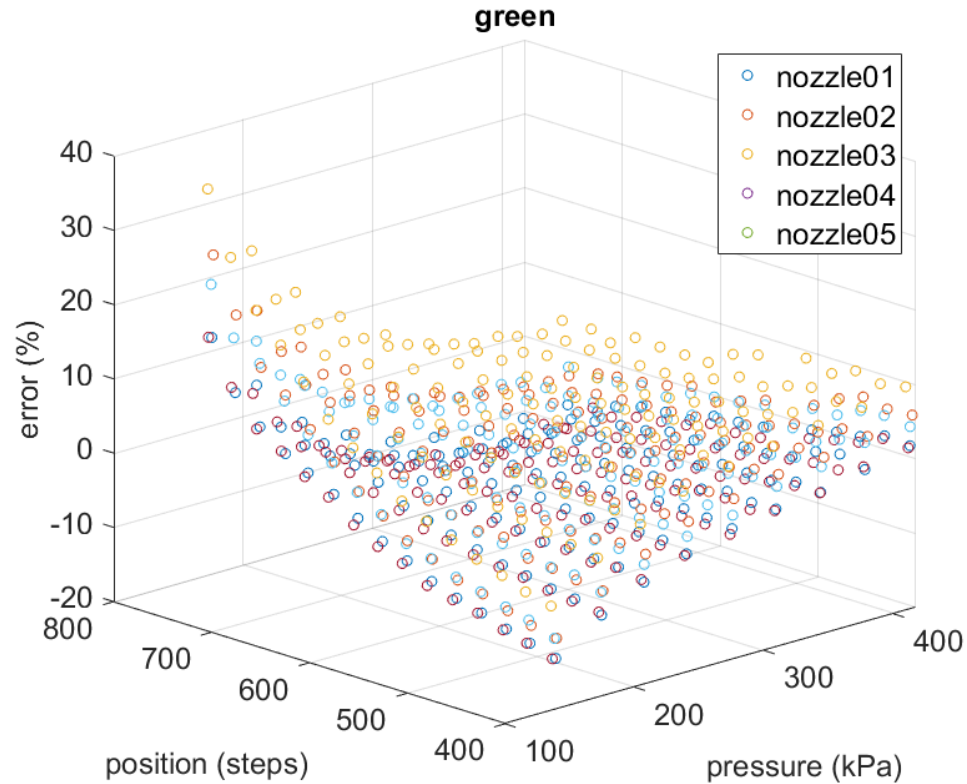


Figure 41 – Percent error between measured flow and expected flow using green nozzle01 polynomial coefficients for each of five green nozzles.

Table 14 - Flow error for five blue nozzles and five green nozzles where expected flow was based on polynomial coefficients from nozzle01.

	error (%)			
	blue nozzles		green nozzles	
	min	max	min	max
nozzle01	-7.5	34.8	-10.4	22.9
nozzle02	-8.8	28.7	-13.1	15.9
nozzle03	-14.0	26.0	-13.1	15.8
nozzle04	-6.2	40.9	-10.4	26.8
nozzle05	-7.5	36.5	-5.9	35.9

The operating envelope may need to be limited by pressure and/or actuator position to avoid operating in areas of flow error that are greater than 10%. Although this ten percent threshold is not a formal industry standard this is a commonly used threshold for nozzle testing and evaluation at the PAT Lab (Kruger, 2020). It may be expected that error for

nozzles 2 through 5 could be reduced by using separate polynomial coefficients for each respective nozzle however this becomes quite cumbersome and impractical to implement for a large system that may involve dozens of nozzles. The quality of the spray pattern (i.e., low coefficient of variation) is an indication that, although there is variability amongst the nozzles, the output is quite uniform at the system level.

5.2 SPRAY SYSTEM DROPLET SIZE VALIDATION

Data were collected at the PAT Lab to evaluate droplet size output of the spray nozzle algorithm. Linear regression was done on one data set to get polynomial coefficients for calculating expected droplet size with equation 4.2. A second data set was collected to be used for validation to find differences between desired droplet size and actual droplet size. Data were also collected from reference nozzles to use for classification of droplet spectra at each operating point. The droplet spectra classification boundaries based on the reference nozzle data are summarized in table 15 and plotted vs. cumulative volume fraction in figure 42.

Table 15 - Reference nozzle droplet diameters for curve fit and validation data collected at PAT Lab 7Dec2020.

Droplet Spectra Classification Boundaries									
categories [†]	mean diameter (μm)								
	$D_{v0.1}$			$D_{v0.5}$			$D_{v0.9}$		
	avg	std dev	sum	avg	std dev	sum	avg	std dev	sum
VF/F	65	0.2	65	142	0.1	142	247	0.7	247
F/M	117	0.4	117	259	0.3	260	425	0.4	425
M/C	170	0.8	169	375	1.0	376	594	1.4	596
C/VC	198	0.7	197	438	0.8	438	730	8.1	738
VC/XC	240	0.7	239	520	1.5	522	832	5.4	838
XC/UC	316	1.5	314	660	2.0	662	1015	1.4	1016

[†]VF = very fine M = medium VC = very coarse UC = ultra coarse
F = fine C = coarse XC = extremely coarse

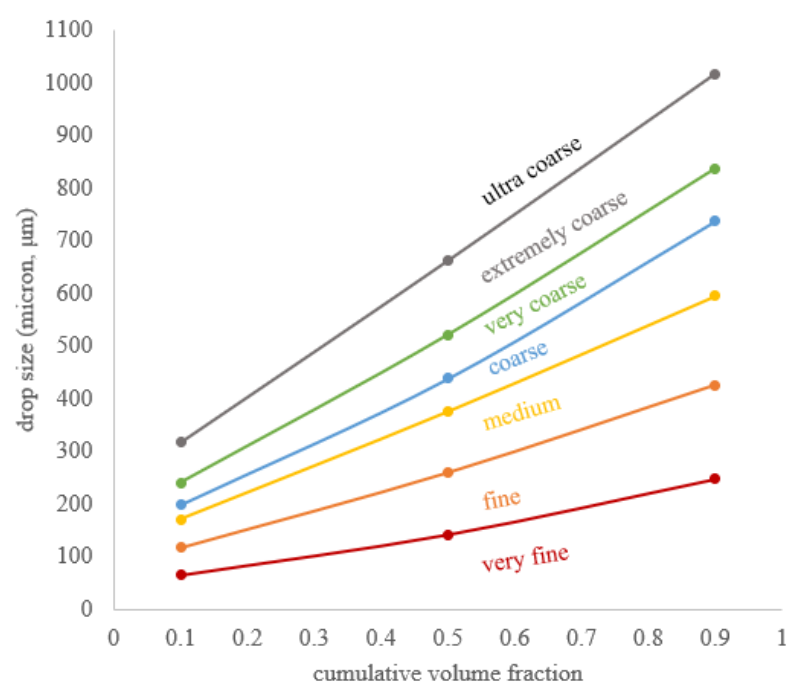


Figure 42 - Reference nozzle droplet size vs. cumulative volume fraction for curve fit and validation data collected at PAT Lab 7Dec2020.

Twenty-five operating points were selected for the curve fit data set that uniformly spanned the spray system operating envelope. There were also twenty-five operating points for the validation data set that spanned the operating envelope, but these were offset from the curve fit operating points as shown in figure 43.

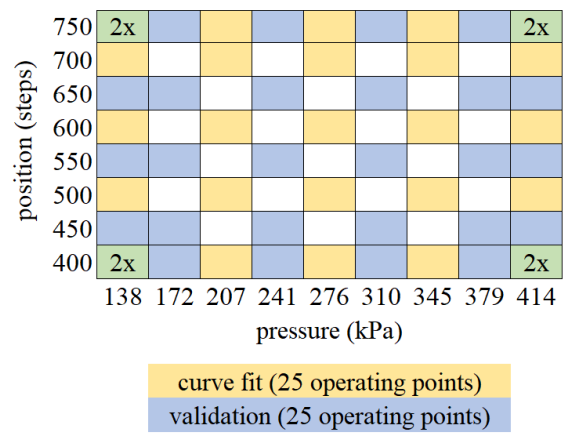


Figure 43 - Operating points for droplet size curve fit and validation data sets.

Using the curve fit data set, linear regression was done on twenty-five mean pressure, actuator position, and $D_{v0.5}$ values measured at the PAT Lab for one blue and one green nozzle as described in section 4.3 (fig. 27). Polynomial coefficients, coefficient of determination, and root mean square error for the regression are in table 11.

$D_{v0.1}$, $D_{v0.5}$, and $D_{v0.9}$ droplet diameters measured for each operating point in the validation data set, (table 16), were compared to the reference nozzle data to find the respective droplet size classifications which are summarized in table 17. The blue nozzle was able to span three droplet size categories, fine to coarse, with a VMD range of 242 to 416 μm . The green nozzle was able to span four categories, medium to extremely coarse, with a VMD range of 279 to 524 μm .

Table 16 - $D_{v0.1}$, $D_{v0.5}$, and $D_{v0.9}$ droplet diameters for droplet validation data set.

		droplet size (μm)											
		blue nozzle01						green nozzle01					
pressure (kPa)	VMD (μm)	position (steps)											
		400	450	550	650	700	750	400	450	550	650	700	750
138	DV10	190	180	158	145	139	130	256	241	209	185	178	181
	DV50	416	398	358	332	323	309	524	497	440	396	383	383
	DV90	698	658	581	555	547	538	824	786	697	612	593	588
172	DV10	181	168	147	133	127	121	238	222	188	169	162	166
	DV50	401	375	336	313	297	288	496	470	404	369	355	359
	DV90	683	600	550	536	508	502	789	764	631	578	561	568
241	DV10	164	153	136	123	117	110	211	198	167	150	146	145
	DV50	374	348	317	288	274	260	452	430	369	339	330	324
	DV90	649	566	540	492	475	460	749	711	582	561	550	537
310	DV10	158	149	131	118	112	107	192	183	158	140	134	132
	DV50	364	344	309	280	265	253	421	402	357	320	310	299
	DV90	643	578	528	484	460	440	710	683	601	537	521	494
379	DV10	151	147	129	117	110	106	178	168	151	133	128	124
	DV50	349	340	303	276	261	248	392	376	338	307	297	283
	DV90	617	582	514	479	457	429	676	648	568	517	498	478
414	DV10	140	137	123	110	106	102	171	163	146	130	125	122
	DV50	330	325	293	265	254	242	382	365	332	303	291	279
	DV90	588	571	503	467	451	423	667	629	573	510	491	474

Table 17 - Droplet classifications for validation data set.

droplet spectra classification												
position (steps)	blue nozzle01						green nozzle01					
	pressure (kPa)											
	138	172	241	310	379	414	138	172	241	310	379	414
400	C	C	M	M	M	M	XC	VC	VC	C	C	C
450	C	M	M	M	M	M	VC	VC	C	M	M	M
550	M	M	M	M	F	F	VC	C	M	M	M	M
650	M	M	M	M	F	F	C	C	M	M	M	M
700	M	M	M	F	F	F	C	M	M	M	M	M
750	M	M	M	F	F	F	C	M	M	M	M	M

Expected droplet size was calculated from mean pressure and position for each respective operating point. Deviation of mean steady-state measured pressure from nominal pressure across all operating points was -6.7 to 9.6 kPa for the blue nozzle and -5.6 to 7.6 kPa for the green nozzle. Percent error between measured and expected droplet size is summarized in table 18. $D_{v0.5}$ droplet size error for blue nozzle01 ranged from -2.9% – 6.2% and for green nozzle01 from -9.5% – 5.0%.

Table 18 - Error between measured and expected $D_{v0.5}$ for validation data set.

$D_{v0.5}$ droplet size error (%)												
position (steps)	blue nozzle01						green nozzle01					
	pressure (kPa)											
	138	172	241	310	379	414	138	172	241	310	379	414
400	-2.0	-0.1	2.2	0.7	0.4	3.5	-9.5	-7.0	-4.2	-3.6	-3.6	-4.2
450	-1.4	2.5	5.2	2.0	-0.9	0.6	-7.3	-5.0	-2.7	-2.7	-3.3	-4.6
550	0.9	4.9	5.8	3.5	0.7	0.8	-2.5	2.9	5.0	0.8	-1.7	-4.9
650	-0.6	3.1	6.2	3.5	-0.7	-0.5	0.4	4.2	5.0	2.7	-2.1	-5.2
700	-2.3	3.4	5.8	3.5	-1.0	-1.6	0.0	3.8	3.4	1.4	-3.9	-6.5
750	-2.9	1.3	5.4	2.4	-1.8	-2.6	-4.3	-1.1	0.7	0.1	-4.2	-7.2

For both blue and green nozzles, the algorithm tended to over-predict droplet size in the middle of the operating range and under-predict droplet size on the edges of the operating range, particularly at low pressures (fig.44 and 45). This is related to the linear curve fit where a flat plane was fitted to a slightly non-linear data set. However, the linear approximation results in small error and seems justified especially when considering the complexity of implementing a non-linear control algorithm.

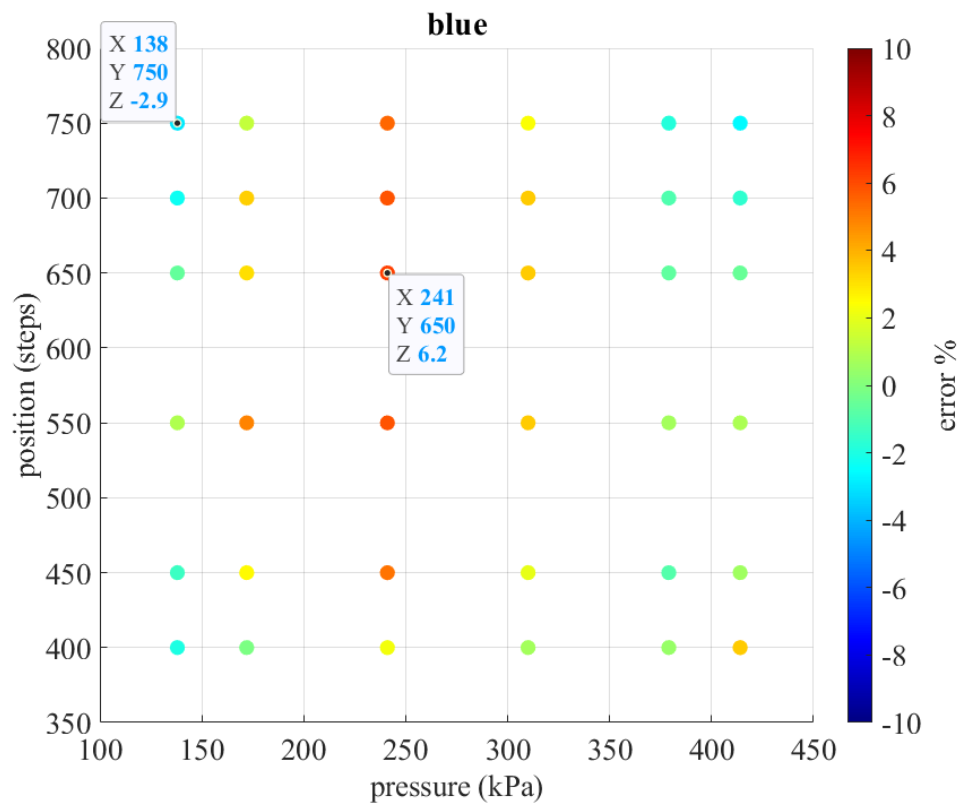


Figure 44 - Error between measured and expected $D_{v0.5}$ for blue nozzle validation data. Minimum and maximum values are tagged.

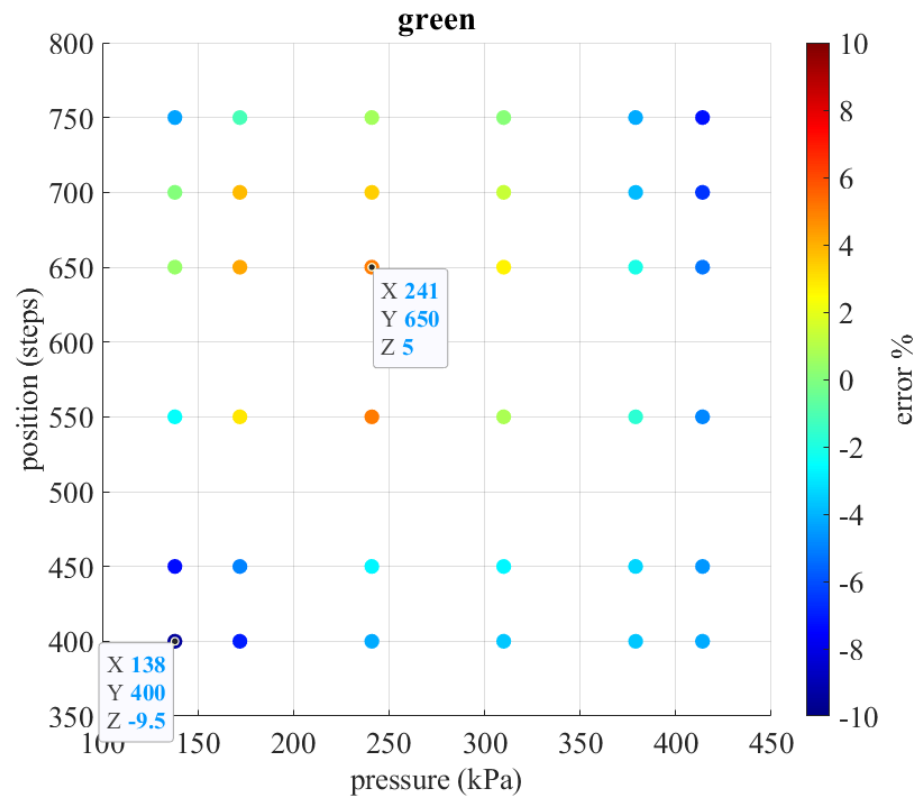


Figure 45 - Error between measured and expected $D_{v0.5}$ for green nozzle validation data. Minimum and maximum values are tagged.

5.3 FIELD PROGRAM VALIDATION

The final validation step was to evaluate the LabVIEW Field Program with the fully implemented algorithm. This was done at the PAT Lab where droplet size was measured in the wind tunnel. Once again, reference nozzles were run so droplet spectra could be determined at each operating point. The droplet spectra classification boundaries based on the reference nozzle data are summarized in table 19 and plotted vs. cumulative volume fraction in figure 46.

Table 19 - Reference nozzle droplet diameters for field program data collected at PAT Lab 8Dec2020.

Droplet Spectra Classification Boundaries									
categories [†]	mean diameter (μm)								
	$D_{v0.1}$			$D_{v0.5}$			$D_{v0.9}$		
	avg	std dev	sum	avg	std dev	sum	avg	std dev	sum
VF/F	64	0.2	64	141	0.4	141	246	0.9	247
F/M	115	0.1	116	257	0.5	258	423	0.3	423
M/C	167	0.3	167	372	0.2	372	594	0.5	595
C/VC	195	1.1	196	434	1.7	435	734	3.8	737
VC/XC	237	0.9	238	518	1.1	519	835	2.2	838
XC/UC	312	0.4	312	655	0.9	656	1028	9.6	1037

[†]VF = very fine M = medium VC = very coarse UC = ultra coarse
 F = fine C = coarse XC = extremely coarse

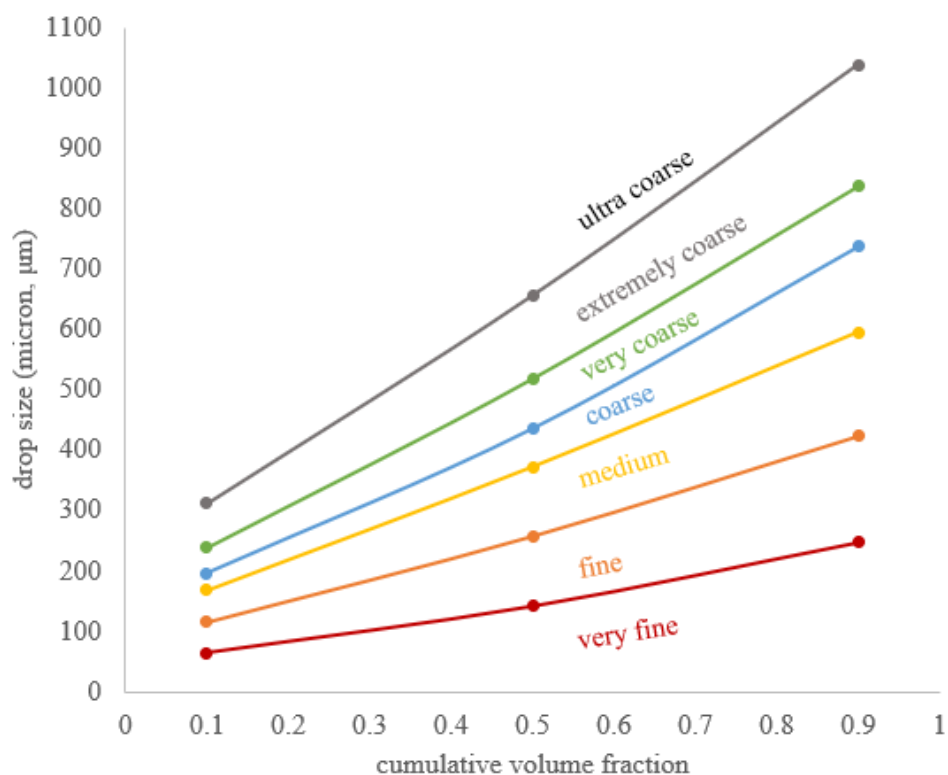


Figure 46 - Reference nozzle droplet size vs. cumulative volume fraction for field program data collected at PAT Lab 8Dec2020.

Final system validation was done by collecting data with the field program at several points spanning the operating range at different droplet sizes but at a fixed ground speed (i.e., constant flow rate). Points were selected at the extremes of the operating range and adjacent to the droplet spectra boundaries along a line of constant ground speed (table 20 points 1-9, fig. 47 for blue nozzle, fig. 48 for green nozzle). With data collected at these points, evaluation could be done to assess the ability of the control system to maintain a constant flow rate while changing droplet size and to understand the transition in droplet spectra at the $D_{v0.5}$ values separating the classification boundaries.

Data were also collected at several ground speeds spanning the operating envelope but along a line of constant droplet size (points 5, 10, and 11 table 20, fig. 47, fig. 48). With these data, the ability of the control system to maintain constant droplet size while varying the flow rate (i.e., ground speed) was evaluated.

Table 20 - Operating points for field program data collection.

		operating points for Field Program							
		blue nozzle01				green nozzle01			
operating point	description	speed (kph)	VMD (%)	pressure (kPa)	position (steps)	speed (kph)	VMD (%)	pressure (kPa)	position (steps)
1	min VMD at speed	14	34	371	750	17.4	10	343	748
2	10 kPa less than lower spectra boundary	14	37	363	734	17.4	41	255	598
3	on lower spectra boundary	14	40	351	714	17.4	44	246	584
4	10 kPa more than lower spectra boundary	14	43	340	694	17.4	48	235	564
5	VMD centered in middle spectra	14	59	279	588	17.4	56	212	526
6	10 kPa less than upper spectra boundary	14	76	214	474	17.4	65	187	482
7	on upper spectra boundary	14	79	203	454	17.4	68	178	468
8	10 kPa more than upper spectra boundary	14	82	191	434	17.4	72	167	449
9	max VMD at speed	14	87	172	401	17.4	82	139	400
10	VMD 50% at left boundary of middle spectra	6.2	59	140	693	11	56	139	621
11	VMD 50% at right boundary of middle spectra	21.5	59	412	486	25.7	56	307	402

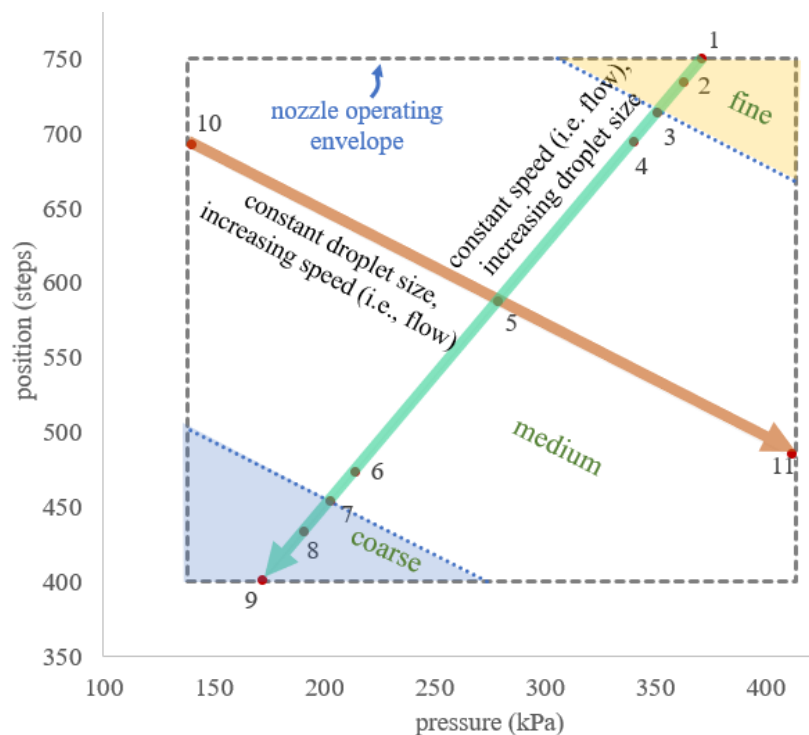


Figure 47 - Operating envelope for blue nozzle spanning three droplet spectra. Lines of constant flow rate (i.e., speed) and constant droplet size are shown along with eleven operating points.

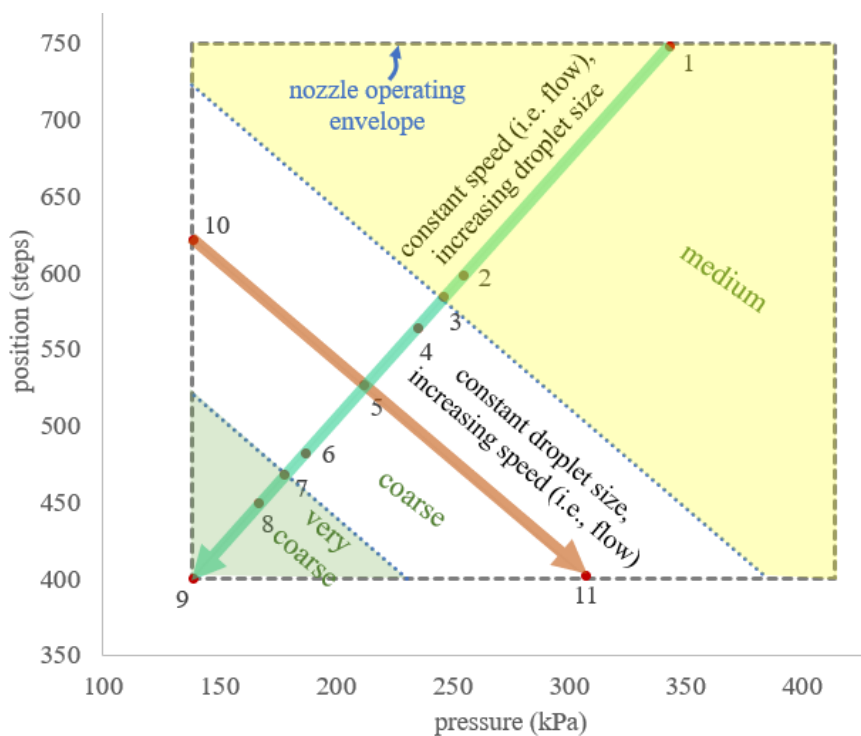


Figure 48 - Operating envelope for green nozzle spanning three droplet spectra. Lines of constant flow rate (i.e., speed) and constant droplet size are shown along with eleven operating points.

For each evaluation, the system was configured with blue nozzle01 or green nozzle01 and the field program used the polynomial coefficients derived from those same nozzles.

Field program UI settings for each respective nozzle are in table 21.

Table 21 - UI settings for field program validation.

Field Program UI input	Blue Nozzle01	Green Nozzle01
Installed nozzle	Blue – Coarse (C)	GREEN - Very Coarse (VC)
Selected droplet spectra	Fine (F)	Medium (M)
	Medium (M)	Coarse (C)
	Coarse (C)	Very Coarse (VC)
Application rate (l/ha)	187	187
Nozzle spacing (m)	0.508	0.508

Once the field program was configured, ground speed was set to a point that would allow the droplet sizes to span as much of the operating envelope as possible. At this fixed

ground speed, the percent VMD was adjusted to achieve each desired operating point.

The nozzle actuator automatically adjusted to the desired position and pressure was set manually.

Across the first nine operating points for the blue nozzle, flow error ranged from 1.6% – 7.8% and error in $D_{v0.5}$ droplet size ranged from -4.8% – 3.0%. Results for the blue nozzle are summarized in fig. 49 and table 22. Across the first nine operating points for the green nozzle, flow error ranged from -10.2% – 0% and error in $D_{v0.5}$ droplet size ranged from -9.4% – 4.7%. Results for the green nozzle are summarized in figure 50 and table 23.

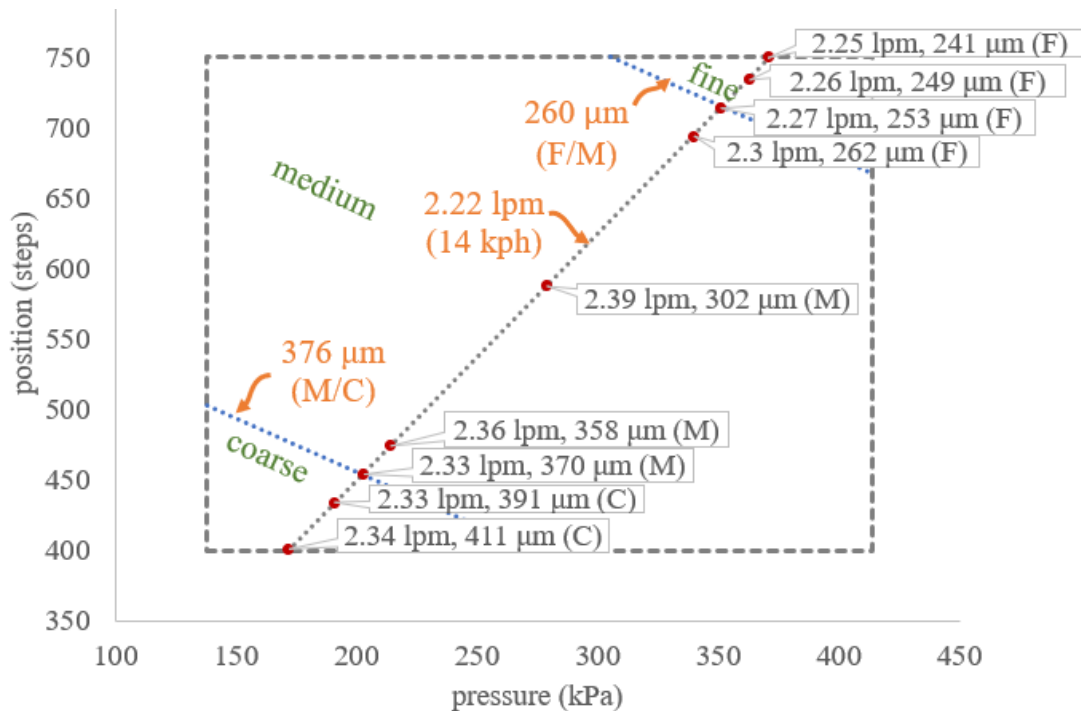


Figure 49 - Nine operating points with blue nozzle01 at constant flow rate (i.e., speed) but varying droplet size ($D_{v0.5}$) spanning three droplet spectra categories. Data tags show flow rate, $D_{v0.5}$, and droplet classification at each operating point.

Table 22 - Summary of blue nozzle01 validation data with field program.

operating point	droplet spectra			classification	Dv50	Dv50	expected	measured	flow
	Dv10	Dv50	Dv90		expected	error	flow	flow	error
	μm	μm	μm		μm	%	lpm	lpm	%
1	102	241	419	F	245	-1.3	2.22	2.25	1.6
2	105	249	428	F	252	-1.1	2.22	2.26	2.0
3	108	253	437	F	260	-3.0	2.22	2.27	2.2
4	112	262	451	F	269	-2.5	2.22	2.30	3.7
5	129	302	514	M	317	-4.8	2.22	2.39	7.8
6	159	358	575	M	367	-2.3	2.22	2.36	6.4
7	166	370	586	M	376	-1.5	2.22	2.33	5.0
8	174	391	658	C	385	1.8	2.22	2.33	5.0
9	186	411	694	C	400	3.0	2.22	2.34	5.4
10	141	323	541	M	317	2.0	0.98	1.22	23.9
11	135	317	539	M	317	0.0	3.40	3.77	10.7

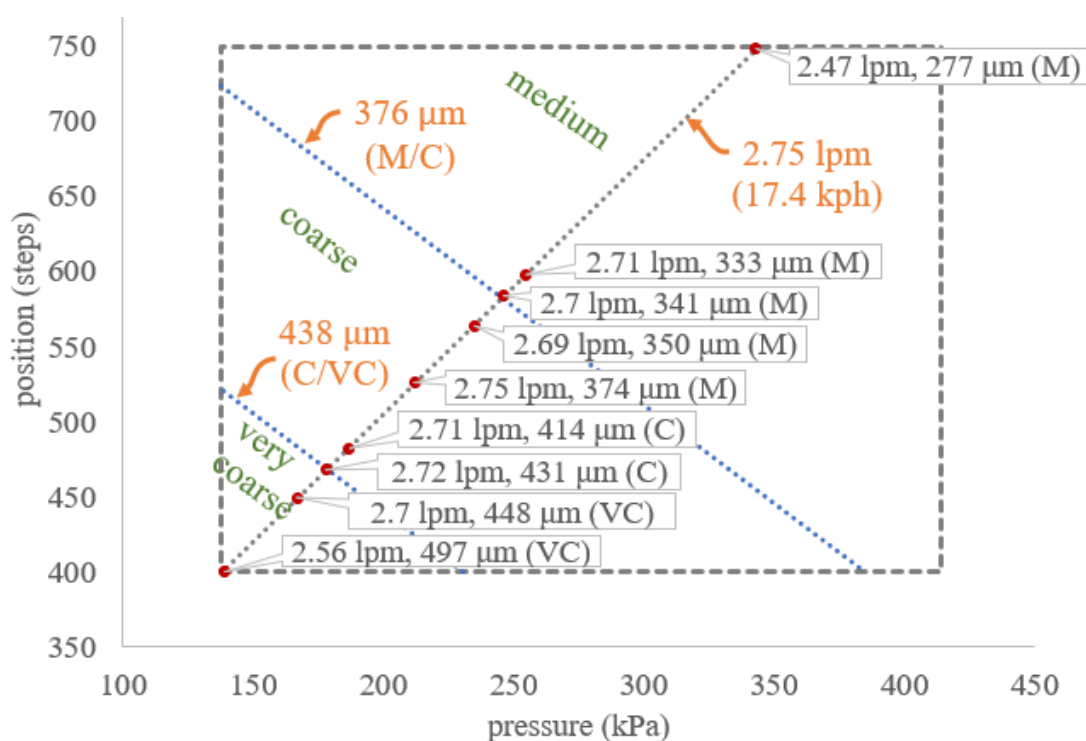


Figure 50 - Nine operating points with green nozzle01 at constant flow rate (i.e., speed) but varying droplet size ($D_{v0.5}$) spanning three droplet spectra categories. Data tags show flow rate, $D_{v0.5}$, and droplet classification at each operating point.

Table 23 - Summary of green nozzle01 validation data with field program.

operating point	droplet spectra			classification	Dv50	Dv50	expected	measured	flow
	Dv10	Dv50	Dv90		expected	error	flow	flow	error
	μm	μm	μm		μm	%	lpm	lpm	%
1	116	277	478	M	286	-3.3	2.75	2.47	-10.2
2	141	333	551	M	367	-9.4	2.75	2.71	-1.6
3	145	341	563	M	375	-9.2	2.75	2.70	-1.9
4	151	350	573	M	386	-9.2	2.75	2.69	-2.3
5	162	374	599	M	407	-8.1	2.75	2.75	0.0
6	182	414	687	C	430	-3.7	2.75	2.71	-1.5
7	190	431	718	C	438	-1.6	2.75	2.72	-1.1
8	198	448	738	VC	449	-0.2	2.75	2.70	-1.9
9	227	497	803	VC	475	4.7	2.75	2.56	-7.2
10	175	393	623	C	407	-3.3	1.74	1.78	2.5
11	178	406	703	C	407	-0.1	4.07	4.24	4.3

Droplet spectra category was also determined at each operating point. The droplet size categories are not precisely aligned with the boundaries in the algorithm, which are based on the VMD (e.g., $D_{v0.5}$ of 258 μm at the blue nozzle F/M boundary), but instead tend to be skewed toward the smaller categories. This was sometimes the result of the $D_{v0.1}$ value being below the reference nozzle $D_{v0.1}$ which forced the droplet spectra classification into the finer droplet size category even though the $D_{v0.5}$ value was above the classification boundary (ANSI/ASABE, 2018). This was the case for point four for the blue nozzle and point five for the green nozzle. In some cases, the droplet size category was the result of less than 2 μm difference in $D_{v0.1}$ or $D_{v0.5}$ relative to that of the reference nozzle.

With the same field program UI settings as indicated above (table 20), data were collected at two additional operating points for each nozzle to evaluate the ability of the system to maintain constant droplet size across varying flow (i.e., ground speed). VMD% was set to the center of the middle droplet size classification for each respective nozzle, 50% of medium for the blue nozzle and 50% of coarse for the green nozzle. Ground

speed was then adjusted to achieve operating points at the extremes of the operating range. These two operating points, along with point number five from the previous data set, fall on a line centered in the medium droplet spectra for blue nozzle01 (fig. 51) and on a line centered in the coarse droplet spectra for green nozzle01 (fig. 52). Target droplet size for the blue nozzle was 318 μm with the three operating points deviating from this target by -15 to 6 μm , resulting in an error of -4.8% – 0%. For these same three operating points the flow error ranged from 7.8% – 23.9%. Target droplet size for the green nozzle was 407 μm with the three operating points deviating from this target by -33 to -1 μm , resulting in an error of -8.1% – -0.1%. For these same three operating points the flow error ranged from 0% – 4.3%.

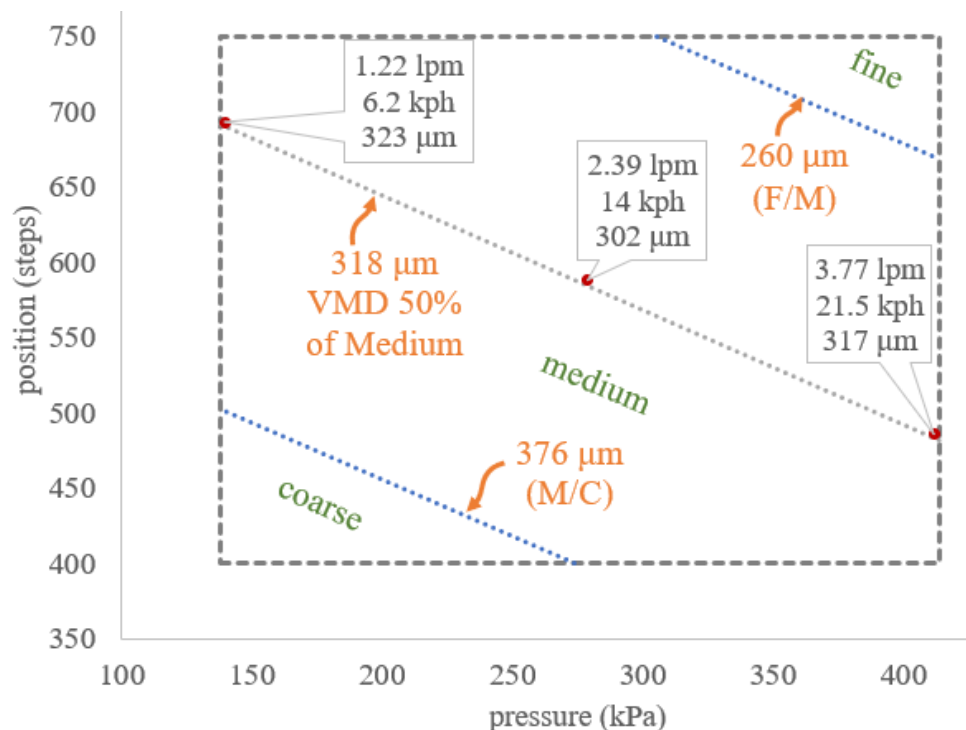


Figure 51 - Three operating points on a line of constant droplet size but varying flow rate for blue nozzle01. Data tags show the respective flow rate, ground speed, and $D_{v0.5}$ droplet size.

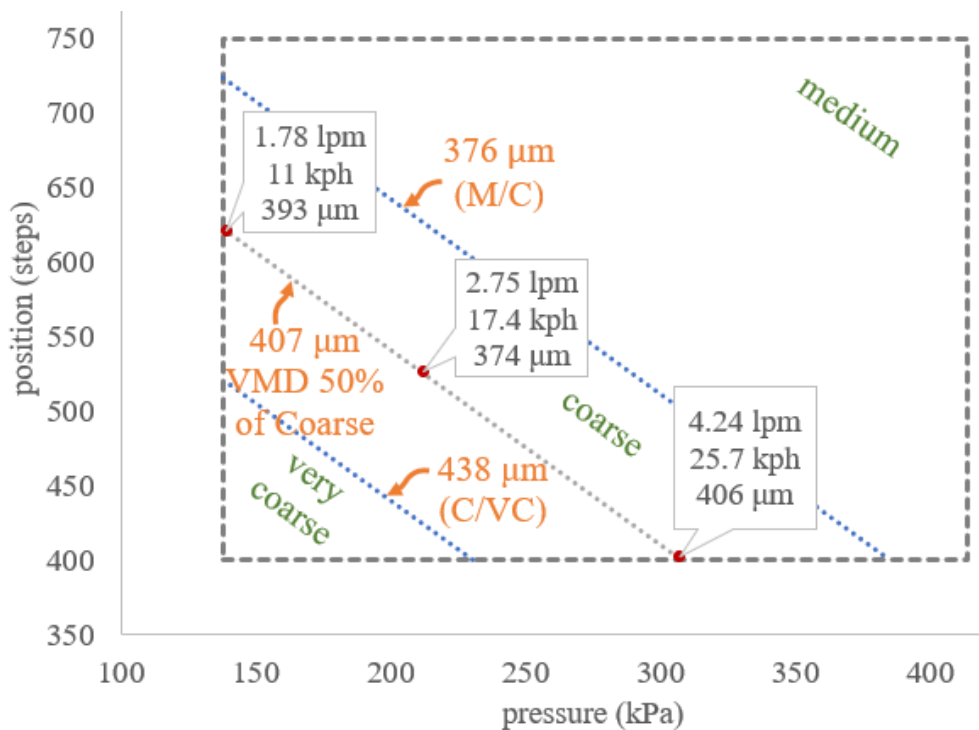


Figure 52 - Three operating points on a line of constant droplet size but varying flow rate for green nozzle01. Data tags show the respective flow rate, ground speed, and $D_{v0.5}$ droplet size.

Note that all field program validation operating points (table 20) were determined from reference nozzles for the curve fit data collected on 7December2020 (table 15, figure 42), however the validation data were measured on a 8December2020 and their droplet spectra categories were based on the reference nozzles (table 19, figure 46) that were measured on that day. Although the data from both days are in quite good agreement this may explain some of the error and subtle shift in droplet spectra categories between the data sets. Additionally, VMD% and ground speed were input as an integer and desired pressure was output as an integer, this coarse resolution likely also contributed to the error.

The three sets of reference nozzle data collected throughout this project are summarized in table 24 and figure 53. All three data sets were collected at the same laboratory with

the same operator but on different days. The maximum difference for $D_{v0.1}$ was 8.8%, for $D_{v0.5}$ 5.4%, and for $D_{v0.9}$ 6.8%. While these differences are not large, they would be enough to change the droplet classification at some operating points. It should be noted that the difference in measurement between two consecutive days is much smaller than that of between March 2019 and December 2020. These results are in alignment with a study by Fritz et al. (2014) which compared similar data from multiple labs and on multiple days concluding that day-to-day variance in droplet size measurement within a laboratory was approximately 5% while variation between laboratories was 4% – 8%.

Table 24 - Variation in droplet size measured from reference nozzles on three different days but at the same laboratory and with the same operator.

		$D_{v0.1}$	$D_{v0.5}$	$D_{v0.9}$
VF/F	19-Mar-19	65	141	241
	7-Dec-20	65	142	247
	8-Dec-20	64	141	247
	max. difference	1.6%	0.6%	2.8%
F/M	19-Mar-19	121	262	425
	7-Dec-20	117	260	425
	8-Dec-20	116	258	423
	max. difference	4.6%	1.5%	0.5%
M/C	19-Mar-19	180	380	590
	7-Dec-20	169	376	596
	8-Dec-20	167	372	595
	max. difference	7.2%	2.3%	0.9%
C/VC	19-Mar-19	207	446	748
	7-Dec-20	197	438	738
	8-Dec-20	196	435	737
	max. difference	5.8%	2.5%	1.5%
VC/XC	19-Mar-19	256	542	856
	7-Dec-20	239	522	838
	8-Dec-20	238	519	838
	max. difference	7.3%	4.6%	2.2%
XC/UC	19-Mar-19	340	692	1086
	7-Dec-20	314	662	1016
	8-Dec-20	312	656	1037
	max. difference	8.8%	5.4%	6.8%

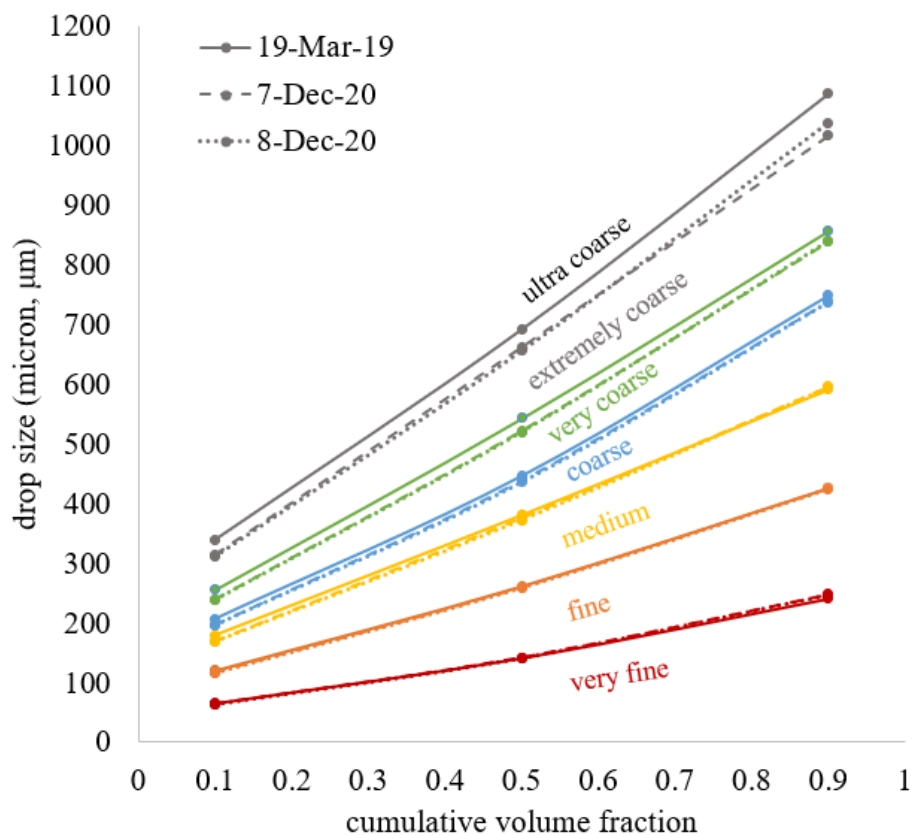


Figure 53 -Variation in droplet size measured from reference nozzles on three different days but at the same laboratory and with the same operator.

5.4 CONCLUSION

The project objective to implement a control system to automatically target (via carrier pressure and metering stem position settings) a desired droplet spectra and desired flow rate based on product application rate was accomplished by the work described in this chapter. With the nozzle control algorithm implemented in LabVIEW, validation data were collected to determine flow rate and droplet size error.

Data were collected at 135 operating points spanning the nozzle operating envelope from which flow error was determined. Actuator position and measured pressure at each steady state operating point were used to calculate expected flow rate.

The difference between expected flow rate and measured flow rate was an indication of how well the linear curve fit modeled the performance of the nozzle. Flow error for blue nozzle01 ranged from -7.5% – 34.8% with thirteen operating points having greater than 10% flow error. Flow error for green nozzle01 ranged from -10.4% – 22.9% with seven points outside of $\pm 10\%$. The most significant flow error occurred at low system pressures and high nozzle actuator position (i.e., small orifice size) and so avoiding operation at pressures below 207 kPa would eliminate the most significant flow error. This could be accomplished by adjusting the operating envelope in the nozzle parameter files.

Data were collected at the PAT Lab at twenty-five operating points spanning the nozzle operating envelope from which droplet size error was determined. Commanded position and measured pressure at each operating point were used to calculate expected $D_{v0.5}$ droplet size. Error between expected droplet size and measured droplet size ranged from -2.9% – 6.2% for blue nozzle01 and from -9.5% – 5.0% for green nozzle01. For both blue and green nozzles the algorithm tends to over-predict droplet size in the middle of the operating range and under-predict droplet size on the edges of the operating range, particularly at low pressures. This is related to the linear curve fit where a flat plane was fitted to a slightly non-linear data set. However, the error is small and the linear approximation seems justified especially when considering the complexity of implementing a non-linear control algorithm.

Final system validation was done to assess the ability of the control system to maintain a constant flow rate while changing droplet size and to understand the transition in droplet spectra at $D_{v0.5}$ values separating the classification boundaries. Across nine constant-flow operating points, flow error for the blue nozzle ranged from 1.6% – 7.8% and error in

$D_{v0.5}$ droplet size ranged from -4.8% – 3.0% while flow error for the green nozzle ranged from -10.2% – 0% and error in $D_{v0.5}$ droplet size ranged from -9.4% – 4.7%.

Data were also collected to evaluate how well the control system could maintain constant droplet size while varying flow rate. For the blue nozzle, three points on a line of constant droplet size deviated from the target by -15 to 6 μm . This resulted in -4.8% – 0% droplet size error while flow error for these same points was 7.8% – 23.9%. It is worth noting that the point with 23.9% error was in the small area of high error that occurred at in the low pressure, high motor step portion of the operating range as discussed above. For the green nozzle, three points on a line of constant droplet size deviated from the target by -33 to -1 μm . Droplet size error was -8.1% – -0.1% and flow error was 0% – 4.3%.

Three sets of reference nozzle data collected throughout this project were compared and maximum difference for $D_{v0.1}$ was 8.8%, for $D_{v0.5}$ 5.4%, and for $D_{v0.9}$ 6.8%. While these differences are not large, they would be enough to change the droplet classification at some operating points. The difference between the measurements taken on two consecutive days was much smaller than that the measurement done the previous year.

CHAPTER 6 RECOMMENDATIONS FOR FUTURE WORK AND SUMMARY

6.1 REDUCING FLOW ERROR WITH HIGHER ORDER CURVE FITS

The control system developed in this project produced favorable results across most of the modified VariTarget nozzle operating range, however, the linear math model for flow caused errors at the extremes of the operating envelope that exceed the acceptable range of $\pm 10\%$. Investigation using higher order curve fits showed favorable results. Four variations of polynomial curve fits, summarized in table 25, were evaluated on the blue nozzle flow validation data that was discussed in section 5.1.

Table 25 - Higher order polynomial curve fits done on blue nozzle flow validation data.

curve fit label	polynomial degree		polynomial equation and coefficients					R ²	RMSE
	pressure (x)	position (y)							
expectedFlow11	1	1	$\text{flow} = p00 + p10*x + p01*y$ <p style="text-align: center;"> $\begin{array}{ccc} p00 & p10 & p01 \\ 2.565 & 0.006208 & -0.00354 \end{array}$ </p>					0.9829	0.1052
expectedFlow21	2	1	$\text{flow} = p00 + p10*x + p01*y + p20*x^2 + p11*x*y$ <p style="text-align: center;"> $\begin{array}{ccccc} p00 & p10 & p01 & p20 & p11 \\ 1.367 & 0.01036 & -0.00139 & 5.89E-07 & -7.80E-06 \end{array}$ </p>					0.9985	0.03228
expectedFlow12	1	2	$\text{flow} = p00 + p10*x + p01*y + p11*x*y + p02*y^2$ <p style="text-align: center;"> $\begin{array}{ccccc} p00 & p10 & p01 & p11 & p02 \\ 1.964 & 0.01069 & -0.00371 & -7.80E-06 & 2.02E-06 \end{array}$ </p>					0.9997	0.01535
expectedFlow22	2	2	$\text{flow} = p00 + p10*x + p01*y + p20*x^2 + p11*x*y + p02*y^2$ <p style="text-align: center;"> $\begin{array}{ccccc} p00 & p10 & p01 & p20 & p11 & p02 \\ 2.002 & 0.01037 & -0.00371 & 5.83E-07 & -7.80E-06 & 2.02E-06 \end{array}$ </p>					0.9997	0.01481

The curve fit polynomials were applied to the flow validation data for blue nozzle01 as shown in figures 54 and 55. Although the linear, first-order, curve fit (expectedFlow11) had an r-squared value of 0.98 there was still significant error at some operating points.

The curve fit that was second-order on pressure and first-order on position

(expectedFlow21) yielded a marginal increase in r-squared value but RMSE was an order

of magnitude lower, resulting in a significant reduction in absolute error. The curve fits that were first-order on pressure and second-order on position (expectedFlow12) and second-order on pressure and position (expectedFlow22) showed similar, but incrementally better, results.

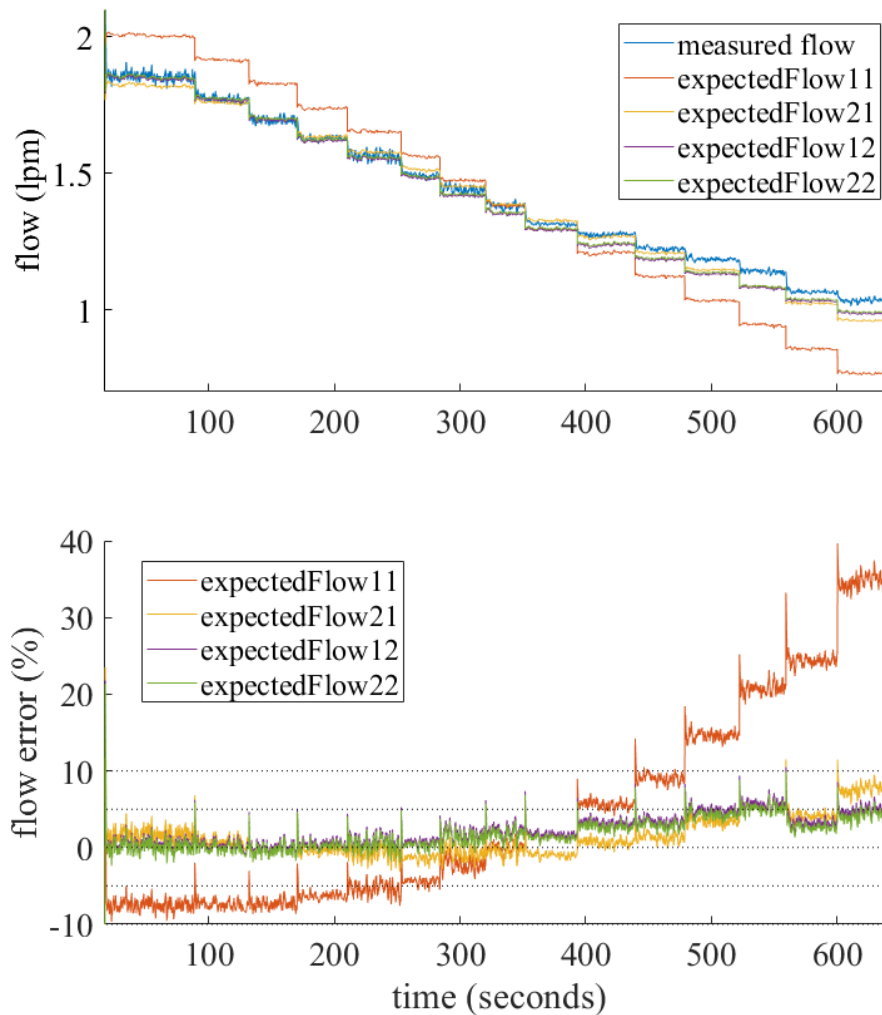


Figure 54 – Plot of blue nozzle01 measured flow along with four variations of expected flow calculated from alternative polynomial curve fits. Data shown is for the lowest pressure of the flow validation data set presented in chapter five.

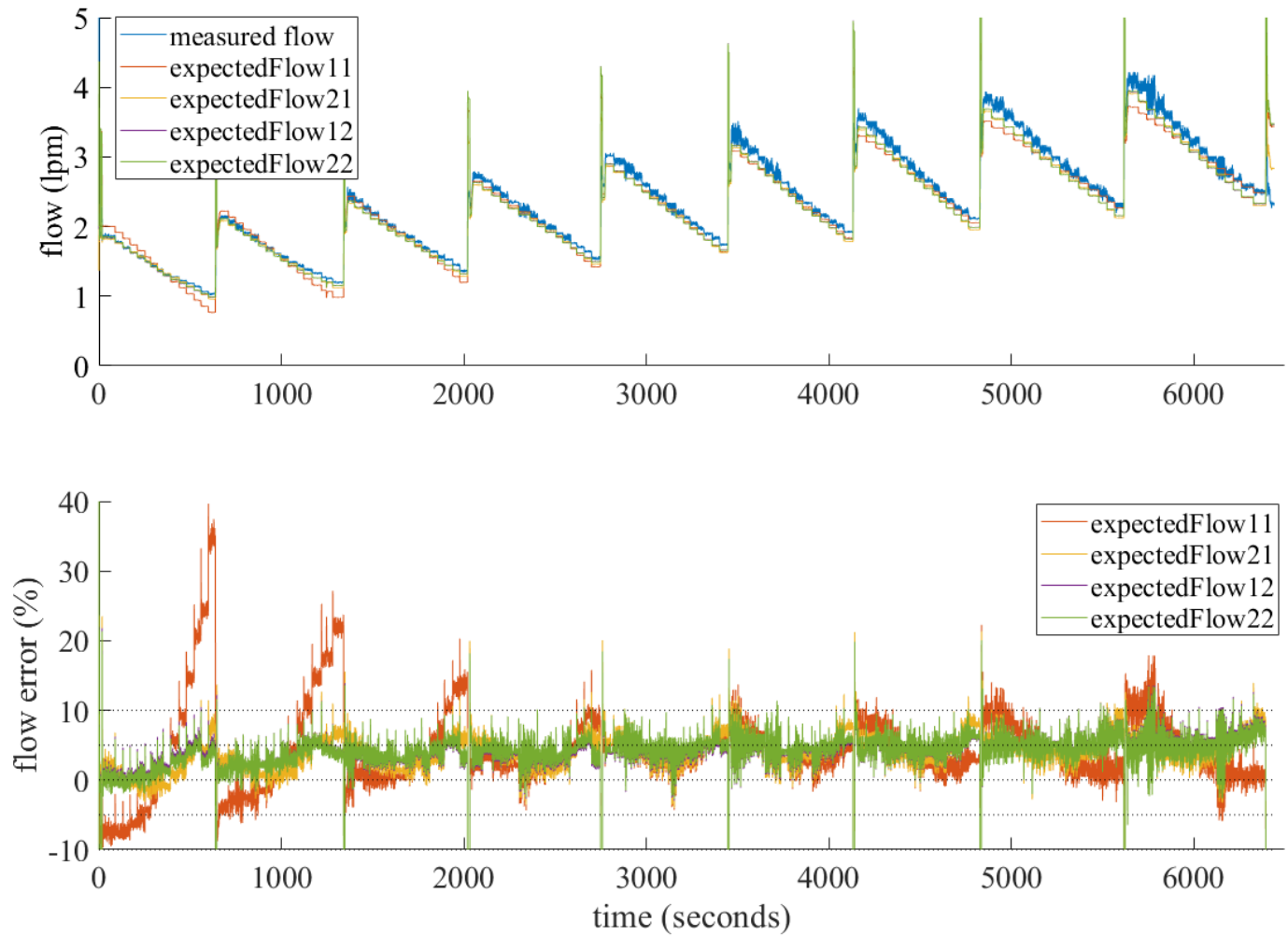


Figure 55 - Plot of blue nozzle01measured flow along with four variations of expected flow calculated from alternative polynomial curve fits. Data shown is for all operating points in the flow validation data set presented in chapter five.

Although polynomial expectedFlow22 produced the best results of the polynomials that were evaluated, due to the two quadratic operators it would be the most difficult to implement in the nozzle control algorithm and most computationally intensive in software. Therefore, it is recommended for future work to investigate use of the polynomial that is first-order for pressure and second order for position (expectedFlow12) as this has lower error than the polynomial second-order on pressure and first order on position (expectedFlow21) and offers less complexity than the polynomial second-order on pressure and position (expectedFlow22).

Figures 56 and 57 show flow error for polynomial expectedFlow12 applied to five blue nozzles using coefficients from nozzle01. Except for nozzle05, the error for all nozzles was reduced from -14% – 40.9% (table 14) to -7% – 10% across the entire operating envelope.

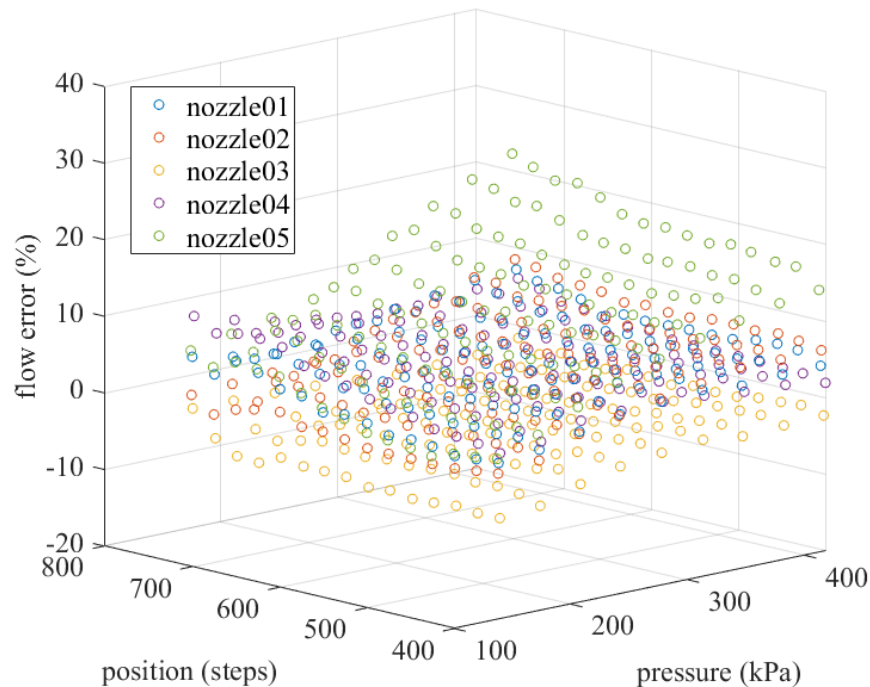


Figure 56 - Flow error vs. pressure and position for five nozzles using nozzle01 coefficients with a polynomial first-order on pressure and second-order on position. Compare to figure 40 which used first-order polynomial for pressure and position.

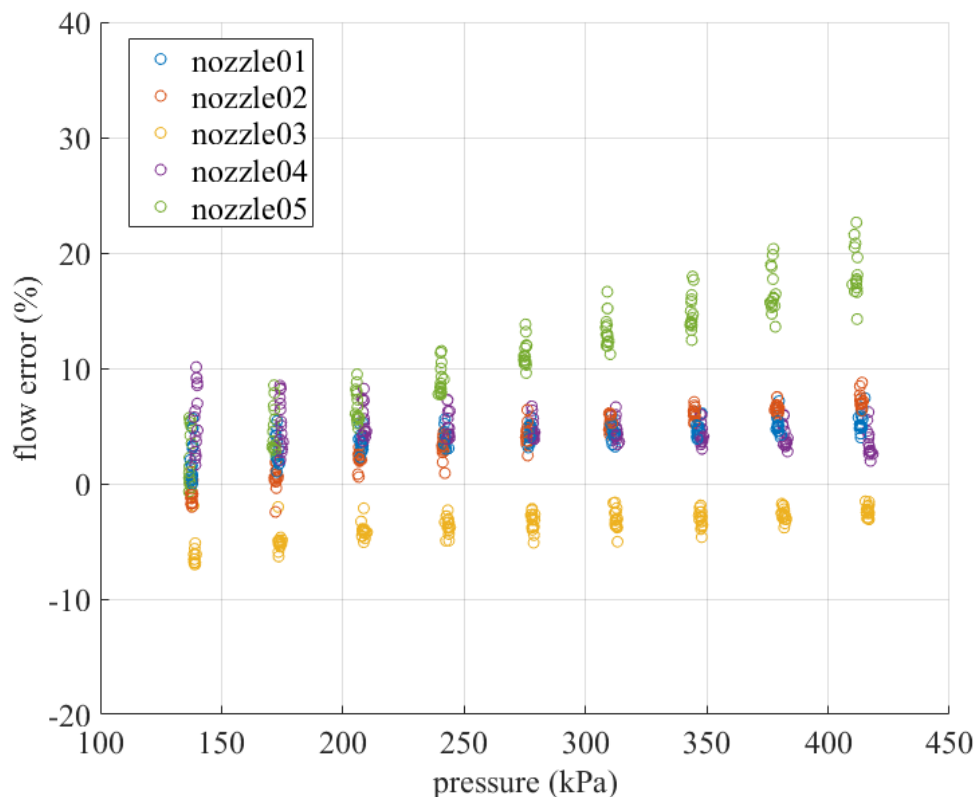


Figure 57 - Flow error vs. pressure for five blue nozzles using nozzle01 coefficients with a polynomial first-order on pressure and second-order on position.

This may allow a curve fit based on data from a single nozzle to produce acceptable performance for many nozzles in a spray system. However, integrating non-linear equations in the control system presents some challenges.

6.2 POTENTIAL APPLICATION OF CONTROL METHOD TO PWM NOZZLES

PWM actuated nozzles are in widespread use in modern agriculture and, while their primary intent is to maintain constant droplet size while varying flow rate, Giles (1996) confirmed experimentally that flow rate and droplet size can be controlled independently. Giles (1997) experimented with several spray nozzles and concluded that the VMD could be controlled over a

two- to threefold range independently of flow rate. Figure 58 shows the relationship between the four variables related to nozzle performance for a PWM nozzle: droplet size, flow rate, pressure, and effective orifice size (i.e., duty cycle, or percent modulation). From the graph it is apparent that flow can be varied across relatively constant droplet size at constant pressure and that droplet size can be varied across a range of constant flow at varying pressure and duty cycle. This is analogous to the modified VariTarget nozzle assemblies used in this study where flow is a function of PWM duty cycle instead of metering stem position. Giles declares that “Within the envelope, any combination of flow and droplet size can be achieved by exciting the valve/nozzle device with a corresponding PWM duty cycle and liquid supply pressure.” Giles continues, “While variable rate technology has been extensively investigated, control of droplet size has not been demonstrated in real time applications. Such capability may reduce off-target movement, e.g., "spray drift" in sensitive areas by allowing the operator to specify desired droplet sizes to be used in specified geographic areas.”

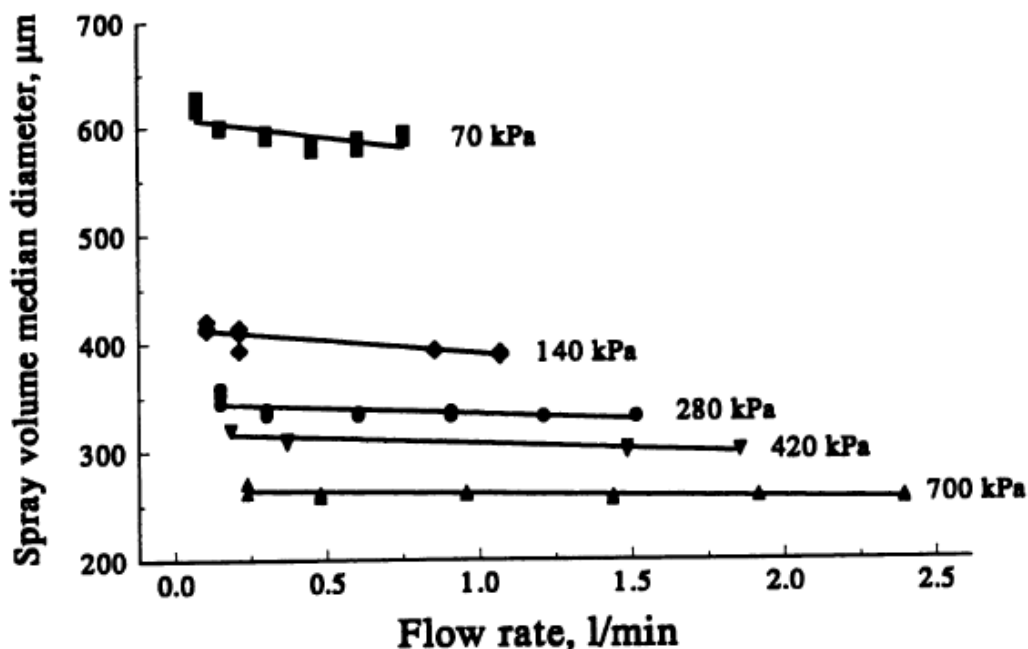


Figure 58 - Spray volume median diameter for various pressures and flow rates achieved by 10% – 100% modulation of control valve with an 8004 nozzle (Giles, 1996).

A related article describes a field experiment where PWM nozzles were used to demonstrate an active drift control concept by maintaining rate and speed but adjusting pressure to change droplet size on demand (Giles, 2009). During the demonstration, the operator was provided wind speed and direction from an on-board weather station and pressure was decreased to increase droplet size in areas of high wind, and vice versa, while the PWM system allowed the application rate to remain the constant.

A more recent study on droplet size performance for PWM nozzles provides data that also shows a relationship between duty cycle, pressure, and droplet size (fig. 59) (Butts, 2019). This study evaluated several spray tips installed on a PWM nozzle body at various duty cycles and pressures. Consistent with what was presented by Giles (1997), the data showed that as PWM duty cycle decreases, spray droplet size slightly increases, at constant pressure, and as pressure

increases, droplet size decreases. Although flow rates were measured for some nozzles evaluated in the study, the flow rate data were not reported.

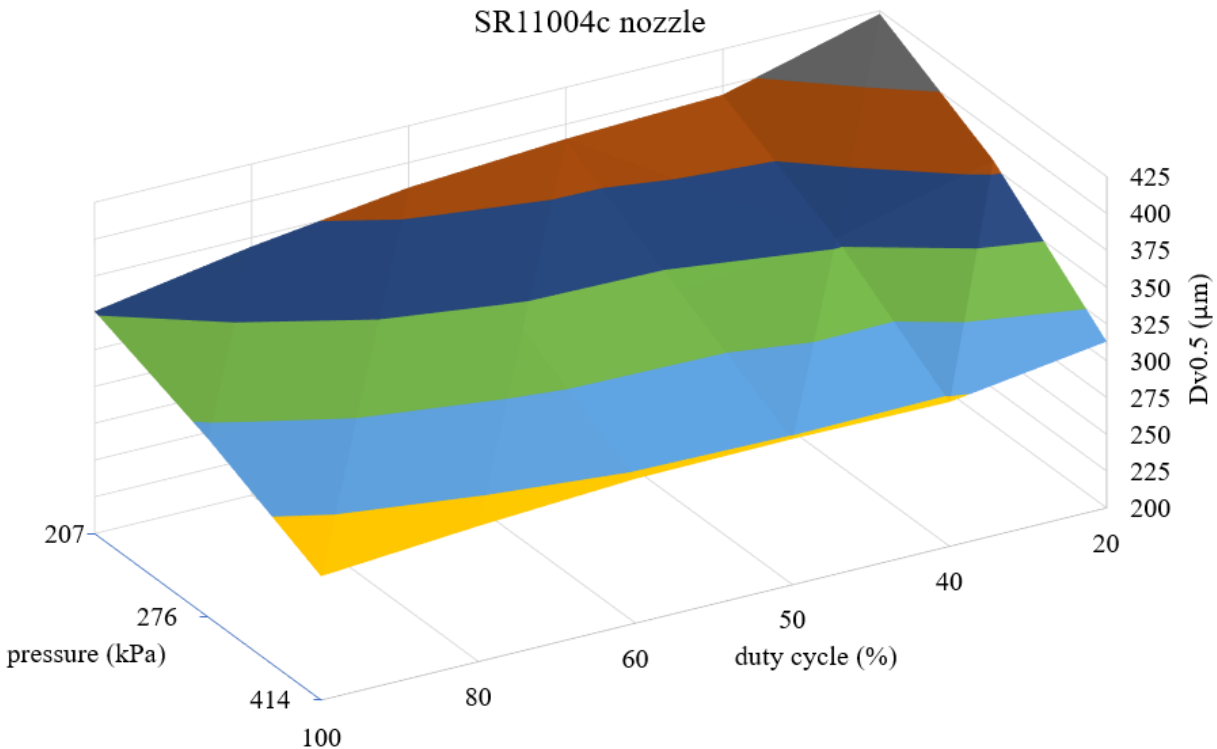


Figure 59 - Surface plot created from data published by Butts, et al. (2019) showing the relationship between pressure, duty cycle and volume median diameter for SR11004c nozzle.

Wei, et al. (2021) studied the relationship of droplet size spectrum, activation pressure, and flow rate from PWM nozzles produced by different manufacturers. From this study, much of the same conclusions as can be drawn as from the data collected by Butts, et al. (2019) and Giles (1997). Future work could include investigating whether the variable-orifice nozzle control method developed in this project could be applied to PWM nozzles for real-time, independent control of flow rate and droplet size where effective orifice size is a function of PWM duty cycle and droplet size is a function of system pressure.

6.3 POTENTIAL CONTROL FEATURES ENABLED BY GPS

With the current control system configuration, the operator must select a desired ground speed and operate the vehicle to closely adhere to that speed to ensure accurate application rate.

However, input from the virtual ground speed selector in the UI could be replaced with a signal from a real time speed sensor connected to the spray system controller. This input, from GPS, radar, or other ground speed sensors, as is done with existing commercial rate controllers, would alleviate of the operator of having to constantly monitor ground speed and make continuous adjustment, resulting in lower application error and reduced operator fatigue. This would also enable other features such as turn compensation where application error during turning could be reduced by adjusting individual nozzle flow rates across the boom while maintaining desired droplet size.

In his patent, Hillger (2017) describes a concept where a spray system would automatically adjust, including altering droplet size, when in close proximity to an area sensitive to spray drift. With addition of GPS input for the embedded controller and associated logic in the software, the control system developed in this project could be adapted to this type of operation where droplet size could change automatically based on geo-location while still maintaining the appropriate application rate. Similarly, Butts et al. (2018) introduced a concept for droplet-size based site-specific weed management which could be implemented in the same way with the variable-orifice nozzle control system. Their study concluding that droplet size is a significant factor in weed control efficacy for both systemic and contact herbicides. Future work could include adding GPS input to the control system to facilitate these uses.

6.4 OTHER POTENTIAL CONTROL FEATURES, DESIGN OPORTUNITIES, AND APPLICATIONS

Weather sensor inputs could be integrated into the control system to enable real-time droplet size control in reaction to changes in local environmental conditions (e.g., wind speed) to mitigate off-target drift. This could be implemented with the intent to limit drift to a determined distance from the spray applicator or in combination with proximity to sensitive areas.

Further development of this control system could include active control of system pressure. A closed loop control strategy, such as PID or Fuzzy Logic, could be implemented within the existing embedded controller and control system software to automatically regulate system pressure based on desired pressure specified by the algorithm. An analog or digital signal could be output from the controller to actuate a pressure regulating valve, bypass valve, or, more directly, to control a variable speed hydraulic motor or electric motor driving a pump.

Future work could also include redesign and optimization of the variable-orifice nozzle assembly that was used in this project. Future design goals could include hardware integration to reduce cost and make a more compact design that is practical for commercial implementation.

Designing the nozzle tip to have a more linear flow and droplet size output would minimize control system complexity and error with a linear system model.

Applications such as irrigation, food processing, or other industrial uses could be investigated and the variable-orifice nozzle redesigned to provide optimized range of droplet size and flow for these uses. For example, the system could be adapted for industrial applications where it is necessary to maintain desired droplet size for spraying a product transported on a conveyor. In

this application constant droplet size could be maintained while flow rate is varied to keep coverage rate constant as conveyor speed, or product throughput, changed. With the same installation, droplet size could also be changed on-the-go as different products are processed on the conveyor.

The variable-orifice nozzle control method is well suited for supporting development of robotic and autonomous farming systems of the future. The ability to change spray system settings on-the-go, and without operator intervention, could enable an autonomous sprayer to automatically adapt to different pesticide applications as it moves between fields and crops. Automated setup could include functionality where an operator could scan a product label and the spray system would auto-adjust based on product and application requirements, or for a network connected machine this could be done remotely while the sprayer is supplied by an automated in-field tender.

6.5 SUMMARY

Real-time simultaneous flow rate and droplet size control for variable-orifice spray nozzles was successfully demonstrated with the control method developed in this project. The prototype spray system had a turn down ratio of approximately five-to-one and maintained spray quality while being able to span up to four droplet spectra with a single nozzle tip. To date, no commercially available product with this capability exists.

Applying this control technology to agricultural sprayers can improve operational efficiency and diminish operator pesticide exposure by reducing the need to change nozzles tips. This adaptable

control system lends itself to the integration of existing spray control processes such as rate control and automatic turn compensation. With these processes, the control method developed in this project could maintain consistent spray quality and droplet size while operating over a wide range of speeds as opposed to the traditional implementation of these processes with fixed orifice nozzles where spray quality may be compromised as flow rates are changed. Additionally, the variable-orifice control method provides a foundation for future development of novel spray technologies including site-specific droplet management for improved pesticide efficacy and weather-based spray droplet management to mitigate off-target drift. The ability of the control system to automatically adjust system settings based on predetermined operating parameters, or in reaction to real-time sensor inputs, makes it well suited for robotic and autonomous spray systems that are likely to play a role in future production ag systems.

REFERENCES

ANSI/ASABE. 2018. S572.2. Spray Nozzle Classification by Droplet Spectra. St. Joseph, MI. ASABE.

ASTM. 2006. E 641-01. Standard Methods for Testing Hydraulic Spray Nozzles Used in Agriculture. West Conshohocken, PA. ASTM International.

Bradley, K. 2017. A final Report on Dicamba-injured Soybean Acres. University of Missouri. https://ipm.missouri.edu/IPCM/2017/10/final_report_dicamba_injured_soybean/. Accessed 25March2019.

Bui, Q.D. 24Oct2006. Nozzle with Flow Rate and Droplet Size Control Capability. U.S. Patent 7,124,964 B2.

Butts, T.R., Samples, C.A., Franca, L.X., Dodds, D.M., Reynolds, D.B., Adams, J.W., Zollinger, R.K., Howatt, K.A., Fritz, B.K., Hoffmans, W.C., Kruger, G.R. 2018. Spray droplet size and carrier volume effect on dicamba and glufosinate efficacy. *Pest Management Science*. Vol. 74 Issue 9. pp. 2020-2029. <https://doi.org/10.1002/ps.4913>.

Butts, T.R., Butts, L.E., Luck, J.D., Fritz, B.K., Hoffman, W.C., Kruger, G.R. 2019. Droplet size and nozzle tip pressure from a pulse-width modulation sprayer. *Biosystems Engineering*, Volume 178, 2019, pp. 52-69, ISSN 1537-5110, <https://doi.org/10.1016/j.biosystemseng.2018.11.004>.

Creech, C.F., Moraes, J.G., Henry, R.S., Luck, J.D., Kruger, G.R. 2016 The Impact of Spray Droplet Size on the Efficacy of 2,4-D, Atrazine, Chlorimuron-Methyl, Dicamba, Glufosinate, and Saflufenacil. *Weed Technology*, 30(2):573-586. Weed Science Society of America. <https://doi.org/10.1614/WT-D-15-00034.1>.

EPA. 2017. Pesticide Industry Sales and Usage 2008-2012 Market Estimates. Available at: <https://www.epa.gov/pesticides/pesticides-industry-sales-and-usage-2008-2012-market-estimates>. Accessed 24March2019.

Fishel, F.M., Ferrell, J.A. 2016. Managing Pesticide Drift. Institute of Food and Agricultural Sciences Extension Service, University of Florida. PI232.

Fritz, B.K., Hoffman, W.C., Kruger, G.R., Henry, R.S., Hewitt, A., Czaczyk, Z. 2014. Comparison of Drop Size Data from Ground and Aerial Application Nozzles at Three Testing Laboratories. *Atomization and Sprays*, 24 (2): 181–192 (2014).

Funseth, T.G., Mercer, D.S., Humpal, R.A. 30Dec2014. Arrangement for Switching Nozzles On the Go for Controlling Spray Rate. U.S. Patent 8,919,676 B2.

Giles, D.K., Comino, J.A. 1992. Electronically Actuated Variable Flow Control System. U.S. Patent 5,134,961.

Giles, D.K., Henderson, G.W., Funk, K. 1996. Digital Control of Flow Rate and Spray Droplet Size from Agricultural Nozzles for Precision Chemical Application. Precision Agriculture. ASA-CSSA-SSSA. Madison, WI.

Giles, D.K. 1997. Independent Control of Liquid Flow Rate and Spray Droplet Size From Hydraulic Atomizers. *Atomization and Sprays*. Vol. 7. pp. 161-181.

Giles, D.K. 16Sept2009. New Spray Technology Delivers Variable Rate Application without a Change in Droplet Size. GRDC Update Papers. Australian Government Grains Research and Development Corporation. <https://grdc.com.au/resources-and-publications/grdc-update-papers/tab-content/grdc-update-papers/2009/09/new-spray-technology-delivers-variable-rate-application-without-a-change-in-droplet-size>. Accessed 13Feb2021.

Hanna, M., Kruckeberg, J., Darr, M., Steward, B. 2009. Nozzle and droplet size effects on pesticide performance and drift. Proceedings of the Integrated Crop Management Conference – Iowa State University.

Hillger, D.E., Jones-Jefferson, T.J., Palmer, D.M. 2017. Spray Drift Systems and Methods. U.S. Patent No. 9,743,655 B2.

Kruckeberg, J.P. 2011. An Automated Nozzle Controller for Self-Propelled Sprayers. Iowa State University. MS Thesis.

Kruger, G.R. Personal communication. 30Oct2020.

Kruger, G.R., Klein, R.N., Ogg, C.L. 2013. Spray Drift of Pesticides. NebGuide G1773. University of Nebraska-Lincoln. Lincoln, NE.

Leonard, R. 2016. Interim study to complete the LR 309 (2014) interim draft report and finalize recommendations to the Legislature.

https://nebraskalegislature.gov/pdf/reports/committee/agriculture/LR536_2016.pdf. Accessed 25March2019.

Luck, J.D. 2012. Development of a Variable-Orifice Spray Nozzle with High Pressure Chemical Injection for Improved Pesticide Efficacy. University of Kentucky. PhD Dissertation.

- Luck, J.D., Pitla, S.K., Sama, M.P., Shearer, S.A. 2015. Flow, Spray Pattern, and Droplet Spectra Characteristics of an Electronically Actuated Variable-Orifice Nozzle. Transactions of the ASABE. Vol. 58(2): 261-269. DOI 10.13031/trans.58.10798.
- Luck, J.D., Shearer, S.A., Sama, M.P., Pitla, S.K. 2015. Control System Development and Response Analysis of an Electronically Actuated Variable-Orifice Nozzle for Agricultural Pesticide Applications. Transactions of the ASABE. Vol. 58(4): 997-1008. DOI 10.13031/trans.58.10945.
- Magnus, D.L., Sharda, A., Engelhardt, A., Flippo, D., Strasser, R., Luck, J.D., Griffin, T. 2017. Analyzing the Nozzle Spray Fan Pattern of an Agricultural Sprayer Using Pulse Width Modulated Technology to Generate an On-Ground Coverage Map. Transactions of the ASABE. 60(2): 315-325. (doi: 10.13031/trans.11835).
- Micron Group. 2002. Micromax Instruction Manual. Micron Group. Bromyard, Herefordshire, UK. https://www.microngroup.com/files/micromax_manual_rev__4.pdf. Accessed 29Jan2021.
- Micron Group. 2021. Micromax. <https://www.microngroup.com/agricultural/micromax1>. Accessed 29Jan2021.
- Sharda, A., Griffin, T., Haag, L., Mangus, D., Fulton, J., Slocombe, F. 2016. Pulse Width Modulation (PWM) Technology for Liquid Application. Kansas State University.
- SprayTarget. 2009. VariTarget Variable Flow Rate Nozzle. <http://spraytarget.com/VariTarget-Brochure-2009.pdf>. Accessed 19Nov2020.1
- Spray Systems Co. 2014. TeeJet Technologies Catalog 51A. https://www.teejet.com/CMSImages/TEEJET/documents/catalogs/cat51a_us.pdf. Accessed 19Nov2020.
- Srivastava, A.K., Goering, C.E., Rohrbach, R.P., Buckmaster, D.R. 2006. Chemical application. Chapter 10 in Engineering Principles of Agricultural Machines, 2nd ed., 269-324. St. Joseph, Michigan: ASABE.
- Wei, Z., Zhu, H., Zang, Z., Salcedo, R., Duan, D. 2021. Droplet Size Spectrum, Activation Pressure, and Flow Rate Discharged from PWM Flat-Fan Nozzles. Vol. 64(1): 313-325 2021 American Society of Agricultural and Biological Engineers ISSN 2151-0032 <https://doi.org/10.13031/trans.14100>

APPENDIX A DRAWINGS OF SYSTEM COMPONENTS

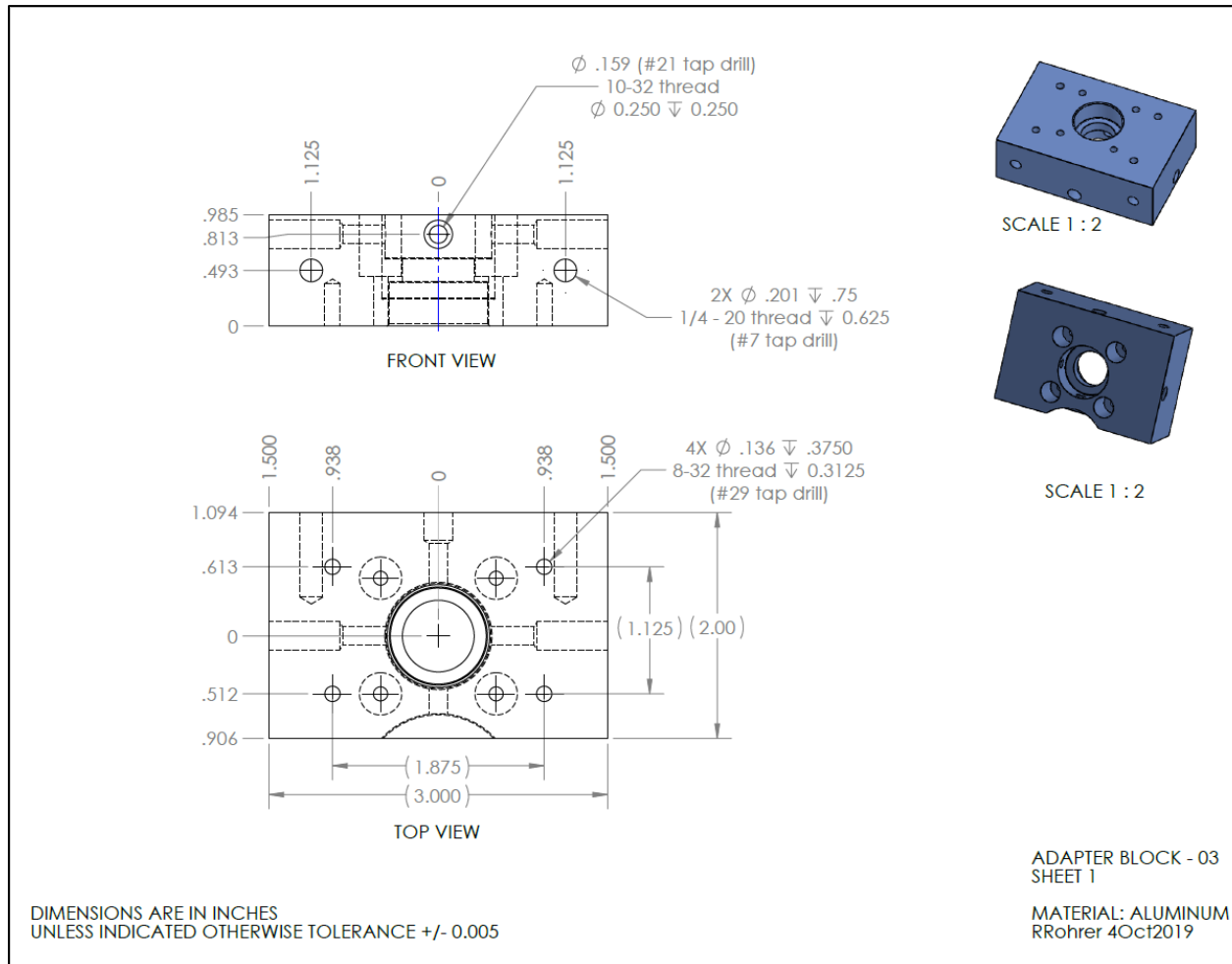


Figure 60 - Engineering drawing for nozzle assembly adapter block sheet 1.

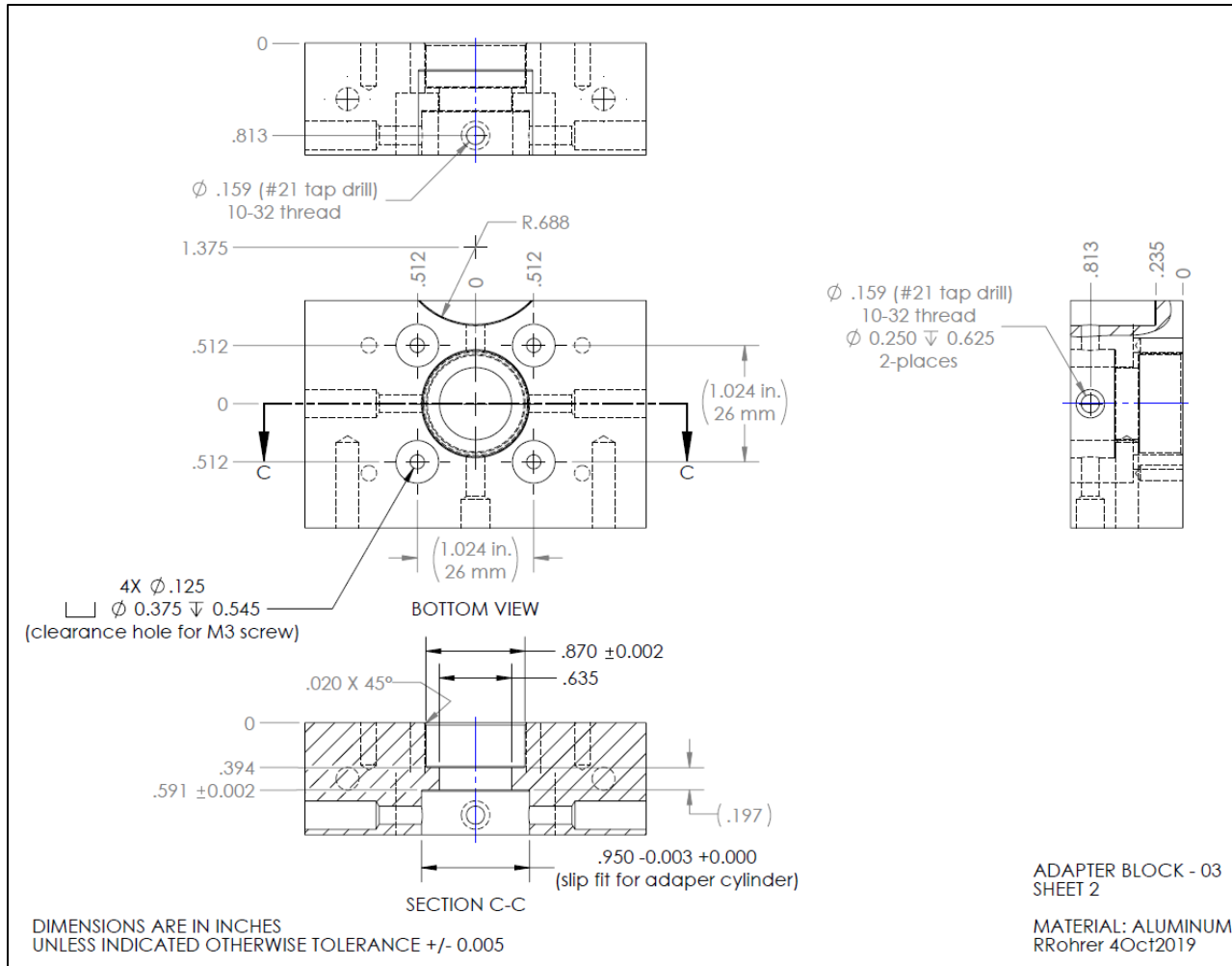


Figure 61 - Engineering drawing for nozzle assembly adapter block sheet 2.

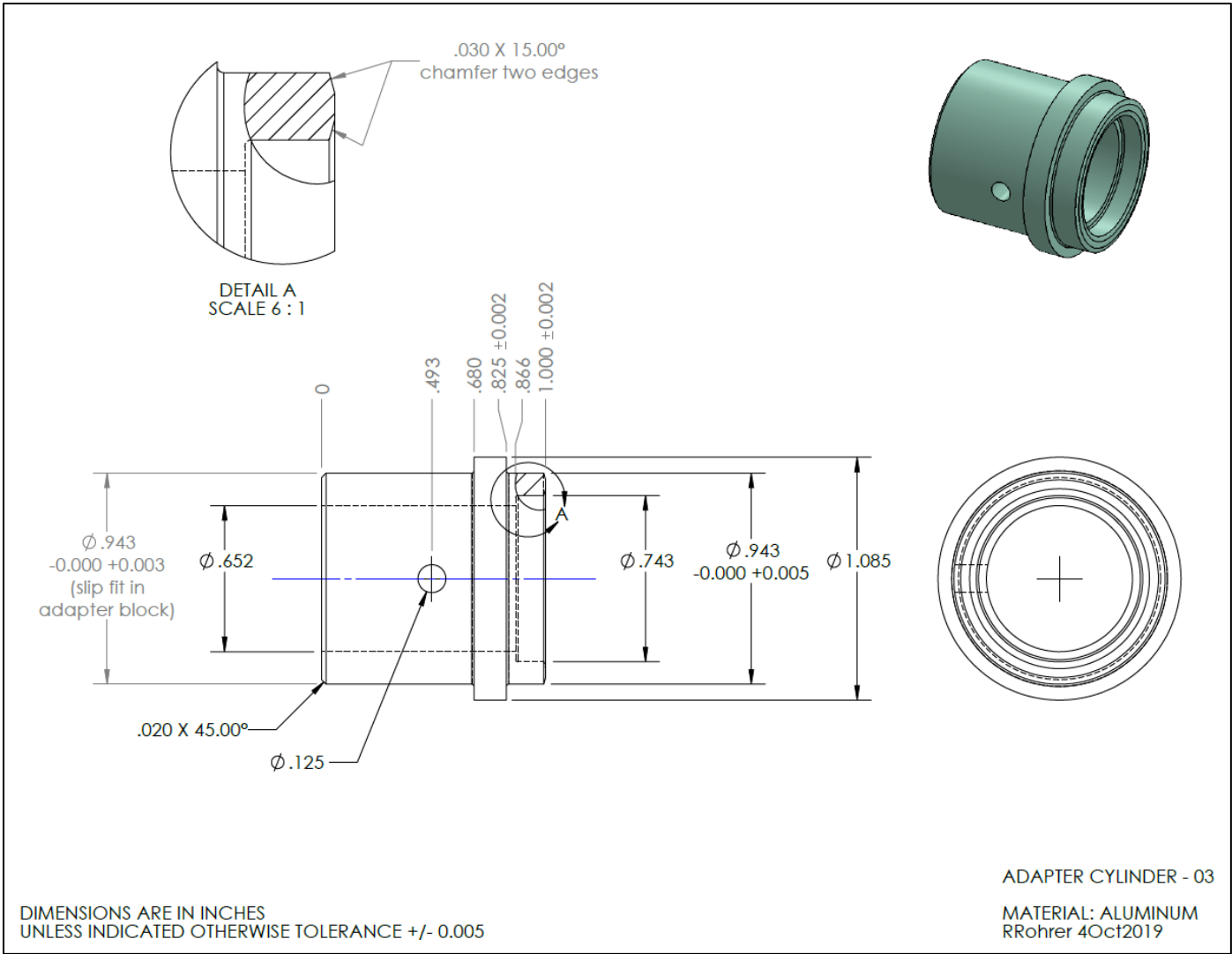


Figure 62 - Engineering drawing for nozzle assembly adapter cylinder.

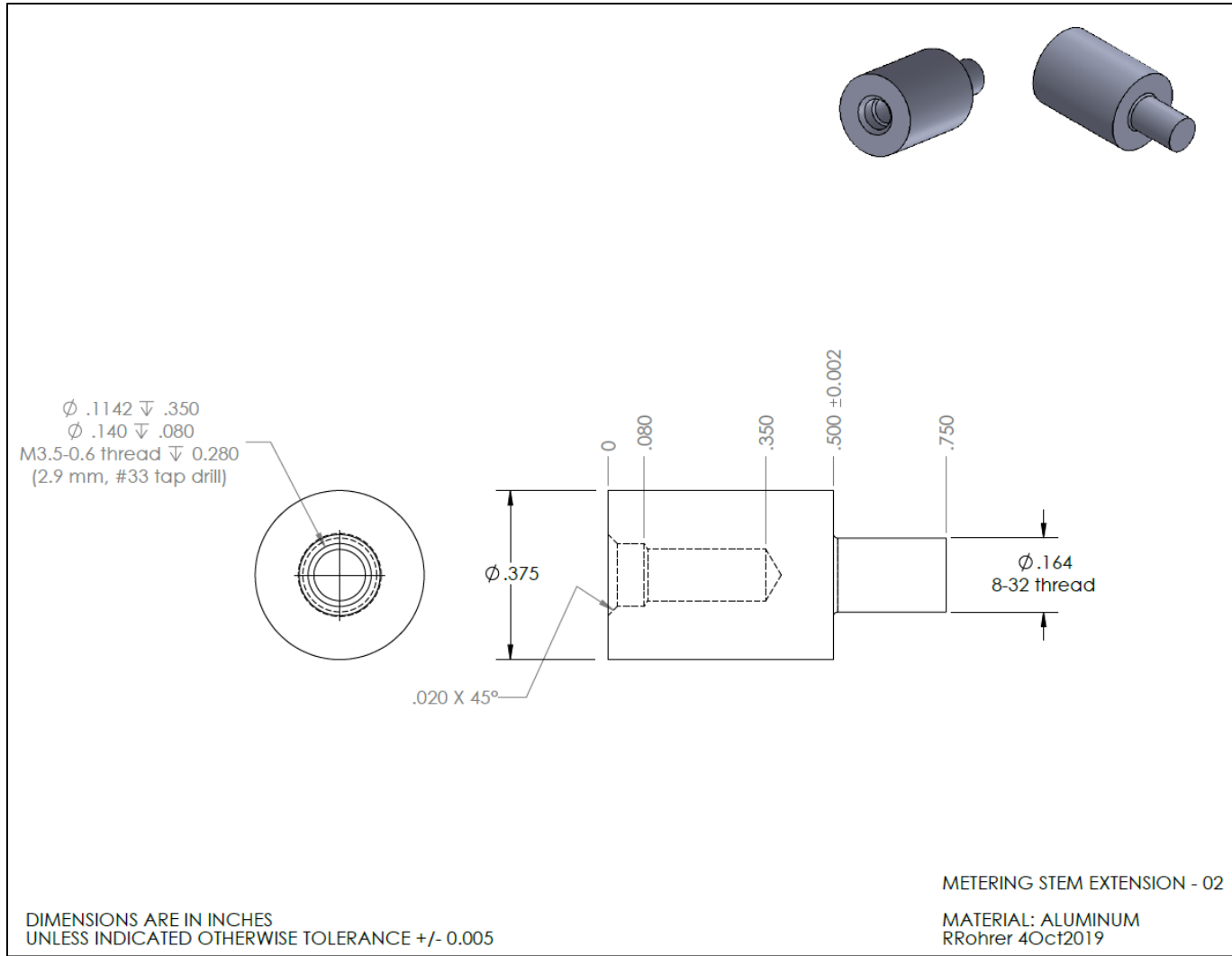


Figure 63 - Engineering drawing for nozzle assembly metering stem extension.

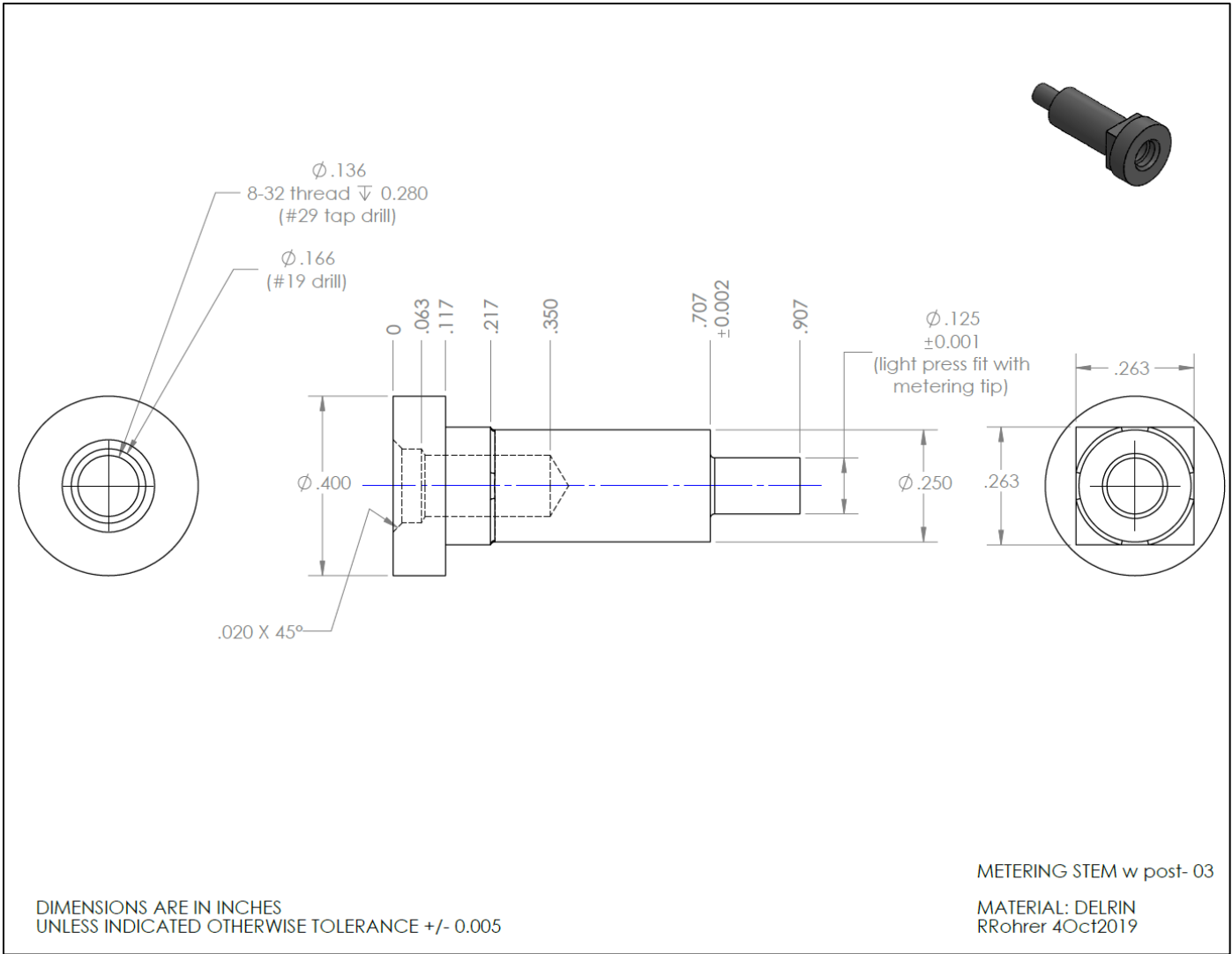


Figure 64 - Engineering drawing for nozzle assembly metering stem.

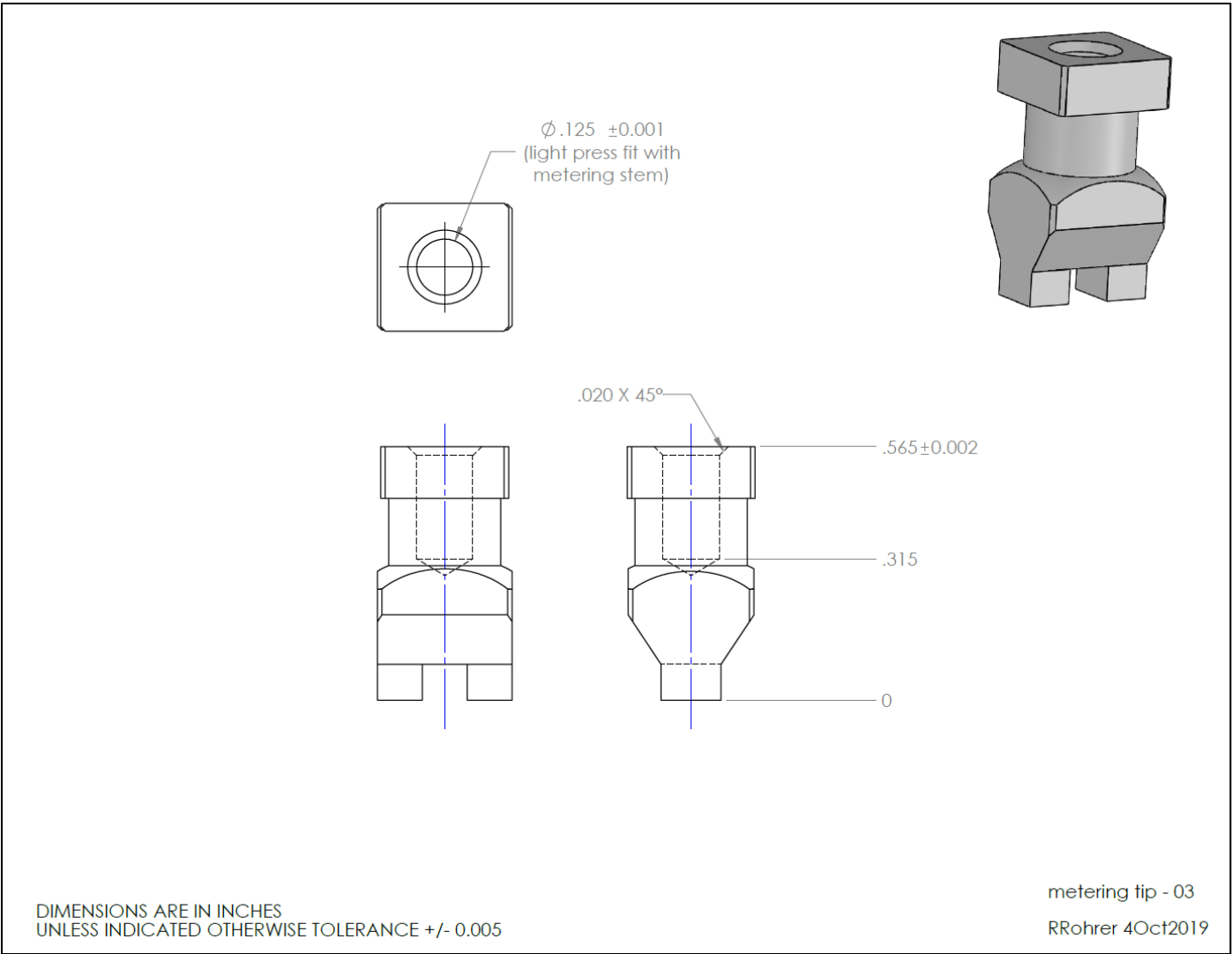


Figure 65 - Engineering drawing for nozzle assembly metering tip.

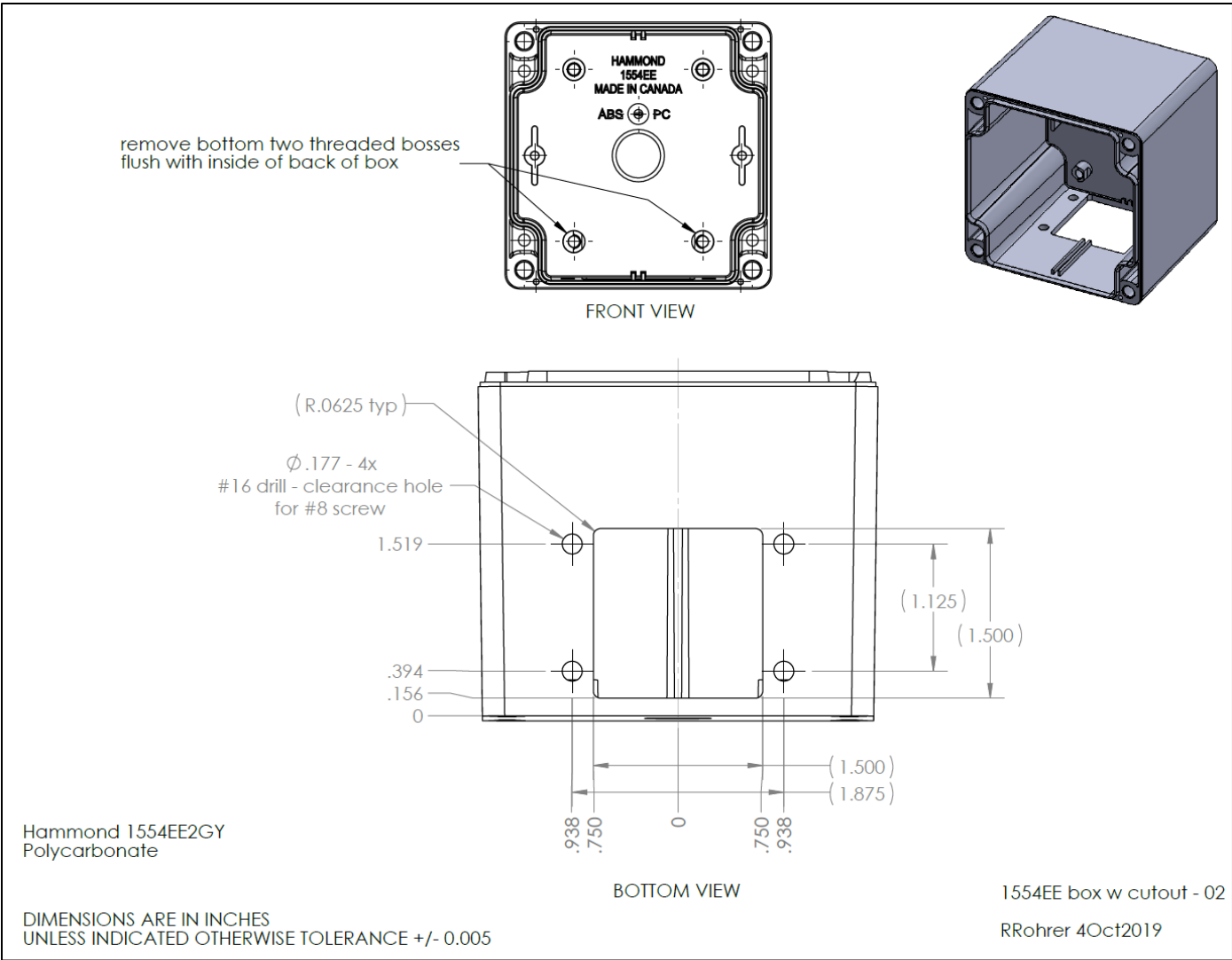


Figure 66 - Engineering drawing for nozzle assembly enclosure.

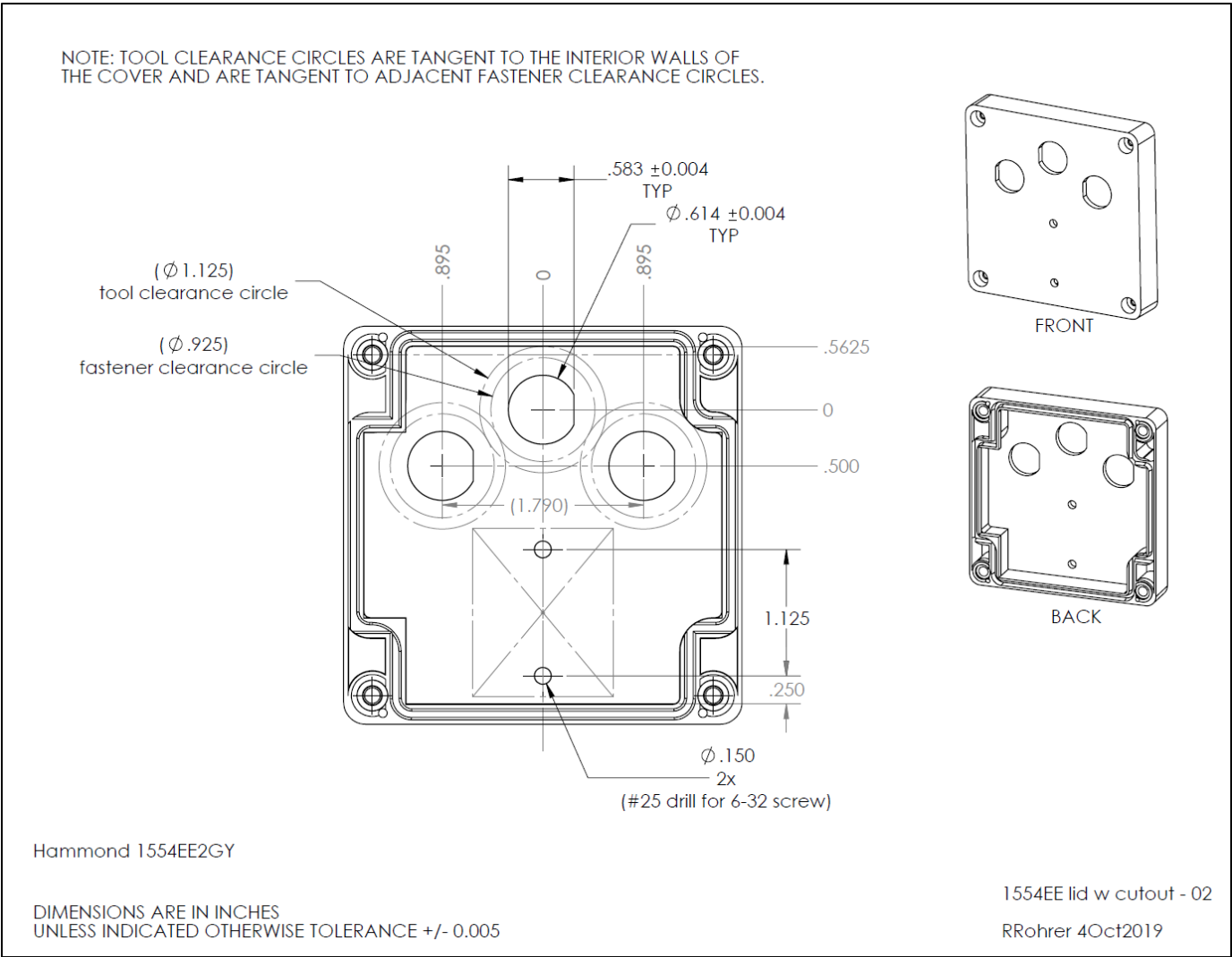


Figure 67 - Engineering drawing for nozzle assembly enclosure lid.

APPENDIX B DROPLET SPECTRA CHARACTERIZATION DATA

Table 26 - Average measured pressure, measured flow, and volume median diameter (Dv0.1, Dv0.5, and Dv0.9) for five nozzles.

nominal pressure (kPa)		red nozzle					orange nozzle				
		position (steps)					position (steps)				
		400	500	600	700	800	400	500	600	700	800
138	pressure (kPa)	--	--	--	--	--	144	146	146	146	146
	flow (lpm)	--	--	--	--	--	0.82	**	**	**	**
	Dv0.1	--	--	--	--	--	128	115	108	105	110
	Dv0.5 (μm)	--	--	--	--	--	286	264	251	245	251
	Dv0.9	--	--	--	--	--	474	460	451	444	431
207	pressure (kPa)	217	215	215	216	216	213	215	215	215	216
	flow (lpm)	**	**	**	**	**	1.15	0.96	0.84	**	**
	Dv0.1	67	68	64	70	67	117	102	95	93	98
	Dv0.5 (μm)	175	171	162	169	168	267	240	226	221	228
	Dv0.9	381	364	358	303	378	454	415	400	394	393
276	pressure (kPa)	286	286	286	286	286	281	283	283	284	285
	flow (lpm)	**	**	**	**	**	1.44	1.24	1.08	0.95	0.83
	Dv0.1	56	53	53	53	55	114	100	91	87	90
	Dv0.5 (μm)	145	137	134	132	136	262	235	217	208	213
	Dv0.9	319	301	288	264	264	450	406	388	370	365
345	pressure (kPa)	353	353	353	353	353	345	350	351	350	351
	flow (lpm)	**	**	**	**	**	1.68	1.47	1.29	1.13	1.00
	Dv0.1	50	48	48	47	48	109	98	89	85	87
	Dv0.5 (μm)	130	121	118	115	118	256	232	212	202	203
	Dv0.9	287	265	255	237	233	439	404	379	355	351
414	pressure (kPa)	419	420	420	420	420	412	414	417	419	420
	flow (lpm)	**	**	**	**	**	1.92	1.71	1.52	1.35	1.17
	Dv0.1	48	46	46	45	45	107	100	90	85	84
	Dv0.5 (μm)	120	114	110	107	106	254	236	214	202	197
	Dv0.9	271	247	232	214	207	437	410	381	357	346
483	pressure (kPa)	487	487	484	484	484	491	490	492	490	488
	flow (lpm)	**	**	**	**	**	2.17	1.99	1.77	1.58	1.39
	Dv0.1	47	45	44	43	43	98	93	87	83	79
	Dv0.5 (μm)	116	108	104	102	101	239	226	212	198	188
	Dv0.9	265	238	216	202	200	419	399	379	349	334
552	pressure (kPa)	566	560	560	558	553	551	556	556	557	559
	flow (lpm)	0.82	**	**	**	**	2.38	2.12	1.96	1.76	1.55
	Dv0.1	47	44	44	43	42	97	93	88	82	80
	Dv0.5 (μm)	115	108	105	101	98	236	225	212	198	190
	Dv0.9	247	233	213	199	181	415	400	373	350	335

** some flow rates were below the sensor operating range and so minimum measurable flow is reported

nominal pressure (kPa)		yellow nozzle					blue nozzle				
		position (steps)					position (steps)				
		400	500	600	700	800	400	500	600	700	800
138	pressure (kPa)	145	142	146	142	141	142	145	145	142	142
	flow (lpm)	1.12	0.93	0.80	**	**	1.77	1.47	1.25	0.99	0.83
	Dv0.1	142	132	118	112	116	207	177	155	143	152
	Dv0.5 (µm)	324	305	277	266	273	439	377	342	320	331
	Dv0.9	543	522	489	481	480	714	583	560	523	530
207	pressure (kPa)	217	210	207	212	208	207	210	209	211	212
	flow (lpm)	1.52	1.34	1.06	0.88	**	2.29	1.92	1.58	1.30	1.10
	Dv0.1	131	129	108	97	98	186	159	137	124	131
	Dv0.5 (µm)	302	291	254	234	235	404	351	313	284	292
	Dv0.9	504	484	437	415	411	676	570	518	473	472
276	pressure (kPa)	279	280	279	280	277	277	283	282	281	284
	flow (lpm)	1.93	1.77	1.39	1.12	0.89	2.88	2.44	2.01	1.64	1.37
	Dv0.1	127	129	104	91	89	175	151	129	119	124
	Dv0.5 (µm)	295	293	246	219	213	386	337	300	271	274
	Dv0.9	499	488	418	390	371	654	556	497	455	446
345	pressure (kPa)	351	350	350	353	352	345	348	351	350	353
	flow (lpm)	2.44	2.04	1.64	1.33	1.07	3.35	2.83	2.39	1.94	1.63
	Dv0.1	136	122	102	87	84	169	147	129	115	114
	Dv0.5 (µm)	310	279	240	208	200	369	325	295	265	257
	Dv0.9	515	469	413	370	346	622	537	489	447	420
414	pressure (kPa)	417	418	420	420	421	413	414	422	422	420
	flow (lpm)	2.84	2.35	1.92	1.58	1.28	3.86	3.33	2.81	2.37	1.91
	Dv0.1	132	116	101	86	81	157	144	127	113	107
	Dv0.5 (µm)	303	270	237	205	189	347	324	290	262	243
	Dv0.9	505	458	405	363	336	592	552	484	443	406
483	pressure (kPa)	476	481	485	487	485	478	488	493	489	490
	flow (lpm)	2.98	2.57	2.14	1.79	1.49	4.04	3.64	3.08	2.61	2.16
	Dv0.1	121	110	96	87	83	140	131	120	108	105
	Dv0.5 (µm)	284	261	229	205	193	327	299	276	251	238
	Dv0.9	481	449	399	359	336	575	500	470	426	405
552	pressure (kPa)	542	555	559	559	558	548	551	559	559	563
	flow (lpm)	3.48	2.98	2.54	2.12	1.78	4.83	4.15	3.60	3.05	2.51
	Dv0.1	121	107	96	87	83	140	129	118	108	102
	Dv0.5 (µm)	285	255	231	207	193	323	298	272	251	233
	Dv0.9	483	449	403	365	341	571	521	468	430	398

** some flow rates were below the sensor operating range and so minimum measurable flow is reported

nominal pressure (kPa)		green nozzle				
		position (steps)				
		400	500	600	700	800
138	pressure (kPa)	143	143	146	146	141
	flow (lpm)	2.55	2.16	1.83	1.51	1.16
	Dv0.1	253	215	193	182	199
	Dv0.5 (μm)	525	459	417	391	420
	Dv0.9	837	752	671	601	652
207	pressure (kPa)	210	210	212	208	212
	flow (lpm)	3.28	2.83	2.39	1.96	1.53
	Dv0.1	227	193	170	155	161
	Dv0.5 (μm)	488	428	382	349	353
	Dv0.9	803	712	639	565	569
276	pressure (kPa)	277	283	284	282	279
	flow (lpm)	4.00	3.41	2.93	2.44	1.92
	Dv0.1	203	193	171	159	161
	Dv0.5 (μm)	445	413	372	342	342
	Dv0.9	745	688	611	558	553
345	pressure (kPa)	349	353	351	349	353
	flow (lpm)	4.69	4.05	3.33	2.80	2.32
	Dv0.1	198	175	152	145	140
	Dv0.5 (μm)	422	382	342	315	308
	Dv0.9	706	656	580	512	502
414	pressure (kPa)	413	420	419	420	420
	flow (lpm)	5.27	4.62	3.88	3.30	2.74
	Dv0.1	172	151	143	131	127
	Dv0.5 (μm)	379	342	324	299	284
	Dv0.9	669	594	560	514	477
483	pressure (kPa)	--	--	--	--	--
	flow (lpm)	--	--	--	--	--
	Dv0.1	--	--	--	--	--
	Dv0.5 (μm)	--	--	--	--	--
	Dv0.9	--	--	--	--	--
552	pressure (kPa)	--	--	--	--	--
	flow (lpm)	--	--	--	--	--
	Dv0.1	--	--	--	--	--
	Dv0.5 (μm)	--	--	--	--	--
	Dv0.9	--	--	--	--	--

APPENDIX C FLOW VALIDATION DATA

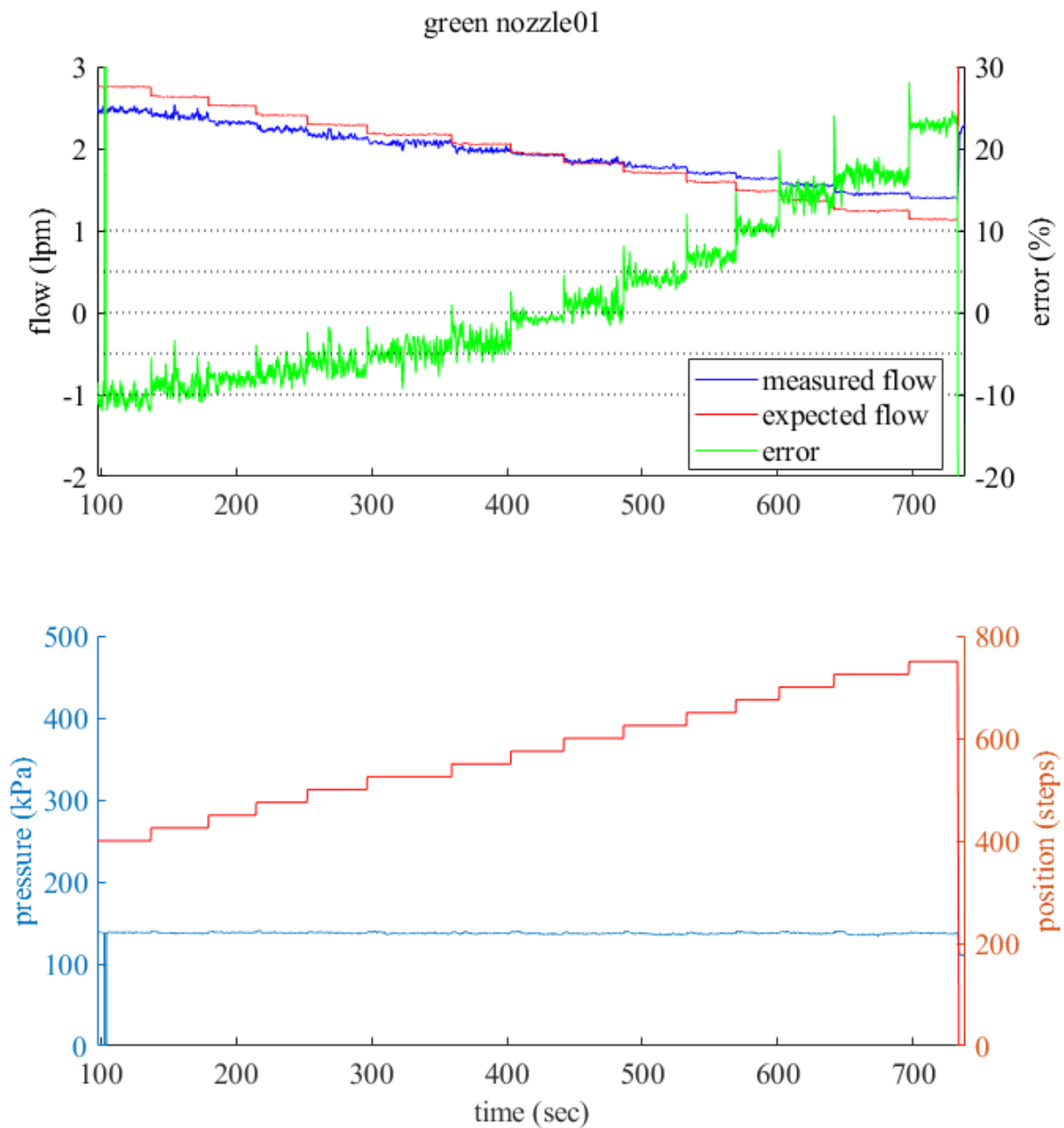


Figure 68 - Detailed view from fig. 69 showing data for varying actuator settings at lowest pressure setting (green nozzle01 flow coefficients).

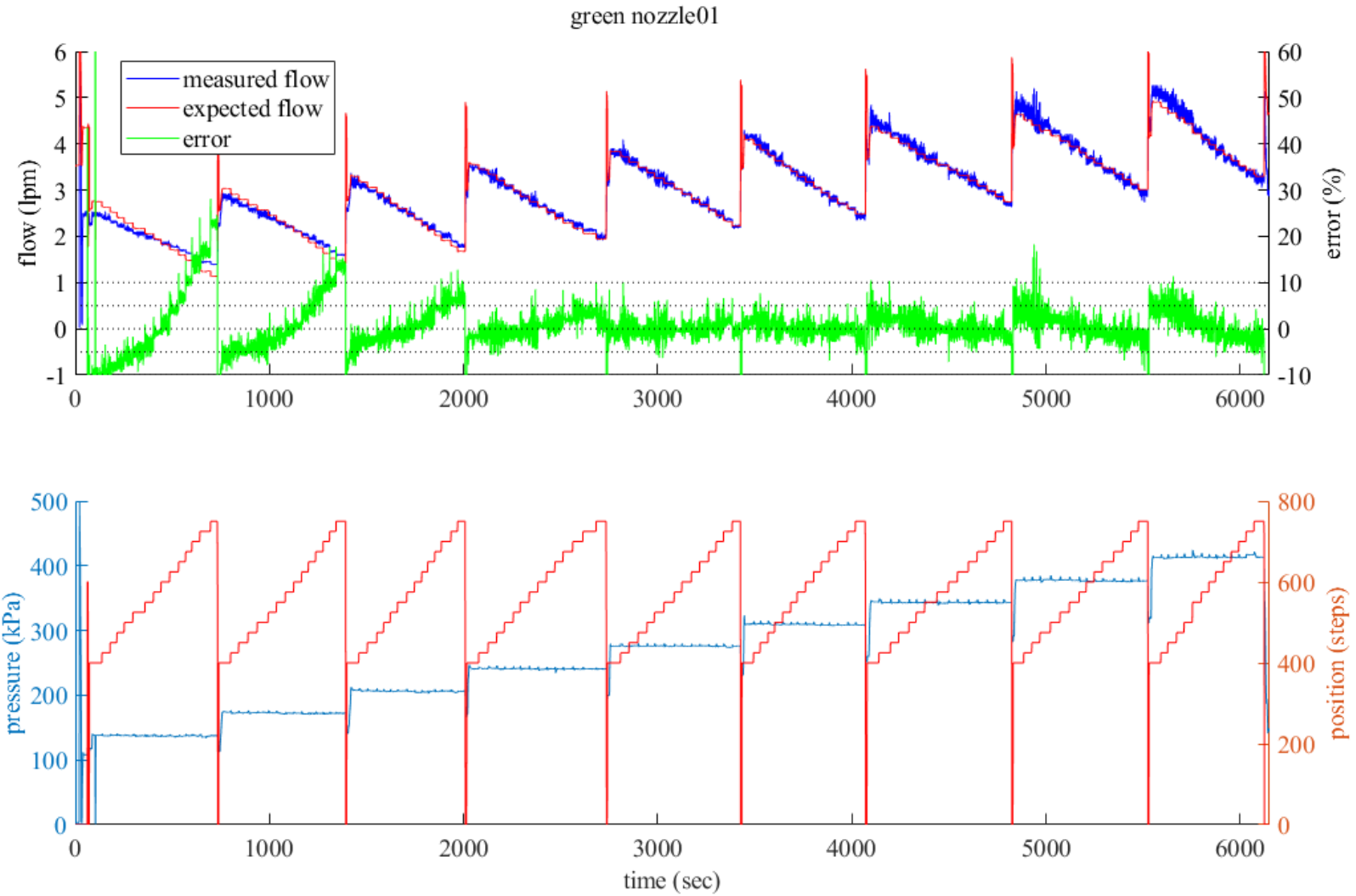


Figure 69 - Plot of time history data for nozzle flow evaluation (green nozzle01 flow coefficients).